A numerical study on the incipient vortices for tropical cyclones: genesis of low level vortices induced by rain evaporation and its sensitivity to vertical wind shear

Masuo Nakano
Department of Earth and Planetary Sciences
Kyushu University

January 2007

Abstract

Two series of systematic parameter experiments using a three dimensional non-hydrostatic model are performed to investigate the effect of environmental wind shear on the genesis and downward development of vortex induced by the cooling associated with the evaporation of rain drops below stratiform cloud. The first series of the experiments, referred to as "dry experiments", the effect of evaporation is represented as a localized cooling in a cylindrical region of various radius and strength in the model. The variable parameters are magnitude of vertical shear, radius and strength of the cooling. Total of 45 systematic parameter experiments are performed. In the second series of the experiments, referred to as "moist experiments", the effect of evaporation is calculated explicitly with the specified mid-tropospheric distribution of precipitation. The variable parameters are magnitude of vertical shear, radius and strength of the stratiform rain. Total of 27 systematic parameter experiments are performed.

In the dry experiments without vertical wind shear, a cyclonic vortex is developed by the stretching of planetary vorticity at the top of the cooling. The vortex is elongated to the ground surface by downward advection. In weak shear experiments, the vortex is slantingly elongated to the ground surface because sheared wind advects the vortex horizontally. In strong shear experiments, the vortex developed at the top of the cooling region is advected downward with large tilt. Moreover, on the way to the ground, the vortex advected away from the cooing

region, and no further downward extension occurs thereafter. The results of the parameter experiments show that the significance of vertical wind shear can be scaled by a non-dimensional number SI which is defined by vertical wind shear, cooling rate and radius of cooling region. When SI exceeds 3, it is shown that the vortex cannot elongate to the ground.

In the moist experiments, temporal and spatial variations of cooling induced by evaporation of stratiform precipitation are observed. The cooling is stronger at the edge of the shower region than at the center in experiments without shear. In the experiments with shear, the cooling at up-wind side is stronger and elongated to lower levels than the cooling at down-wind side. The strong cooling region descents with time as the air in the upper portion becomes mostly saturated. In experiments with halved rain intensity, however, the cooling does not occur in the levels near the ground surface. In spite of the existence of spatial and temporal inhomogeneity of the cooling, general characteristics of the evolution of vortex is qualitatively similar to that of the dry experiments. The results of the moist experiments show that the vortex cannot reach the ground surface when SI estimated using spatially and temporally averaged cooling rate in each case exceeds 3, which is in fairly good agreement with that in the dry experiments.

Contents

1 General introduction

1.1 Role of vertical wind shear during TC genesis

Tropical cyclones (TCs) are vortical storms with the radius of O(100-1000km) which form on the tropical ocean. In each year, roughly 80 TCs are formed on the globe (Emanuel 2003). For a variety of reasons, genesis has remained as one of the least understood stages of the TC's life-cycle. The most fundamental difficulty is the shortage of conventional observations over oceanic regions on which TCs form (WMO 2006). On the other hand, the climatological large-scale condition favorable for TC genesis has been well known as a combination of dynamical and thermodynamic factors (Gray 1968). This includes warm ocean surface temperature ($> 26°$C), potentially unstable moist-lapse rate that allows deep convection, small vertical shear of the tropospheric horizontal wind, low-level cyclonic vorticity, moist mid-troposphere, and sufficiently large Coriolis parameter (or large-scale absolute vorticity; Chang *et al.* 2003).

It is widely accepted that tropical cyclogenesis do not occur in region where vertical wind shear is large. Widely accepted explanation for the fact is that vortex is blown off by the vertical sheared environmental flow (e.g. Gray 1968; McBride and Zehr 1981). If vertical wind shear has only detrimental effects for tropical cyclogenesis, genesis may occur only in environment where vertical shear is nearly zero. Indeed, Gray (1968) recognized that small vertical shear (i.e., $\leq$ 10-15 m s^{-1} between 200 hPa and 850 hPa) environment is favorable for genesis. McBride and Zehr (1981) shows that vertical wind shear at incipient vortex center

is nearly zero at the time of genesis.

On the other hand, Jones (1995, 2000a, b) found that the vortex has a mechanism to oppose the destructive effects of vertical shear. She argued that combination of the flow associated with large-scale asymmetric PV anomaly at radii larger than radius of maximum wind and the flow induced by vertical projection of the tilted PV anomaly play a crucial role in counteracting the effect of vertical shear. Reasor *et al.* (2004) found that, when inverse time scale of the advection shearing apart the vortex is shorter than the frequency of precession induced by vertically projected PV anomaly, the vortex can resist the destructive effect of vertical shear and the vortex can be in the steady state with downshear-left tilt after the damp of vortex Rossby waves.

Moreover, in recent years, some authors have suggested that small, but non zero vertical shear is favorable for cyclogenesis. Bracken and Bosalt (2000) found that mean shear between 900 hPa and 200 hPa was 10.5 m s^{-1} and standard deviation of shear was 4.8 m s^{-1} at the time of genesis in Atlantic region. Through the diagnosis using the quasi geostrophic ω equation, they pointed out that large scale ascent conducive to genesis is presented in the vertically sheared environmental flow region. Montgomery and Farrell (1993) argued that vertical shear was required to couple the disturbances at lower and upper levels. Molinari *et al.* (2004) who analyzed ignition stage of Hurricane Danny (1997) found that convection in down shear side was active and that down shear vortex spin-up was occurred.

The relationship between vertical wind shear and TC genesis has been also

studied from the viewpoint of climate variation or climate change. For example, Camargo *et al.* (2006) compare Emanuel and Nolan's (2004) genesis potential index which computed using monthly data obtained from the NCEP/NCAR reanalysis with the same index which computed using data from three atmospheric general circulation models (AGCMs) forced by observed SST. They found that AGCMs can reproduce the ENSO response; genesis potential index anomalies appear in ENSO year, and that anomalies appearing in Atlantic and eastern North Pacific result from intensity change of vertical wind shear in ENSO years. Latif *et al.* (2007), who investigated the possible link between TCs activity in North Atlantic region and global warming, show that TC activity in the North Atlantic is modulated by vertical wind shear over the North Atlantic which is controlled the temperature difference between the tropical North Atlantic and the tropical Indian and Pacific Oceans. As discussed above, influence of vertical shear on tropical cyclogenesis remains very much under debate.

1.2 Incipient vortex formation as a major issue in the tropical cyclogenesis

Observations show that the TCs form in the presence of mesoscale convective systems (MCSs) in tropical disturbances, such as easterly waves (e.g., Gray 1968, 1998; Cotton and Anthes 1989; Raymond et al. 1998). Therefore cumulus convection is believed to be an essential ingredient in the TC formation process.

Ooyama (1964) and Charney and Eliassen (1964) hypothesized that, in conditionally unstable atmosphere, cumulus convection cooperates with the large scale

vortex in a positive feedback process; this idea was later coined the conditional instability of the second kind, or "CISK". The CISK hypothesizes only convective available potential energy (CAPE) in the ambient atmosphere as a energy reservoir of TC. However sea surface exchanges of heat and moisture plays important role in the stage of TC genesis. Indeed, Riehl (1954) estimated that ambient CAPE contributes no more than 15 hPa pressure drop. In Ooyama's (1969) simulation, only a weak vortex occurred when sea surface flux turned off. Rotunno and Emanuel (1987) demonstrated another feedback process, called wind-induced surface heat exchange, or "WISHE", that tropical storm can intensify itself enhancing sea surface energy flux by vortical wind even in mostly no CAPE atmosphere.

It is worth noting that, as some authors (e.g. Montgomery and Farrell 1993; Hendricks *et al.* 2004) pointed out recently, neither the CISK nor WISHE theories are appropriate descriptions of TC genesis process. Both of them assume that low-level concentrate rotational system (i.e., incipient tropical cyclone) already exists from the beginning; it is implicitly assumed that the transformation from tropical disturbance to incipient tropical cyclone has been already finished. How weak-amplitude tropical disturbances are transformed into a surface vortex of sufficient strength that can then intensify via CISK or WISHE process remains as a major unsolved problem in TC genesis.

1.3 Bottom-up and top-down scenarios

Recently, increased satellite sensors, improved analysis techniques of remotely-sensed data and increased power of computers have provided better representation of the TC formation process and have led to two primary scenarios for organization of a precursor tropical disturbance into a surface vortex of sufficient strength. One scenario is referred as "bottom-up" (Montgomery and Enagonio 1998; Hendricks *et al.* 2004; Montgomery *et al.* 2006) and another is referred as "top-down" (Ritchie and Holland 1997; Bister and Emanuel 1997, hereafter BE). In the bottom-up scenario, pre-existing low-level cyclonic vorticity is intensified through convergence and stretching associated with deep cumulus convection. In MCSs associated with easterly waves or extratropical troughs which penetrate into tropics, small-scale cores of towering cumulonimbus convection, or hot towers, are frequently observed to exists (e.g., Zehr 1992; Gray 1998). Simpson *et al.* (1998) put forth the idea that the hot towers were a positive influence to TC genesis via subsidence warming around them and the associated surface pressure fall through the hydrostatic balance. Montgomery and Enagonio (1998) and Möller and Montgomery (2000) demonstrated that low-level vortex merger and axisymmetrization of small-scale diabatically generated cyclonic potential vorticity (PV) anomalies could intensify a large-scale vortex on realistic time scales. Hendricks *et al.* (2004) analyzed a numerical simulation of Hurricane Diana (1984) using 3-km horizontal grid spacing. Hendricks *et al.* (2004) suggested that convective plumes forming intense vertical vorticity in their cores are the preferred convective

structures. The simulated plumes forming in a environment with rich cyclonic vorticity acted to generate multiple small-scale [O(10-30 km)] intense cyclonic vortex tubes. As demonstrated by Reasor *et al.* (2004), these tubes have coherent structure since they have vortex-Rossby elasticity. Hendricks *et al.* (2004) coined the term vortical hot towers (VHTs) to describe these tubes. In the pre-Diana environment, the generation of VHTs led to multiple mergers/axisymmetrization of the VHTs and corresponding upscale vorticity cascade to the tropical storm scale. Montgomery *et al.* (2006) performed idealized numerical simulations by introducing mesoscale convective vortex (MCV) embryo into the model. They suggested that while the each VHT has short lifetime nature, the aggregate of VHTs mimic a quasi-steady heating rate on the cyclone-scale circulation. For the cyclone-scale system to be kept in thermal wind balance, a thermodynamically direct toroidal circulation with a thin outflow at the tropopause and a thick inflow extending from surface to upper troposphere is generated. This circulation converges cyclonic vorticity of initial MCV and convective scale positive vorticity patches generated by VHTs.

In the top-down scenario, a precursor tropical disturbance may one or more MCSs with an accompanying MCV induced by evaporation of stratiform precipitation. Ritche and Holland (1997) reported that merger of MCSs within the original disturbance results in a more intense MCV that may eventually extend downward to increase the cyclonic vorticity at low levels. BE hypothesized that vertical vorticity of MCV was advected via mesoscale subsidence associated with evaporation of stratiform precipitation based on observation of Hurricane

Guillermo (1992) genesis and they demonstrated the theory by using axisymmetric model.

1.4 The focus of this thesis

In this thesis, I investigate the effect of environmental wind shear on the top-down scenario proposed by BE. In particular, genesis of MCV induced by evaporation of stratiform precipitation and its touchdown to the ground surface are focused. Among several senarios on the genesis of incipient vortex for TC, the mechanism proposed by BE is cleanest in the sense that it requires only stratiform precipitation and the earth's rotation; other mechanisms can be activated only if a number of preconditioning are finished. On the other hand, the mechanism proposed by BE may have its own weakness. As was speculated by BE themselves, the downward development of the vortex tube may be strongly affected by environmental vertical shear. If the effect of the shear is very destructive, it can not work at all in the real atmosphere where some degree of vertical shear exists everywhere.

Two series of systematic parameter experiments using a three dimensional non-hydrostatic model are performed. One of the series of experiments is named dry experiments. In these experiments, a localized cylindrical cooling region representing the effect of evaporation of stratiform precipitation is introduced to the model. Intensity of cooling, radius of cooling region, and magnitude of vertical wind shear are varied. Another series is named moist experiments. In these experiments, stratiform precipitation from "shower head" is imposed. The effect

of the evaporation is calculated explicitly in the model. Intensity of precipitation, radius of shower head, and magnitude of vertical wind shear are varied.

The outline of this article is as follows. The detail description of numerical model appears in section 2. Specification and results of dry/moist experiments are presented in sections 3 and 4, respectively. A summary and recommendation for future work are presented in section 5.

2 Numerical model

2.1 The dynamics formulation

The dynamics formulation presented in Klemp and Wilhelmson (1978) is mainly employed. The equation of state of moist atmosphere is conventionally written as follows

$$p = \rho R_d T(1 + 0.61 q_v), \tag{1}$$

where p is the pressure, ρ the density of moist air, R_d the gas constant for the dry air, T the temperature and q_v the mixing ratio of water vapor. For convenience, non-dimensional pressure Π (a.k.a. Exner function) is derived from (1) as follows

$$\Pi \equiv \left(\frac{p}{p_0}\right)^{R_d/C_p}. \tag{2}$$

Here p_0 is the basic state pressure at the ground and θ_v the virtual potential temperature defined by

$$\theta_v = \theta(1 + 0.61 q_v). \tag{3}$$

The potential temperature θ is then simply written in the form

$$\theta = \frac{T}{\Pi}.$$

The momentum equations are derived from the Navier-Stokes equations with the aid of Eq. (1). The results on an f-plane in the Cartesian coordinates (x, y, z) can be expressed in tensor form as

$$\begin{aligned} \frac{du_i}{dt} + C_p\overline{\theta}\frac{\partial(\pi - \alpha Div)}{\partial x_i} &= \delta_{i3}\left[\frac{\theta}{\overline{\theta}} - 1 + 0.61(q_v - \overline{q_v}) - q_c - q_r\right] - \epsilon_{ij3} f u_i \\ &\quad + D_{u_i} + F_{u_i}^{sponge} + F_{u_i}^{sfc}. \end{aligned} \tag{4}$$

The u_i (i=1, 2, 3) are the velocity u, v, w, respectively, π is the deviation of pressure from the initial unperturbed state $\overline{\Pi}$, and q_c and q_r are the mixing ratios of cloud drops and rainwater, respectively. The f is the Coriolis parameter. Bars over individual variables refer to the initial undisturbed state which is a function of z only. The operator $\frac{d}{dt}$ denotes the substantial derivative given by

$$\frac{d}{dt} \equiv \frac{\partial}{\partial t} + u_i \frac{\partial}{\partial x_i}.$$

Term α and Div are defined as follows

$$Div \equiv \frac{\partial u}{\partial x} + \frac{\partial v}{\partial y} + \frac{\partial w}{\partial z},$$

$$\alpha = 2.5 \times 10^{-4} \text{ (s)},$$

and the term αDiv is introduced as an artificial damping for acoustic wave to keep numerical stability (Skamarock and Klemp 1992). Terms denoted by D_{u_i}, $F_{u_i}^{sponge}$ and $F_{u_i}^{sfc}$ represent the subgrid turbulent mixing (see subsection 2.3), the friction in the sponge layer (see subsection 2.4) and the drag force on the surface (see subsection 2.5), respectively.

The prognostic equations for θ, q_v, q_c, and q_r can all be written in the form

$$\frac{d\phi}{dt} = M_\phi + D_\phi + F_\phi^{sponge} + F_\phi^{sfc} + F_\phi^{rad}, \tag{5}$$

where M_ϕ refers to microphysical terms described in subsection 2.2 and D_ϕ to turbulence terms defined in subsection 2.3. The term F_ϕ^{sponge} and F_ϕ^{sfc} refer to Newtonian damping in the sponge layer (see subsection 2.4) and surface flux (see subsection 2.5), respectively. In the dry experiments, all water substance term

set to be zero and thermodynamic equation is modified in the form

$$\frac{d\theta}{dt} = D_\theta + F_\theta^{sponge} + F_\theta^{sfc} + C, \tag{6}$$

where the C represents cooling by the evaporation of stratiform precipitation, whose detail will be described next section. The term F_ϕ^{rad} refers to radiative cooling defined by

$$F_\phi^{rad} \equiv -\frac{(\theta - \overline{\theta})}{\tau_r}, \tag{7}$$

where $\tau_r = 12$ hours (after Rotunno and Emanuel 1987) which is only added to θ equation in moist simulation.

The continuity equation for compressible atmosphere can be written in the form

$$\frac{\partial \rho}{\partial t} + \frac{\partial}{\partial x_j}(\rho u_j) = 0. \tag{8}$$

By taking substantial derivative of Eq. (1) and using Eq. (8) and thermodynamic equation, the pressure equation is obtained in the form

$$\frac{\partial \pi}{\partial t} + \frac{\overline{c}^2}{c_p \overline{\rho}\,\overline{\theta_v}^2} \frac{\partial}{\partial x_j}\left(\overline{\rho}\overline{\theta_v} u_j\right) = f_\pi, \tag{9}$$

$$f_\pi = -u_j \frac{\partial \pi}{\partial x_j} + \frac{R_d \pi}{c_v} \frac{\partial u_j}{\partial x_j} + \frac{c^2}{c_p \theta_v^2} \frac{d\theta_v}{dt} + D_\pi, \tag{10}$$

where c is the speed of acoustic wave given by $c^2 = c_p R_d \Pi \theta_v / c_v$. In the model, f_π is set to be zero. This specification causes negligible difference on the pressure fields (Klemp and Wilhelmson 1978).

2.2 Formulation of cloud microphysics

The cloud microphysical processes represented by M_ϕ in Eq. (5) are given by

$$M_\theta = \gamma \left(\frac{dq_{vs}}{dt} + E_r \right), \tag{11}$$

$$M_{q_v} = \frac{dq_{vs}}{dt} + E_r, \tag{12}$$

$$M_{q_c} = -\frac{dq_{vs}}{dt} - A_r - C_r, \tag{13}$$

$$M_{q_r} = \frac{1}{\overline{\rho}}\frac{\partial}{\partial z}\left(\overline{\rho} V q_r\right) - E_r + A_r + C_r. \tag{14}$$

Here $\gamma = L/(c_p\overline{\Pi})$, L is the latent heat of vaporization, q_{vs} represents the saturation mixing ratio, and $\frac{dq_{vs}}{dt}$ refers to the rate of condensation or evaporation of cloud water q_c. The terms A_r, C_r and E_r represent the rates of autoconversion, collection and evaporation of rain, respectively, and V is the terminal velocity of the rain water.

Condensation and evaporation represented by the $\frac{dq_{vs}}{dt}$ term are governed by the thermodynamic equation

$$\frac{d\theta}{dt} + \gamma\frac{dq_v}{dt} = D_\theta + \gamma D_{q_v}. \tag{15}$$

Tetens' formula is employed to determine the saturation vapor pressure. The formula is in the form

$$q_{vs} = \frac{380}{p}\exp\left(17.27\frac{\overline{\Pi}\theta - 273}{\overline{\Pi}\theta - 36}\right). \tag{16}$$

In the moist experiments, significant pressure drops associated with developed vortices are observed in the later time period. To express the evolution of hurricane strength vortices accurately, the pressure p, which is replaced by basic state pressure $\overline{p}$ in Klemp and Wilhelmson (1978), is employed in this study. Eqs.(15) and (16) are sufficient to uniquely determine θ and q_v in a saturated region in which supersaturation is not permitted. Summing the q_v and q_c equations results

in

$$\frac{dq_l}{dt} = D_{q_v} + D_{q_c} + (E_r - A_r - C_r), \tag{17}$$

and thus $q_l = q_v + q_c$ is a conservative variable in the absence of rain processes and turbulent mixing.

Autoconversion (A_r) and accretion (C_r) rates are determined using warm rain parameterization (Kessler 1969), where C_r is based on a Marshall-Palmer distribution for q_r. These rates are defined by

$$A_r = k_1(q_c - a), \tag{18}$$

$$C_r = k_2 q_c q_r^{0.875}, \tag{19}$$

where $k_1 = 0.001$ s^{-1}, $a = 0.001$ kg kg^{-1} and $k_2 = 2.2$ s^{-1} (Soong and Ogura 1973). The evaporation of rain is calculated using a rate equation similar to that described by Ogura and Takahashi (1971), i.e.,

$$E_r = \frac{100}{\rho} \frac{(1 - q_v/q_{vs})C(0.001\overline{\rho}q_r)^{0.525}}{5.4 \times 10^5 + 2.55 \times 10^8/(\overline{p}q_{vs})}, \tag{20}$$

where C is the ventilation factor given by

$$C = 1.6 + 124.9(\overline{\rho}q_r)^{0.2046}. \tag{21}$$

The first term on the RHS of Eq. (14) represents the vertical flux of rainwater. The expression for the terminal fall velocity V is similar to that given by Soong and Ogura (1973) but is adjusted for mean density variations as suggested by Kessler (1969) and commented on by Beard (1977):

$$V = 36.34(\overline{\rho}q_r)^{0.1364} \left(\frac{\rho_0}{\overline{\rho}}\right)^{\frac{1}{2}}, \tag{22}$$

where ρ_0 is the basic state density at the ground.

2.3 Subgrid turbulence parameterization

Subgrid turbulence parameterization, the closure linking the resolved scales and the unresolved subgrid-scale, is desired to make a simulation successfully. In this study, 1.5 order turbulent kinetic energy (TKE) scheme and Smagorinsky scheme are employed for moist and dry simulation, respectively. The Smagorinsky scheme is a special case of the TKE scheme.

The general approach taken in TKE scheme is to close the subgrid transports using mixing length theory on conservative variables. In unsaturated motion θ and q_v are conserved. In saturated motion $q_l \equiv q_v + q_c$ is conserved ignoring rain process, while Eq. (15) governs conservation in the thermodynamic process. Based on these considerations, the expressions for $D_\phi = D_\theta$, D_{q_v}, D_{q_c} and D_{q_r} can be approximated for both unsaturated and saturated motion as

$$D_\phi = -\frac{\partial}{\partial x_j}\left(\overline{u_j'\theta'}\right) \sim \frac{\partial}{\partial x_j}\left(K_h \frac{\partial \phi}{\partial x_j}\right), \tag{23}$$

where K_h is an eddy mixing coefficient to be defined later. Here, primed variables refer to deviations from the grid volume average and overbars denote an average taken throughout the grid volume. Hereafter, unprimed variables represent grid volume averages and thus their overbars are omitted to avoid confusion with those used for the undisturbed initial state variables.

At first glance, it may not be evident that these expressions provide closure on conservative quantities when the air is saturated. However, as discussed above, the moist processes are governed by Eqs. (15)-(17) and consequently, the closures

denoted in Eq. (23) imply a closure for Eq. (15) given by

$$D_\theta + \gamma D_{q_v} = \frac{\partial}{\partial x_j}\left(K_h \frac{\partial \theta_e}{\partial x_j}\right) - K_h q_v \frac{d\gamma}{dz} \cdot \frac{\partial}{\partial z}\left[\ln\left(k_h q_v^2 \frac{d\gamma}{dz}\right)\right] \tag{24}$$

and for Eq. (17) by

$$D_{q_v} + D_{q_c} = \frac{\partial}{\partial x_j}\left(K_h \frac{\partial q_l}{\partial x_j}\right). \tag{25}$$

The subgrid momentum terms are given by

$$D_{u_i} = -\frac{\partial}{\partial x_j}\left(\overline{u_i' u_j'}\right), \tag{26}$$

where

$$\overline{u_i' u_j'} = -K_m\left(\frac{\partial u_i}{\partial x_j} + \frac{\partial u_j}{\partial x_i}\right) + \frac{2}{3}\sigma_{ij} E. \tag{27}$$

Here K_m is the momentum eddy mixing coefficient and E is the subgrid-scale kinetic energy given by

$$E = \frac{1}{2}\overline{(u_i')}^2. \tag{28}$$

In deriving these expressions, motion on the subgrid scale is assumed to be incompressible which is a good approximation for motion at scales smaller than the grid interval. The remaining mixing term D_π is set to be zero since it has virtually no influence on the solutions.

It now remains to determine E, K_m and K_h. The turbulence energy E is represented by a prognostic equation of the form

$$\frac{dE}{dt} = \overline{gw'\left(\frac{\theta'}{\overline{\theta}} + 0.61 q_v' - q_c'\right)} - \overline{u_i' u_j'}\frac{\partial u_i}{\partial x_j} + \frac{\partial}{\partial x_j}\left(K_m \frac{\partial E}{\partial x_j}\right) - (C_\epsilon / l) E^{\frac{2}{3}}, \tag{29}$$

where l is the mixing length which is set to Δz in this study and $E \geq 0$ is enforced. All the subgrid terms have been defined except for the vertical buoyancy flux

in saturated motion. This term can be expressed as a function of the nearly conservative variables θ_e and q_l, and then closed using mixing length theory. This is accomplished by relating the saturation mixing ratio and θ through the Clausius-Clapeyron equation which yields

$$\overline{u_i' q_v'} = \frac{\epsilon L^2 q_v}{R_d T \theta} \overline{u_i' \theta'}, \tag{30}$$

where $\epsilon = 0.622$. Employing the definition of the θ_e, Eq. (30) becomes

$$\overline{u_i' \theta'} = \overline{u_i' \theta_e'} \left(1 + \frac{\epsilon L^2 q_v}{c_p R_d T^2} \right)^{-1}. \tag{31}$$

Coupling these expressions with Eq. (3) and closing on θ_e and q_l yields

$$\overline{w' \left(\frac{\theta'}{\overline{\theta}} + 0.61 q_v' - q_c' \right)} = -A K_h \frac{\partial \theta_e}{\partial z} + K_h \frac{\partial q_l}{\partial z}, \tag{32}$$

$$A = \frac{1}{\overline{\theta}} \left\{ \frac{1 + \frac{1.61 \epsilon L q_v}{R_d T}}{1 + \frac{\epsilon L^2 q_v}{c_p R_d T^2}} \right\}. \tag{33}$$

Once E is known, K_m can be determined on dimensional grounds using

$$K_m = C_m E^{\frac{1}{2}} l. \tag{34}$$

Following Deardorff (1975), the coefficients are defined by $C_m = C_\epsilon = 0.2$. K_h is then related to K_m by a proportionality constant, i.e., $K_h = 3K_m$. The factor of 3 was used in Deardorff (1972).

To increase coding efficiency the subgrid-scale kinetic energy equation (29) is actually written in terms of K_m. Using Eq. (34) and assuming that l is constant, Eq. (29) is rewritten in the form

$$\frac{dK_m}{dt} = \frac{C_m^2 l^2}{2K_m}(B + S) + \frac{1}{2} \left(\frac{\partial^2 K_m^2}{\partial x^2} + \frac{\partial^2 K_m^2}{\partial y^2} + \frac{\partial^2 K_m^2}{\partial z^2} \right) - \frac{C_\epsilon K_m^2}{2 C_m l^2}. \tag{35}$$

B denotes the buoyancy term and its evaluation depends on whether or not the air is saturated ($q_c > 0$). When $q_c = 0$,

$$B = -g\frac{K_h}{\theta}\frac{\partial\theta}{\partial z}, \tag{36}$$

and when $q_c > 0$

$$B = -gAK_h\frac{\partial\theta_e}{\partial z} + gK_h\frac{\partial q_l}{\partial z}, \tag{37}$$

where A represents the term defined in Eq. (33).

In Eq. (35), S represents the shear term and approximated by

$$\begin{aligned} S &= -\overline{u_i' u_j'}\frac{\partial u_i}{\partial x_j} \\ &= K_m\left\{2\left[\left(\frac{\partial u}{\partial x}\right)^2 + \left(\frac{\partial v}{\partial y}\right)^2 + \left(\frac{\partial w}{\partial z}\right)^2\right]\right. \\ &\quad \left. + \left(\frac{\partial v}{\partial x} + \frac{\partial u}{\partial y}\right)^2 + \left(\frac{\partial w}{\partial x} + \frac{\partial u}{\partial z}\right)^2 + \left(\frac{\partial w}{\partial y} + \frac{\partial v}{\partial z}\right)^2\right\}. \end{aligned} \tag{38}$$

Smagorinsky's (1963) first order scheme usually defines K_m as

$$K_m = C_s l[\max(|Def|^2 - N^2/Pr, 0)]^{\frac{1}{2}} \tag{39}$$

where C_s is empirical constant and takes a value of 0.21 after Deardorff (1972), N is Brunt Väisällä frequency defined as B/K_h, P_r is the turbulent Prandtl number and is usually a constant having a value between 1/3 and 1, Def^2 is squared magnitude of deformation defined as $B/K_m - \frac{2}{3}(Div)^2$. In dry simulation, K_m is obtained by setting $\frac{dK_m}{dt}$ and diffusion and dissipation term in Eq. (35) to be zero for re-usability of the code.

2.4 Sponge layer

In order to absorb upward propagating wave disturbances and to eliminate spurious wave reflection at the top boundary, an artificial damping is added in a layer near the top boundary. The terms F^{sponge} in Eqs. (4) and (5) is defined as follow

$$F^{sponge} = -R_D(z)(\phi - \overline{\phi}), \tag{40}$$

where R_D is the vertical profile of the inverse damping time scale and ϕ is u, v, w, θ or a water substance.

The profile of R_D has the form

$$R_D = \begin{cases} 0 & \text{for } z < z_D \\ \frac{1}{\tau_D}\frac{z-z_D}{z_T-z_D} & \text{for } z \geq z_D, \end{cases} \tag{41}$$

where z_D is the height of the bottom of the damping layer and z_T the height of the model top boundary. τ_D is the e-folding time scale of damping at $z = z_T$.

2.5 Surface flux parameterization

The surface fluxes enter the model as the lower boundary conditions for the momentum stresses (F^{sfc} in Eqs. (4) for u, v), turbulent heat flux (F^{sfc} in Eq. (5) for θ), and turbulent moisture flux (F^{sfc} in Eq. (5) for q_v) at the ground surface.

The surface momentum fluxes are defined as

$$F_u^{sfc} = -\frac{1}{\Delta z/2}\frac{\overline{\rho}(z=0)}{\overline{\rho}(z=\Delta z/2)}C_D V(u - \overline{u}), \tag{42}$$

$$F_v^{sfc} = -\frac{1}{\Delta z/2}\frac{\overline{\rho}(z=0)}{\overline{\rho}(z=\Delta z/2)}C_D V v, \tag{43}$$

where u and v are the horizontal velocity components evaluated at the lowest grid level above the ground surface and

$$V \equiv \sqrt{(u - \overline{u})^2 + v^2} \tag{44}$$

is the wind speed at the same level. The reason for subtracting $\overline{u}$ from u will appear in section 4.2.2.

The drag coefficient $C_D = 1.5 \times 10^{-3}$ is used.

The surface sensible heat flux is defined as

$$F_\theta^{sfc} = -\frac{1}{\Delta z/2}\frac{\overline{\rho}(z=0)}{\overline{\rho}(z=\Delta z/2)} C_D V(\theta(z=0) - \overline{\theta}(z=0)), \tag{45}$$

where $\theta(z = 0)$ is obtained by linear extrapolation. The moisture flux at the surface is

$$F_\theta^{sfc} = -\frac{1}{\Delta z/2}\frac{\overline{\rho}(z=0)}{\overline{\rho}(z=\Delta z/2)} C_D V(q_v(z=0) - \overline{q_{vs}}(z=0)), \tag{46}$$

where $q_v(z = 0)$ is calculated by using extrapolated θ and π.

The procedure for obtaining a numerical solution of the finite-difference analogues to the model equation is similar to Klemp and Wilhelmson (1978). The horizontal advection terms are approximated with forth-order finite differences, and the vertical advection terms are approximated with second-order finite differences. For water substances and TKE, MPDCD scheme (Lafore *et al.* 1998) is used to avoid negative values. In this study, horizontal domain size of 1500 km is used in both directions, z_T of 15 km (dry simulation) or 30 km (moist simulation) is used. The horizontal grid space $\Delta x = \Delta y = 10$ km and the vertical grid space $\Delta z = 500$ m are used. The starting level of sponge layer z_D is set to be 12.5 km

(dry simulation) or 25 km (moist simulation). For time integration, Klemp and Wilhelmson's (1978) time-splitting technique is employed. The large time step of $\Delta t = 30$ s (dry simulation) or $\Delta t = 10$ s (moist simulation) is used.

3 Dry experiments

3.1 Introduction

It is widely accepted that tropical cyclogenesis require a finite amplitude incipient vortex near sea surface level which can initiate CISK (Ooyama 1964; Charney and Eliassen 1964) or WISHE (Rotunno and Emanuel 1987). BE observed that such an incipient vortex was formed through following steps: (1) development of stratiform region in later stage of life cycle of tropical cloud cluster (Fig. 1a), (2) atmosphere under stratiform cloud was cooled by evaporation of raindrops (Fig. 1b). (3) Mesoscale convective vortex (MCV) was developed at the middle level of troposphere (Fig. 1c), (4) MCV elongated toward the ground and that the vortex developed into Hurricane Guillermo (1991) (Figs. 1d and e). They, further, speculated that aforementioned mechanism is fragile to vertical wind shear by thought experiment.

A systematic parameter experiments using a three dimensional non-hydrostatic model are performed to investigate the effect of environmental vertical wind shear on the genesis and downward development of vortex induced by evaporational cooling. In this section, to investigate the condition for vortex elongation toward the ground surface and to reveal the mechanism which determine the condition of vortex elongation, total of 45 systematic parameter experiments are performed. The variable parameters are magnitude of vertical shear, radius and strength of cooling.

The outline of this section is as follows. Subsection 3.2 explains detail of series

of numerical experiments. Subsection 3.3 shows structure of vortices induced by the cooling. The condition in successful elongation of mid-level vortices to the ground is discussed and non-dimensional number SI which indicates the amount of influence of vertical shear is introduced in section 3.4. Subsection 3.5 shows conclusion.

3.2 Specification of the dry experiments

3.2.1 Initial profiles of temperature and wind

The temperature is set to be 300 K at the ground. The lapse rate for the initial state of the model is set to be 6.5 K km^{-1} up to 10 km height from the ground. At layers higher than 10 km, temperature is set to be 235 K. Linearly sheared westerly wind

$$\overline{u} = \begin{cases} U_{7.5}(z/H) & (z < H) \\ U_{7.5} & (z \geq H), \end{cases}$$

where $H = 7.5$ km is introduced into the model (Fig. 2). $U_{7.5}$ of 0, 3, 6 or 9 m s^{-1} is used in each experiment. In the present model, meridional potential temperature gradient balancing the prescribed vertical shear is not considered. No significant differences are observed between the model run with and without temperature advection term in the thermodynamic equation responsible for temperature gradient balanced to shear.

3.2.2 Specification of eveporational cooling effect of stratiform precipitation

The term C in Eq. (6) represents the effect of the cooling by evaporation of raindrops from a stratiform cloud. In dry experiments, a localized cylindrical region with 5 km height is cooled. The translation velocity of the stratiform cloud is assumed to be same as the initial wind speed at 5 km height (Fig. 2). The term C is given as a function of distance from center of the cylindrical region r and height z

$$C(r, z) = \frac{R(r)Z(z)}{\overline{\rho}(z)} C_0, \tag{47}$$

where $\overline{\rho}$ represents dry air density of the basic state and C_0 is a parameter discussed later and

$$R = \begin{cases} 1 & (r \le r_0) \\ \frac{r_1 - r}{r_1 - r_0} & (r_0 \le r \le r_1) \\ 0 & (r_1 \le r) \end{cases}$$

$$Z = \begin{cases} 1 & (z \le 5\text{km}) \\ 0 & (z > 5\text{km}). \end{cases}$$

The stratiform precipitation region observed by BE had radius of ∼100 km (see their rader images, Figs. 4a and 5a). I examine three cases 50, 100 or 200 km for r_0, and $r_1 = r_0 + 40$ km.

The cooling rate by evaporation under stratiform cloud varies widely (e.g., 4.8-144 K day^{-1}; Leary and Houze 1979). Hence some C_0 should be examined. BE employed 0.1425 g kg^{-1} as fixed rain water mixing ratio in their numerical experiments. The mixing ratio has 25 % larger value than that deduced from their rader observation. Assuming that terminal velocity of raindrops is 5 m s^{-1}, this water mixing ratio corresponds to precipitation rate of 6.2 cm day^{-1}. Houze (1989, Fig. 23) shows that cooling rate in the stratiform precipitation region can be estimated to be about (3 K day^{-1})/(1.4 cm day^{-1}). Therefore the stratiform precipitation region observed by BE results in the cooling rate of about 10 K day^{-1}. According to Johnson *et al.* (2002) who simulated tropical convection system observed in TOGA COARE (Webster and Lukas 1992) by using a cloud resolving model, the cooling rate under the melting layer of stratiform system is 5-10 K day^{-1}. In this study, cooling rate C_0 of 5, 10 or 20 K day^{-1} is employed. BE concluded that, for a significant incipient vortex to be formed, stratiform precipitation should last longer than the positive potential vorticity (PV) anomaly

dominates at the surface in the precipitation region. In their study, precipitation duration time of 36 hours are required. In each of the experiment, for simplicity, the cooling rate is assumed to be independent of time during whole integration time (100 hours). One might claim that evaporational cooling does not last 100 hours in nature. As you can see in later section, however, in experiments with realistic cooling rate (e.g., 10 K day^{-1}), the vortex can extend to the ground in less than 40 hours, which is nearly same time required precipitation duration time by BE.

In summary, total number of 45 systematic parameter experiments are performed in this study. The parameter variables are C_0, r_0, and $U_{7.5}$. Hereafter, for example, the experiment in which parameters $C_0 = 10$ K day^{-1}, $r_0 = 100$ km, and $U_{7.5} = 3$ m s^{-1} are used is named as C10R100S3.

3.3 Structure of vortex induced by cooling.

In this section, time evolution of the vortex is presented by mainly focusing onto vorticity. To understand the evolution of the vortex, budget analyses are performed. The vorticity tendency equation can be written as follows

$$\frac{\partial \zeta}{\partial t} = -u\frac{\partial \zeta}{\partial x} - v\frac{\partial \zeta}{\partial y} - w\frac{\partial \zeta}{\partial z} - (f+\zeta)(\frac{\partial u}{\partial x} + \frac{\partial v}{\partial y}) + \frac{\partial w}{\partial y}\frac{\partial u}{\partial z} - \frac{\partial w}{\partial x}\frac{\partial v}{\partial z} + F, \quad (48)$$

the first and the second terms on the RHS represent horizontal advection, the third term represents vertical advection, the fourth term is the generation term by stretching, and fifth and sixth terms are the generation rate by tilting of x-component and y-component of vorticity vector, respectively. The last term of RHS represents the effect of friction or diffusion.

3.3.1 No shear Experiments

Figure 3 shows the time evolution of the vorticity and its generation terms on the vertical plane at $y = 750$ km, the center of cooling region, in the experiment C10R100S0. As shown in Figs. 3a-c, at first, positive vorticity appears at the top of the cooling, and it extends downward. The vorticity is produced at the top of the cooling by stretching (Figs. 3d-f) and the vorticity produced at the top of the cooling is advected downward (Figs. 3g-i).

Figure 4 shows time evolution of vorticity at $z = 750$ m in the experiment C10R100S0. At first, negative vorticity surround the positive vorticity. The negative vorticity is produced at the edge of cooling region by the tilting of horizontal component of the vorticity vector whose horizontal component directed to the

center of the cooling region and accounted mostly by the increase of tangential velocity with altitude inside the cooling region.

Subsidence in the cooling region (not shown) is 1.5-2 cm s^{-1} in cases of $C_0 = 5$ K day^{-1}, 3-4 cm s^{-1} in cases of $C_0 = 10$ K day^{-1} and 5-7 cm s^{-1} in cases of $C_0 = 20$ K day^{-1}, supporting the common assumption for the tropical atmosphere that cooling rate is proportionality relation to subsidence velocity. The temperature in the cooling region decreases only 1-2 K except in lowest level in cases of $C_0 = 10$ K day^{-1}. This also suggests that the term C in Eq. (6) is approximately balanced to adiabatic heating in the cooling.

Elapsed time required for vortex to extend to the ground, defined here as the time when a closed vorticity contour of 5×10^{-5} s^{-1} can be written at z =750 m, are 18-24 hours in case of $C_0 = 20$ K day^{-1}, 35-43 hours in case of $C_0 = 10$ K day^{-1}, 69-80 hours in case of $C_0 = 5$ K day^{-1}. These result show the elapsed time before the vortex touchdown is approximately in inverse proportion to cooling rate.

3.3.2 Experiments with vertical shear

Figure 5 shows evolution of vorticity at $y = 750$ km for the experiments C10R100S3, C10R100S6 and C10R100S9. As no shear cases, vorticity is produced at the top of the cooling region and advected downward. The vortex tilt is larger as the prescribed shear is larger. In particular, in the experiment C10R100S9 (lowest panel), vortex cannot reach the ground but blown off away from the cooling region.

Figure 6 shows time series of vorticity and wind vector relative to the translation velocity of the cooling at $z = 750$ m for the experiments C10R100S3, C10R100S6 and C10R100S9. In contrasted to the no shear cases, negative vorticity is mostly concentrated at the southern edge of cooling. In the experiments with $U_{7.5}$ of 3 and 6 m s^{-1} cases, the negative vorticity is winded by positive vorticity with time. In the experiment C10R100S9, the positive vorticity maximum of 1×10^{-4} s^{-1} is small in magnitude and lies outside of the cooling region. The shape of positive vorticity distribution is largely elongated toward downshear side[1].

Figure 7 shows time mean (0-30 hours) vertical velocity and potential temperature anomaly at altitude of 2250 m. The time mean downward velocity is larger in the downshear side, and potential temperature in the downshear side is warmer than opposite side. From hydrostatic relation, the asymmetry of the thermal structure is consistent with the offset of the vorticity maximum or the pressure minimum to the west in the lower altitude.

At 60 hour, azimuthal wave number 1 structures are dominant in potential temperature and vertical velocity fields in the cooling region. The downshear side is warmer and the upshear side is cooler (Fig. 8a). It is also observed that an ascent exists in the southern side and a descent exists northern side of vortex (Fig.8b). The vorticity maxima shifts to the downshear side in lower altitude

[1]Usually eastern side should be called as downshear side in westerly shear configuration. However, in this article, western side is called as downshear side because the translate velocity of cooling is assumed to be same as background flow speed at 5 km height. Therefore the parcels start at the top of the cooling region, which posses positive vorticity, experience easterly shear along with their downward motion.

(Figs. 5 and 9).

The wave-number 1 structures of vortex are similar to the relationship among vertical velocity, potential temperature deviation and the tilt of vortex observed by Jones (1995). She interpreted the observed precession of the vortex as interaction of lower and upper portion of vortex; upper (lower) vortex rotate anticlockwise around vortex center in mid-level due to upward (downward) projected lower (upper) vortex. Figure 9 shows the time evolution of the vertical tilt of vorticity maxima in the experiments C10R100S3, C10R100S6 and C10R100S9. In the dry experiments with shear, no precession of vortices like those found in Jones (1995) is observed. What is responsible for the difference between the results of Jones (1995) and ours is that local penetration depth defined as $(f_{loc}(f+\zeta))^{\frac{1}{2}}L/N$ ($f_{loc} \equiv f + 2v_T/r$, ζ: relative vorticity, v_T: tangential velocity) (Hoskins *et al.* 1985) is much smaller than that in Jones (1995). In this study, local penetration depth is only 2.3 km ($f = 3\times10^{-5}$ s^{-1}, $L = 100$ km, $N^2 = 10^{-4}$ s^{-2}, $\zeta = 1\times10^{-4}$ s^{-1}, $v_T = 10$ m s^{-1}, $r = 50$ km) but that of Jones' is 14 km. Jones (1995) initialized her experiments by introducing a relatively strong upright vortex placed in a vertically sheared flow environment. On the other hand, in the present experiments, vortices are gradually built up with time in the sheared environment. Moreover, vortices formed in the present model are not axisymmetric. This difference may be responsible for the weaker interaction between upper and lower portion of vortex in the present study.

3.3.3 Asymmetry of vorticity generation at the northern and southern edges of the cooling region

Figure 10 shows time evolution of each term of vorticity equation calculated for the experiment C10R100S6 at the southern edge of the cooling and $z = 1250$ m. We can observe that negative vorticity is continually produced from the tilting of y-component of vorticity vector, most of which is composed of $\frac{d\overline{u}}{dz}$. On the other hand, Fig. 11 shows the same as Fig. 10 except for the northern edge of the cooling region and z=1750 m. In contrast to the southern edge, positive vorticity is produced from the tilting of y-component vorticity. However this is not persistent; after 23 hours, vorticity produced from the tilting of y-component vorticity falls down to negative. At 30 hours, total tendency of vorticity changes sign to negative.

Figure 12 shows vertical profile of zonal flow for the experiment C10R100S6 at the southern and northern edges and t =20 hours. At the southern edge, westerly shear is enhanced because the vortex descending from the top of the cooling has stronger circulation in higher altitude. On the other hand, at the northern edge, the flow accompanied by descending vortex weaken and even reverse the westerly shear in the environmental flow. This explains the asymmetry of the vorticity generations by tilting term at the northern and the southern edges of the cooling region.

3.4 Condition for vortex touchdown to the ground.

As noted in section 3.1, cyclonic vorticity on the ground surface are required for TC genesis. In this section, condition for vortex touchdown to the ground is discussed based on the results of the dry experiments.

3.4.1 Time evolution of vorticity near the ground surface level.

Figure 9 shows that the tilt of the vortex induced by cooling is larger when the environmental shear is larger. In particular, in cases with $U_{7.5} = 9$ m s^{-1}, the location of the vorticity maximum on $z = 750$ m surface is more than 100 km away from that on $z = 1750$ m, indicating that the vortex is blown off in the lower level.

Figure 13 shows the time evolution of maximum values of vorticity on the $z = 750$ m surface. Cases with $U_{7.5} = 1$ m s^{-1} (Fig. 13b) are difficult to distinguish from the no shear cases. In cases with $U_{7.5} = 3$ m s^{-1} (Fig. 13c) the effect of the environmental shear becomes noticeable; in the experiment C5R50S3 little increase of vorticity is observed. In the experiment C10R50S3, large decrease in the maximum value of the vorticity is observed after the initial increase, although the vorticity recovers afterwards. This behavior of vorticity maximum value suggests that the existence of the vertical shear influences the vortex built-up process by cooling. In cases of $U_{7.5} = 6$ m s^{-1} (Fig. 13d), little increase in vorticity is observed in the experiment C5R50S6. In addition to case C10R50S6, cases C10R100S6 and C20R50S6, are significantly affected by the shear; large decreases in vorticity are observed after initial buildups. In cases of $U_{7.5} = 9$

m s^{-1} (Fig. 13e), little increase in vorticity is observed in all cases of $C_0 = 5$ K day^{-1} (experiments C5R50S9, C5R100S9 and C5R200S9) and C10R50S9. In experiment C10R100S9, vorticity decreases after the initial moderate increase. Other cases exhibit large fluctuations of vorticity maximum value, but the vortex seems to reach to the ground surface.

Table 3 summarizes whether the vortex extended to the ground or not. The judgement for all dry experiments is performed based on the following criteria; (1) the maximum value of vorticity on z=750 m surface reaches $> 2 \times 10^{-4}$ s^{-1} (Table 1), (2) vorticity is at least two times the value of the rate of the deformation defined as follows

$$deformation = \sqrt{\left(\frac{\partial u}{\partial x} - \frac{\partial v}{\partial y}\right)^2 + \left(\frac{\partial u}{\partial y} + \frac{\partial v}{\partial x}\right)^2},$$

at the point of vorticity maximum (Figs. 14-18 and Table 2). The final judgement is obtained from the logical multiplication (AND operation) of above results.

Figures 14 and 15 show the vorticity and ratio of deformation rate to vorticity for experiments with no shear and 0 m shear at z=750 m. In all these experiments, the shape of vorticity is nearly circular and the deformation rate at the point of vorticity maximum is nearly zero. In cases of $U_{7.5} = 3$ m s^{-1} (Fig. 16), the vortex in experiments with smaller or weaker cooling (C5R50S3, C5R100S3 and C10R50S3) is distorted. In the cases of $U_{7.5} = 6$ m s^{-1} (Fig. 17), the vorticity in experiments with smaller or weaker cooling is elongated to down shear side. In particular, in the experiments C5R50S6 and C10R50S6, the deformation rate at the point of vorticity maximum exceeds our criterion value. In the cases of

$U_{7.5}$ = 9 m s^{-1} (Fig. 18), the vortex is elongated to down shear side in all experiments except for C20R200S9. In more than half experiments (C5R50S9, C5R100S9, C10R50S9, C10R100S9 and C20R50S9), the deformation rate at the point of vorticity maximum exceeds our criterion value.

The Table 3 illustrate a general tendency that vortex cannot reach the ground as vertical shear is larger. Comparing cases with the same wind shear, it is more difficult for the vortex to touch down to the ground surface when the cooling region is more localized and/or the cooling is less intense.

3.4.2 Condition of vortex touch down.

In this study, the vortex is generated by introducing a prescribed cylindrical region having constant cooling rate. In the cooling region, downward motion is driven and, consequently, vorticity and PV are produced by stretching of planetary vorticity. The PV is advected downshear side by the background zonal flow as it is advected downward by subsidence associated with the cooling. It is noted that PV of the air parcel with a parcel is conserved in the cooled region because, in this series of experiments, density weighted cooling rate is homogeneous (see Holton (2004); Eq. (4.36)). So we can predict whether the vortex can touch down to the ground or not by considering the trajectories of parcels which start from the top of the cooling.

For simplicity, it is assumed that the parcel moves in the x-z plane on the center of cooling region. The parcels which start at the top of the cooling are advected horizontally by the background flow. Here, we define downward and

horizontal displacement of a parcel which starts from the top of the cooling as $\Delta\chi$ and $\Delta\xi$, respectively (Fig. 19). The radius and the depth of the cooled region are L and D, respectively. Horizontal displacement $\Delta\chi$ at time t is written by

$$\begin{aligned}\Delta\chi &= \int_0^t u(z,t)dt = \int_0^t \frac{d\overline{u}}{dz}\Delta\xi dt = \int_0^t \frac{d\overline{u}}{dz} wtdt = \frac{1}{2}\frac{d\overline{u}}{dz}wt^2 = \frac{1}{2}\frac{d\overline{u}}{dz}w\frac{\Delta\xi^2}{w^2} \\ &= \frac{1}{2}\frac{d\overline{u}}{dz}\frac{\Delta\xi^2}{w} \quad (t = \Delta\xi/w), \end{aligned} \tag{49}$$

so that each parcel follows a parabolic path. Note that, for simplicity, it is assumed that constant subsidence w exist not only in the cooling but also outside of cooling; in reality, no subsidence exist outside of cooling.

When the parcel reaches to the ground, $\Delta\xi \to D$, so that

$$\Delta\chi = \frac{1}{2}\frac{d\overline{u}}{dz}\frac{D^2}{w}. \tag{50}$$

Recalling that downward flow w exists only inside of cooling. If $\Delta\chi \leq L$ at $t = D/w$, more than half of parcels which start from top of the cooling can reach to the ground. Conversely, if $\Delta\chi > L$ at $t = D/w$, more than half of parcels which start from the cooling is blown away from the cooling.

The assumption that downward velocity in the cooled region is constant is, of course, not perfectly valid. Fig. 7b illustrates , however, that amount of cooling resulting in the potential temperature decrease is much smaller than total amount of introduced cooling, so that the cooling term mostly balances the adiabat compression term in Eq. (6). Then, Eq. (6) can be approximated as

$$\frac{1}{w} = \frac{1}{C}\frac{d\overline{\theta}}{dz}. \tag{51}$$

By substituting Eq. (51) into Eq. (50) and dividing the result by L, a nondimensional number SI is obtained which is

$$SI \equiv \Delta\chi/L = \frac{1}{2}\frac{d\overline{u}}{dz}\frac{D^2}{CL}\frac{d\overline{\theta}}{dz}. \tag{52}$$

If $SI > 1$ more than half of the parcels start from the top of the cooling cannot reach to the ground because the parcels are advected in the region $w \approx 0$ (outside of cooling) on the way to the ground. If $SI > 2$ all of the parcels cannot reach to the ground.

The values of SI calculated for all the dry experiments with shear are presented in Table 4. Comparing this table with Table 3, it is clear that $SI \leq 3$ is the condition for vortex touch down. The value is larger than the value estimated from the parcel consideration. This inconsistency is resolved by considering the effect of tilting of background vertical wind shear as described below.

3.4.3 The effect of tilting induced vorticity

As shown in Fig. 6, a concentrated negative vorticity developed at the southern edge of the cooling region in cases with environmental wind shear. Therefore vertical wind shear near the cooling becomes weakened by the circulation around negative vorticity. Now, we assume that zonal flow is given as

$$u(z,t) = \overline{u}(z) + u_{vort}(z,t) + \tilde{u}(z,t), \tag{53}$$

where $\overline{u}(z)$ is initially prescribed zonal wind relative to translated velocity of cooling region, $u_{vort}(z,t)$ represents zonal flow induced by the axially symmetric component of vorticity and $\tilde{u}(z,t)$ denotes the zonal flow induced by the non-

symmetric component of vortex. Hereafter, we assume that only tilting of vertical wind shear (y-component of vorticity vector) contribute to $\tilde{u}(z,t)$.

In order to examine the magnitude of $\tilde{u}$ quantitatively, as illustrated in Fig. 20, we define a rectangular loop C1 and C2 which encircles the southern and northern edges of the cooling region, respectively. we also define loop C3 as southern semicircle of cooling and C4 as northern semicircle. Positive vorticity produced from the stretching is distributed mostly in the cooling. On the other hand, negative vorticity produced from the tilting of the environmental vertical shear is mainly distributed outside of cooling. Therefore the integral of vorticity within C1 minus the integral of vorticity within C3 approximately equal to the circulation induced by negative vorticity produced by tilting of vertical shear in C1. The circulation divided by the length of C1 is regarded as the averaged tangential velocity u_{C1} on C1 from the definition of circulation. Same as u_{C1}, we can calculate u_{C2} for C2. If both vorticity distributions inside and outside of the cooling region are axisymmetric, $u_{tilt} \equiv u_{C1} + u_{C2}$ should be exactly zero. As long as the vortex can reach to the ground, vorticity distribution in the cooling is nearly axisymmetric. Therefore u_{tilt} is mainly composed by asymmetric distribution of vorticity outside of cooling region.

Figure 21b shows evolution of vertical distribution of u_{tilt} for the experiment C10R100S6. Figure 21a shows zonal flow realized in the model for the same case averaged in the cooling region minus the prescribed initial vertical sheared flow $\overline{u}$. Comparison between Fig. 21a and Fig. 21b shows u_{tilt} roughly explains the magnitude and the nearly barotropic structure of u in the model. The Values of

u_{tilt} for all the dry experiments with shear are presented in Fig. 22. The figure suggests that u_{tilt} is roughly proportional to vertical wind shear and the constant of proportionality does not the radius and the strength of the cooling.

The proportional relationship can be interpreted as following. Assume that uniform negative vorticity of ζ_T is formed from the tilting of vertical shear is concentrated in area of $r\Delta\theta\Delta r$ located at the southern edge of the cooling region (Fig. 23). Circulation induced by the ζ_T is given by using cooling elapsed time Δt as

$$C = \zeta_T \times r\Delta\theta\Delta r = \frac{\partial w}{\partial y}\frac{\partial u}{\partial z}\Delta t \times r\Delta\theta\Delta r. \tag{54}$$

Appropriate length of Δt for each experiment can be scaled by the time required for a parcel to reach the ground, so that $\Delta t = D/w$, then

$$C = \frac{w}{\Delta r}\frac{d\overline{u}}{dz}\frac{D}{w}\Delta r \times r\Delta\theta = \frac{d\overline{u}}{dz}Dr\Delta\theta. \tag{55}$$

Divide Eq. (55) by length of closed loop C1 and C2 and one can calculate averaged tangential velocity u_{tilt} along the loop. Equation (55) shows that C (therefore also u_{tilt}) is proportional to vertical wind shear $\frac{d\overline{u}}{dz}$. Note that C and u_{tilt} are uniform on z and do not depend in the intensity or area of cooling region.

Now we examine how SI is modified by including u_{tilt} to initial vertical shear flow. The u_{tilt} can be written by using proportional coefficient $A \equiv Dr\Delta\theta/l_C$

$$u_{tilt} = \frac{C}{l_C} = A\frac{d\overline{u}}{dz}$$

Displacement of a parcel which starts at the top of the cooling region in horizontal direction is denoted $\Delta\chi$, in vertical direction is denoted $\Delta\xi$. Assuming constant

subsidence w exists everywhere, horizontal displacement $\Delta\chi$ at time T can be written

$$\begin{aligned}\Delta\chi &= \int_0^T u(z,t)dt = \int_0^T \left(\frac{d\overline{u}}{dz}\Delta\xi - A\frac{d\overline{u}}{dz}\right)dt = \int_0^T \frac{d\overline{u}}{dz}\left(wt - A\right)dt \\ &= \frac{1}{2}\frac{d\overline{u}}{dz}\left(wT - 2A\right)T. \end{aligned} \tag{56}$$

Recalling that $T = D/w$,

$$\Delta\chi = \frac{1}{2}\frac{d\overline{u}}{dz}\left(D - 2A\right)\frac{D}{w},$$

which we divide by L, and we obtain the

$$SI' \equiv \frac{1}{2}\frac{d\overline{u}}{dz}\left(1 - \frac{2A}{D}\right)\frac{D^2}{wL}, \tag{57}$$

or by using Eq. (51)

$$SI' \equiv \frac{1}{2}\frac{d\overline{u}}{dz}\left(1 - \frac{2A}{D}\right)\frac{D^2}{CL}\frac{d\overline{\theta}}{dz}. \tag{58}$$

Compare with Eq. (52), $SI' = \left(1 - \frac{2A}{D}\right)SI$. Remember $\frac{2A}{D} = \frac{2r\Delta\theta}{l_C}$ and l_C is several times of $2r\Delta\theta$, then SI' is about 50-80 % of SI value.

This fact suggests that vortex spin-up process by cooling in the vertically sheared environment has a mechanism to resist to destructive effect of shear. The value of SI' becomes, however, larger as the shear becomes larger. Therefore it is difficult for building up the vortex in very large vertical shear environment to touch down . Compare Table 3 with Table 4, criteria of SI' for vortex touchdown is $\leq 1.5 - 2$. Hence we may conclude that we can predict whether vortex can reach to the ground or not by referring the SI based on the parcel consideration accounting the effect of tilting of environmental vertical shear.

3.5 Discussion and conclusions

In this section, I have investigated the influence of vertical wind shear on the incipient vortex formation mechanism observed by BE, cyclonic mid-level vortex induced by evaporational cooling of stratiform precipitation extend to ground surface, by using three dimensional non-hydrostatic dry model. In no shear experiments, cyclonic vortex is formed at mid-level and anti-cyclonic vortex is formed at ground surface at first. As the time goes on, the anticyclonic vortex is weaken and the cyclonic vortex at mid-level extend into the ground as reported by BE. The time that elapses before the vortex touch down is inversely proportional to prescribed cooling rate. In cases with small shear, the vortex can extend to the ground with a bit tilt. In cases with large vertical shear, however, the vortex is blew off completely before it reaches the ground.

I have defined a non-dimensional number SI that represents the influence of vertical wind shear on vortex touch down referring to the cooling rate and radius of prescribed cooling by considering the parcel orbit in the cooling. The value of SI above which the vortex is blown off is 3. which is larger than the intuitive estimation ($\sim$1-2). I, therefore, have modified SI by investigating the results of numerical experiments which show zonal flow in the cooling is influenced by concentrated negative vorticity at the edge of the cooling which is generated by the tilting of environmental vertical wind shear. Calculated values for all numerical experiments show that the vortex is blown off before touchdown in cases with $SI' > 1.5 - 2$, which is within the range of the present parcel theory.

For the cases in the real atmosphere, we can suppose a stratiform precipitation region with radius of 100 km and cooling rate of 10K day^{-1} (reduced precipitation of 2 mm hour^{-1}; House 1989). If the precipitation occurs in the environment with vertical shear of 10 m s^{-1} between the ground and z=7.5 km , SI=5 with no consideration of influence of u_{tilt} or $SI' = 2.5$ with consideration of influence of u_{tilt} ($(1 - 2A/D) = 1/2$ is assumed.) is estimated. These results indicate that cooling induced incipient vortex formation does not occur with such large vertical shear. It has been conventionally believed that tropical cyclogenesis does not occur in the environment with large vertical shear because WISHE or CISK can not work even if incipient vortex exists. The result suggests, however, at least one route for incipient vortex formation is shut in such environment from the beginning.

Whether the results can be applied to incipient vortex formation directly is not clear due to the following reasons. First, I prescribed vertically uniform cooling rate in 5 km tall cylindrical region supposing evaporational cooling of stratiform precipitation. In reality, however, the cooling has considerable vertical structure as shown by Leary and Houze (1979) and Houze (1989). Second, it is likely that vertical structure of cooling may evolve in time. BE reported that cooling induced stratiform precipitation creates an incipient vortex of tropical cyclone and it is required that stratiform precipitation must last until sufficiently broad area is moisten at ground to form the incipient vortex. These results by BE suggest that vortex feeds back to cloud activity. Raymond and Jiang (1990) found that circulation formed by positive PV anomaly at lower level in MCS

and slope of isentropic surface induced by the PV anomaly can cause ascent in upshear side and make MCS long-lived. Frank and Ritchie (1999) pointed out secondary circulation is stronger in case the maximum vertical shear level exists in lower level. This implies that vertical profile of background flow can influence on the structure of vortex. Their moist calculation with vertical wind shear shows azimuth wavenumber 1 structure in convection activity. Calculation of Jones (2000b) with dry model shows static stability is reduced in vortex tilt side. She argued that it is likely convection activity is concentrate on vortex tilt side. In these studies, they introduce hurricane strength vortex into vertically sheared environment. On the other hand, I do not introduce such vortices but only cooling. In dry model, vortex is driven by cooling. In such situation, whether the anomaly of convective activity is formed or not is intriguing theme. To attack above problems, experiments by using three dimensional cloud resolving model is desired.

4 Moist experiments

4.1 Motivation for the moist experiments

In the dry experiments, neither the effect of "real" evaporation of raindrops nor the effect of the circulation which maintains the mesoscale convective systems (MCSs) are not considered. As is frequently noted in the literature regarding genesis and intensification of TCs (e.g.,Gray 1998), there are many wrong ways to the right answer. Thus, it is needed to evaluate the plausibility of the hypothesis demonstrated in the previous section that the possibility of touchdown of rain evaporation driven vortex can be evaluated by calculating SI, the shear index, in the real atmosphere. As the first step of the evaluation, additional experiments by using the model including the effect of evaporation of raindrops are performed. In these experiments, stratiform precipitation from "shower head" is imposed. The effect of the evaporation is caluculated explicitly in the model. Intensity of precipitation, radius of shower head, and magnitude of vertical wind shear are varied. It is worth noting that the cooling is not prescribed; temporal and spatial variations of cooling are permitted in the model since the effect of evaporation is calculated explicitly.

The outline of the moist experiments is as follows. The specifications of the experiments are described in subsection 4.2. The structure of the cooling induced by evaporation of raindrops and the structure of the vortex induced by the cooling for the experiments with no shear (with shear) are illustrated in subsection 4.3 (in subsection 4.4), respectively. The criterion of vortex touchdown and discussion

of applicability of SI appear in subsection 4.5.

4.2 Specification of moist experiments

The schematic view of the rain shower head and wind configuration is shown in Fig. 25. In this series of the experiments, the "shower head" which provides stratiform precipitation is introduced in the model following BE. Three kinds of the shower intensity, three kinds of radius of the shower and three kinds of magnitude of wind shear are employed. Total of 27 parameter experiments are performed in the series of the moist experiments.

4.2.1 Specification of "rain shower"

BE observed that incipient vortex of Hurricane Guillermo (1993) was formed as a by-product of stratiform precipitation with radius of $\sim$ 100 km. They employed radius of 116 km "shower head" for their axisymmetric numerical experiments. Following BE, the rainwater mixing ratio is set to 0.07125 g kg^{-1} (intensity halved hereafter HI), 0.1425 g kg^{-1} (control, hereafter CI) or 0.285 g kg^{-1} (intensity doubled, hereafter DI) at 4.75 km altitude during first 36 hours of the simulation. The radius of the rain shower R_{rain} set to be 58 km (radius halved, hereafter HR), 116 km (control, hereafter CR) or 232 km (radius doubled, hereafter DR), outside of which the imposed flux of rainwater decreases linearly to zero over a radial distance of 37.5 km.

4.2.2 Initial wind profiles

In this study, linearly sheared environmental westerly wind is introduced in the model. The initial wind profiles are

$$\overline{u} = \begin{cases} U_{shear}/H(z - 4.75 \text{ km}) & (z < H) \\ U_{shear}/H(H - 4.75 \text{ km}) & (z \geq H), \end{cases} \tag{59}$$

where U_{shear} is the magnitude of shear defined in the form

$$U_{shear} \equiv \overline{u}(z = 15\text{km}) - \overline{u}(z = 0\text{km}), \tag{60}$$

$H = 15$ km is the top level of the shear layer. U_{shear} of 0, 20 or 40 m s^{-1} is employed in the each experiment. Although Eq. (59) shows non-zero wind exists on the ground surface, from Eqs. (44), (45) and (46), no momentum, no moisture, and no sensitive heat flux by initial surface wind are permitted. This experimental design will yield the same results as obtained from the experiments employing the moving coordinate with the speed of cloud and no initial wind on the ground surface configuration.

4.2.3 Vertical profiles of temperature and moisture

Many of the earlier studies (i.e., Rottuno and Emanuel, 1987; Montgomery et al., 2006) which examine TCs by idealized simulation use the mean hurricane season sounding in the West Indies area observed by Jordan (1958). This profile is unstable to moist convection (Fig. 24; black lines). In moist experiments, downdraft is induced by evaporational cooling in the "shower" region. The cooled downdraft spread out from the shower region on the ground surface as gravity current. The gravity current will uplift high-θ_e air near the surface and will

trigger new deep convective clouds which will make the simulation results very complex. To avoid such situation, the Jordan's profile is stabilized by mixing the atmosphere artificially. The modified profile is created in a similar way of Rotunno and Emanuel (1987). A two dimensional version of the model with 1500 km horizontal domain size is prepared, setting $f = 0$. Then, a convective activity is forced at the center of the model by forcing a convergence zone. Convection is freely allowed, and the horizontal mean values of θ, π, q_v after 50 hours integration are taken as the modified Jordan's profile. The modified sounding is shown in Fig. 24 (red lines); the stabilization is manifested by drying and warming of the lower levels and moistening in middle and upper layers.

All experiments are named conventionally as 0mCICR, which means the experiment in which U_{shear} of 0 m s^{-1} (0m), the shower intensity of 0.1425 g kg^{-1} (CI), and the shower radius of 116 km (CR) are employed.

4.3 Experiments with no shear

4.3.1 Structure of cooling and vertical velocity

In contrast with the prescribed cooling used for the dry experiments, the intensity of the cooling is not homogeneous in horizontal and vertical directions.

Fig. 26 (Fig. 27) shows the time evolution of mixing ratio of rainwater and relative humidity (cooling rate) in experiment 0mCICR at $y = 750$ km. At 10 hours, few raindrops are observed below z=1500 m; most raindrops evaporate above z=1500 m, and the air above z=1500 m is moistened. The cooling is stronger at the higher level than the level near the surface. The vertical structure of the cooling results from inhomogeneity of raindrops mixing ratio; much of the raindrops evaporate at the higher level, so that few raindrops to evaporate exist at the level near the ground surface. In lower levels, the air at the center of the shower is more moistened than the air near the edge of the shower.

Corresponding to this moist structure, the raindrops near the center of the shower ($x = 750$ km $\pm$ 50 km) can reach lower levels than the raindrops at the edge of the shower. The cooling is stronger at the edge of the rain shower than at the center of the shower. The horizontal distribution of cooling results from inhomogeneity of moisture field; the relative humidity is higher at the center of the shower region where the evaporation of raindrops is suppressed.

The cooling intensity also varies with time. At 20 hours, the air at $x = 750$ km $\pm$ 30 km is mostly saturated above z= 1000 m, and the raindrops can reach to the ground surface. At the edge of the shower, however, only the air above z=4000 m are nearly saturated, and the raindrops can reach to only z=2000 m. Raindrops

can fall down to the surface and can evaporate in the levels near the surface as the air above becomes almost saturated. The cooling extends downward to the surface. On the other hand, the cooling in the layers above z= 3000 m is weakened since the air is moistened.

Corresponding to the structure of cooling, the vertical velocity also have spatial and temporal structure (Fig. 28). At 10 hours, stronger subsidence is observed at the edge of shower, where the cooling is stronger than the center of the shower. At 20 hours, as the air is moistened and the cooling is weakened, the subsidence is weakened. In particular, quite small subsidence is observed at the center of the shower.

The time evolution of potential temperature deviation is shown in Fig. 29. Although the huge amount of cooling is supplied by the rain evaporation, the potential temperature decrease of at most 2-3 K is observed. This is because the cooling induced by evaporation of rain drops is mostly balanced by adiabatic heating associated with the subsidence. This implies that the distribution of evaporational cooling determines the distribution of subsidence. Of course this balance is not perfect. For example, the temperature rising is observed in the lower levels near the surface.

The cooling structure depends on the radius of the rain shower (Fig. 30); the cooling extends small (large) area when the radius of the rain shower is small (large). Moreover the weak cooling area near the center of the shower is small (large) when the radius of the shower is small (large). The cooling structure also depends on the intensity of the rain shower (Fig. 31); the cooling is strong (weak)

when the intensity of the shower is doubled (halved). It should be noted that few raindrops can reach the ground and little cooling is observed on the ground surface until the rain shower stops (t= 36 hours).

Corresponding to the dependency of cooling structure on the radius and the intensity of the rain shower(Figs. 32 and 33), the vertical velocity also depends on the radius and the intensity of the shower; the subsidence extends small (large) region when the radius of shower is small (large) and the magnitude of subsidence is small (large) when the intensity of shower is small (large). It should be also noted that little subsidence is observed when the intensity of shower is halved.

Figure 34 shows the time evolution of vertical structure of horizontal mean of cooling in the shower region for all the no shear experiments. The cooling is weakened (enhanced) in upper (lower) levels with time. It should be noted again that, in half intensity shower cases, we can find little evaporational cooling in the layers near surface because almost rain drops evaporate on the way to the ground surface.

4.3.2 Structure of vortex driven by evaporational cooling

Figure 35 shows the time evolution of vorticity at y=750 km, at the center of the shower, for the experiment 0mCICR. As in the dry experiments, at first (t=4 hours), positive vorticity appears at about z=4000 m, and it extends downward. At t=12 hours, the vortex reach the ground surface. Similar to the dry experiments, the vorticity is produced in the layers z=2000-4000 m and advected downward (Fig. 36). In the shower region, subsidence of about 0.1 m s^{-1} is

observed. Therefore the vorticity produced at z= 4000m takes about 10 hours to travel to the ground surface. It is consistent with Fig. 35; the vorticity takes about 8 hours to reach the ground surface.

The vertical section of vorticity at t=12 hours for all the no shear experiments are shown in Fig. 37. At this time. the cyclonic vorticity have already reached the lowest level in the experiments with standard or doubled rain intensity. In the experiments with halved rain intensity, the vorticity does not reach the lowest model level until the end of integration, not only because the downward advection does not occur in the layers near the ground but also because the negative vorticity is produced by the shrink of vorticity below z=2000 m. In the experiments with doubled radius of shower, the vorticity is stronger at the edge of the shower region than the center. These results from the structure of the subsidence; the vorticity production by stretching and vertical advection occurs mainly at the edge of the cooling since the subsidence exists mainly at the edge of the cooling region (Fig. 32).

4.4 Experiments with shear

4.4.1 Structure of cooling and vertical velocity

Same as the no shear experiments, the cooling also has variations in space and time. General feature of the structure of the cooling is similar to those of no shear cases; the cooling is large (small) at the edge (center) of the shower. Figures 38 and 39 show the time evolution of rainwater mixing ratio and relative humidity at y=750 km in the experiments 20mCICR and 40mCICR, respectively. At 20 hours, the air is a bit more moistened in up-wind side, and the raindrops in the up-wind side can reach lower levels than down-wind side. At 40 hours, the air in the down-wind side is also moistened, however the raindrops in the up-wind side can reach lower levels than up-wind side.

The cooling is shown in Figs. 40 and 41 for the experiments 20mCICR and 40mCICR, respectively. Corresponding to the distribution of raindrops and moisture, the cooling is stronger in the up-wind side than in the down-wind side, and the cooling in the up-wind side is elongated to lower altitude downward than in the down-wind side. The vertical velocity (Figs. 42 and 43) and the potential temperature deviation (Figs. 44 and 45) are shown for 20mCICR and 40mCICR, respectively. Corresponding to the cooling structure, the subsidence in the up-wind side is elongated to the lower level than in the down-wind side, and the negative deviation of potential temperature is observed in the lower layers in the up-wind side. It is worth noting that the negative deviation of potential temperature at the mid-level (z=2000-3000 m) is larger in the up-wind side than that in the down-wind side. This feature is also observed in the dry experiments (Figs.

7 and 8).

The time evolution of vertical structure of horizontal mean of the cooling in the shower region has little dependency on the shear (Fig. 46); it depends mainly on the intensity and radius of the shower as seen in Fig. 34. In other words, the cooling has wavenumber 1 structure in the azimuth direction from the center of the shower, superposed the wavenumber 0 structure observed in the no shear experiments.

4.4.2 Structure of vortex driven by evaporational cooling

The time evolution of vorticity in the vertical section at y= 750 km is shown for the experiments 20mCICR (Fig. 47) and 40mCICR (Fig. 48). As in the dry experiments with shear, the vorticity extends downward with down shear tilt. At 12 hours, the trailing vorticity from the shower region is observed in the levels z= 2000-500 m in the experiment 40mCICR. This shows that the vertical sheared environmental wind has blown off the vortex tube out of the shower region in the lower levels.

Figure 49 shows the vorticity production by stretching for the experiments 20mCICR and 40mCICR. Same as the no shear experiments, the stretching occurs in thick layers (z=1000-5000 m). Moreover, the stretching is more intense at the up-wind side than at the down-wind side since the cooling (Figs. 40 and 41) and the subsidence (Figs. 42 and 43) in the up-wind side are stronger. Figure 50 shows the vorticity production by the vertical advection for the experiments 20mCICR and 40mCICR. Compared to the down wind side, larger amount of

vorticity convergence is observed; convergence extends to the ground since the subsidence is stronger and extends more downward.

Figure 51 shows the horizontal distribution of the vorticity at z=250 m and t=12 hours. A positive vorticity exists in the shower region. As in the dry experiments, a negative vorticity exists at the southern edge of the shower in the experiments with shear, which is produced by the tilting of the vertical sheared wind. No positive vorticity is observed at the northern edge since the vertical shear is weakened there (Fig. 52) as in the dry experiments with shear (Fig. 12). In the experiment 20mCICR, the shape of the closed contour denoting vorticity of 1.0×10^{-4} s^{-1} is nearly circular. However, in the experiment 40mCICR, the contour denoting vorticity of 1.0×10^{-4} s^{-1} is elongated westward by the vertically sheared environmental wind.

4.5 Judgement of vortex touchdown

4.5.1 Methodology

General characteristics of the vortex induced by the evaporational cooling in the moist experiments are common to the dry experiments; the vortex tends to be difficult to make touchdown when the radius or the intensity of cooling is small or the vertical shear is large. Therefore the SI defined for the dry experiments can likely be applied to the moist experiments. The judgement of vortex touchdown is performed based on following three criteria; (1) the maximum value of vorticity on $z = 250$ m surface at 36 hours $> 2 \times 10^{-4}$ s^{-1}, (2) the vorticity maxima are connected from the level of shower head to the lowest model level, (3) the vorticity on $z = 250$ m is at least two times larger than the value of rate of deformation at the point of vorticity maximum. This last criterion examines that the shape of vorticity is near circular or not; the vorticity associated with shear line should be rejected. The final judgement is obtained from the logical multiplication (AND operation) of three criteria.

4.5.2 Results

In Table 6, maximum value of vorticity on $z = 250$ m surface is examined. In almost all the experiments with intensity halved shower, the value of vorticity observed at $z = 250$ m is smaller than the threshold. This is not only because the bulk of raindrops evaporate on the way to the low levels therefore the vorticity produced in upper levels cannot advected to the ground surface but also because the negative vorticity is produced by vorticity shrinking in the layers near the

ground. In the experiments with shear and halved rain, the vortices are too weak except for the experiments with large shower.

Table 7 shows whether the vorticity tube is continuous or not. Upright vortices are observed in all the experiments with no shear. In cases with vertical shear, vortices in the experiments with smaller intensity of precipitation or with smaller radius of shower head are blown off near the ground surface.

Table 8 shows the results of judgement based on the ratio of the deformation rate to vorticity on the lowest model level surface at the vorticity maximum. In cases with no shear, the shape of vortex is nearly circular (Fig. 53) and the value of deformation rate is below our criterion. In cases with U_{shear} of 20 m s^{-1} (Fig. 54), the shape of the vortex in the experiments 20mHIHR, 20mHICR, 20mHIDR, and 20mCIHR is heavily distorted and the value of deformation rate is larger than our criterion. In cases with $U_{shear}$of 40 m s^{-1} (Fig. 55), the shape of the vortex in all the experiments is heavily distorted. In only two experiments (40mDICR and 40mDIDR), the value of deformation rate is below our criterion.

In cases with shear, the positive vorticity is significantly distorted in the experiments with smaller radius of shower head or smaller intensity of shower. This reflects that the vortex tubes are blown off in the low levels near the ground surface.

The final results of judgement of vortex touchdown are summarized by taking a AND operation of above three results (Table 9). It is more difficult to make touchdown for the vortex which is produced in experiments with smaller radius of shower, with smaller intensity of shower, or with larger vertical shear. This is

consistent with the results of dry experiments; it is difficult to make touchdown for the vortex in the experiments with smaller radius of cooling, with smaller intensity of cooling, or larger vertical shear. In cases with the halved intensity of rain, it is difficult to make touchdown for the vortex even if no shear exists.

4.5.3 Application of SI for the results of moist experiments

As mentioned above, the vorticity is mainly produced at z=2000-4000 m and then advected downward. To calculate SI, we must obtain cooling rate below the levels where the vorticity is produced.

Table 10 shows average cooling rates $\overline{C}$ for all the experiments calculated as follows,

$$\overline{C} \equiv \frac{1}{N} \sum_{r=0}^{R_{rain}} \sum_{z=0}^{3750 \text{ m}} \sum_{t=0}^{36 \text{ hours}} C(r, z, t),$$

where N is the total number of grid, C is the cooling rate, $r = \sqrt{(x - x_c) - (y - y_c)}$, $x_c = 750$ km and $y_c = 750$ km are the coordinates of shower center. The cooling rates depend heavily on the rain intensity and the radius of rain shower, although not depend on the magnitude of shear.

Now, we can calculate SI by using Table 10 and values of $D = 3750$ m and $\frac{d\overline{\theta}}{dz} = 3$ K km^{-1}. The values of SI for all experiments are summarized in Table 11. Comparing with Table 9, we can say that the vortices can make touchdown in the experiments $SI < 3$ except for 40mCICR and 40mCIDR. This result is in the fairly good agreement with the corresponding discussion of the dry experiments. In the experiments 40mCICR and 40mCIDR, the vortex cannot make touchdown in spite that SI < 3. This may result from inhomogeneous structure of cooling in

temporal and spatial direction. This problem remains for future works.

4.6 Summary and Conclusions

In this section, the influence of vertical wind shear on the incipient vortex formation mechanism observed by BE, cyclonic mid-level vortex induced by evaporational cooling of stratiform precipitation extend to the ground surface, has been investigated by using three dimensional non-hydrostatic moist model. Temporal and spatial variations of the cooling induced by the evaporation of stratiformed rain are observed. In the no shear experiments, the cooling is stronger at the edge of shower region than at the center. The strong cooling region descents with time as the air in the upper portion becomes nearly saturated. In the experiments with shear, the cooling at the up-wind side is stronger and elongated to the lower levels than down-wind side. In the experiments with weak rain intensity, the cooling does not reach to the levels near the ground surface. This behavior is directly reflected in the structure of subsidence.

The cyclonic vortex is formed by stretching mainly in the layer z = 2000-4000 m and advected downward. The vortex produced by stretching reaches the ground surface within about 10 hours in the no shear experiments except for the halved rain intensity cases. In the experiments with halved rain intensity, the vortex does not reach the ground because no cooling (therefore no downward advection) exists in the levels near the surface.

In the experiments with shear, the vortex extends with downshear tilt. In particular, in the experiments with strong shear, the trailing vorticity is observed to be advected out of the shower region. As in the no shear experiments, the

vortex does not reach the ground surface in the experiments with halved rain shower. Also as in the dry experiments, the negative vorticity is observed at the southern edge of shower and is wound onto the main positive vortex with time.

The judgements about touchdown of vortex for all the experiments are performed based on the value of vorticity maxima at the lowest level at the end time of shower, the ratio of deformation rate to the vorticity near vorticity maxima on the lowest level and the vertical continuity of vorticity maxima over all levels. The judgements show that the vortex does not reach the ground surface in the experiments with larger shear, weaker rain intensity and/or smaller radius of the shower.

The values of SI are calculated for all the experiments with shear by using temporally and spatially averaged cooling rate. Comparing the values of SI with the results of the experiments, we can conclude that vortex can reach the ground surface in $SI < 3$ cases. This result is in fairly good agreement with the corresponding discussion of the dry experiments by using parcel method in the previous section.

5 Concluding remarks

In this thesis, two series of systematic parameter experiments using a three dimensional non-hydrostatic model are performed to investigate the effect of environmental wind shear on the incipient vortex formation by the evaporation of rain observed and suggested by BE. One is a series of the dry experiments which examines the basic dynamics of vortex behavior created by the specified cooling and another is a series of the moist experiments which examines the vortex behavior in more realistic atmosphere.

General features of the time evolution of vortex in the dry experiments are qualitatively similar to each other. In the experiments with no shear, the cyclonic vorticity generated at the mid-troposphere by stretching and then the vorticity is advected downward by the subsidence associated with the cooling and reaches the ground surface. In the moist experiments with no shear, the vortex is produced by stretching in thicker layers than in the dry experiments. In the moist experiments with weak rain intensity, when the raindrops do not reach the lower levels, the vorticity cannot make a touchdown due to little vertical advection of vorticity near the ground. In the experiments with shear, the vortex develops to the ground with down shear tilt. In the experiments with stronger shear, the vortex extends downward with larger tilt and are blown off completely out of the cooling region in the experiments, especially, with smaller radius of cooling (shower) and/or smaller intensity of cooling (shower).

By considering trajectories of the parcels in the subsidence region, I intro-

duced a non-dimensional number SI that presents the influence of environmental vertical wind shear on the downward extension of the vortex referring to the cooling rate and the radius of prescribed cooling. In both the dry and moist experiments, the vortex is blown off when $SI > 3$. This value is larger than a naive estimation ($SI >$ 1-2) by parcel method. This difference is found to come from the effect of the circulation induced by the negative vorticity at the southern edge of the cooling (shower).

The present study establishes that SI can serve as a useful measure whether the vortex can reach to the ground or not. To apply SI for forecasting of vortex touchdown in MCSs, the cooling rate or the magnitude of subsidence must be estimated. Recent satellite sensors such as precipitation radar mounted on TRMM, have provided three-dimensional structure of MCSs. With those informations, it will be possible to estimate the cooling rate. Then it is now possible to evaluate the SI as a criterion of TC genesis.

In this study, only the touchdown of MCVs in the vertically sheared environment is considered. To understand the whole stages of TCs genesis in the top-down scenario, the intensification from the touchdown vortex to TC is left to be examined. In this stage, since cumulus convection may play crucial role, the cloud-resolving (grid spacing $<$ 2 km) calculation is required. The circulation which maintains the stratiform precipitation associated with MCSs is also outside of this study. Many studies (e.g., Raymond and Jiang 1990) showed the existence of vertical wind shear makes MCSs long lived. BE suggested that stratiform precipitation lasting enough to moisten the lower levels is necessary to

TC formation. To understand the whole stages of TCs genesis in the top-down scenario, numerical experiments which include all of effect mentioned above are required. This is a subject for future study.

Acknowledgments

I would like to express my deepest respect and most sincere gratitude to my supervisor, Dr Kensuke Nakajima at the Department of Earth and Planetary Sciences, for the patient guidance, encouragement and advice he has provided throughout the present study. I am thankful to Prof. Saburo Miyahara for his kind advice and continuous encouragement. Lots of discussion in lectures and seimners during my stay in this laboratory is very inspired me. I am also grateful to Profs. Hisanori Itoh, and Toshihiko Hirooka for their helpful comments. If I had not received the support from other members of the Geophysical Fluid Dynamics Laboratory, the Middle Atmosphere Sciences Laboratory and the Tropospheric Sciences Laboratory, I would not have finished this work. My friends in Department of Earth and Planetary Sciences, sometimes shared drinking party with me, also deserve many thanks. They have provided many ways to escape from my tough studies. I express my gratitude to my parents for their continued support and encouragement.

I am indebted to the Kyushu University Foundation, which provide an opportunity to attend the 26th Conference on Hurricanes and Tropical Meteorology at Miami, USA. I express my gratitude to Drs. Wataru Ohfuchi, Tetsuya Nakazawa, Kotaro Bessho, and Prof. Hiroshi Niino, who organized of the conferences held at Ohtsuchi in 2005 and 2006. The coversations with the researchers at the frontier of tropical cyclone studies in the conferences deeply inspired me.

This work was supported by a Grant-in-Aid on JSPS Research Fellowships for

Young Scientists. All of the moist experiments are performed on the VPP5000/64 at the Computing and Communications Center, Kyushu University. The campaigns named as “haru no muryou campaign” and “natu yasumi ni omoikkiri keisan shiyou campaign” in 2006 that provided opportunity for me to use supercomputers at the center freely are acknowledged. I am thankful to Associate Prof. Yoshitaka Watanabe, who take care of my use of the supercomputers at the Computing and Communications Center. I am also grateful to Yasuhiro Morikawa, the developer of gt4f90io library, for resolving the issues that I had on VPP5000 so quickly. GPhys, a nice library for handling gridded data developed by Dennou Ruby Project, is used for analyzing data. Other resources developped by GFD-Dennou Club are also used for drawing the figures. LAPACK is used to solve the pressure equation in the numerical model.

References

Bister, M., and K. Emanuel, 1997: The genesis of hurricane Guillermo: TEXMEX analyses and a modeling study, *Mon. Wea. Rev.*, **125**, 2662-2682

Beard, K. V., 1977: Terminal velocity and shape of cloud and precipitation drops aloft, *J, Atmos. Sci.*, **33**, 857-864

Bracken, W. E., and L. F. Bosart, 2000: The role of synoptic-scale flow during tripical cyclogenesis over the north Atlantic ocean, *Mon. Wea. Rev.*, **128**, 353-376

Camargo, S. J., K. A. Emanuel, and A. H. Sobel, 2006: ENSO and genesis potential index in reanalysis and AGCMs, 15C.2, 27th Conference on Hurricanes and Tropical Meteorology, *Amer. Meteor. Soc.*, Monterey, CA

Chang, C.-P., C.-H. Liu, and H.-C. Kuo, 2003: Typhoon, Vamei: An equatorial tropical cyclone formation, *Geophys. Res. Lett.*, **30**, 1150, doi:10.1029/2002GL016365

Charney, J., and A. Eliassen, 1964: On the growth of the hurricane depression., *J. Atmos. Sci.*, **21**, 68-75

Cotton, W. R., and R. A. Anthes, 1989: Storm and Cloud Dynamics, Academic Press, 883 pp.

Deardorff, J. W., 1972: Numerical investigation of neutral and unstable planetary boundary layers, *J. Atmos. Sci.*, **29**, 91-115

Deardorff, J. W., 1975: The development of boundary-layer turbulence models for use in studying the severe storm environment, *Proc. SESAME Meeting*, Boulder, NOAA-ERL, 251-264

Emanuel, K. A., 2003: Tropical cyclones, *Ann. Rev. Earth Planet. Sci.*, **31**, 75-104

Emanuel, K. A., and D. Nolan, 2004: Tropical cyclone activity and global climete, 10A.2, 26th Conference on Hurricanes and Tripical Meteorology, *Amer. Meteor. Soc.*,Miami, FL

Frank, W. M. and E. A. Ritchie, 1999: Effects of environmental flow upon tropical cyclone structure, *Mon. Wea. Rev.*, **127**, 2044-2061

Gray, W. M., 1968: Grobal view of the origin of tropical disturbances and storms, *Mon. Wea. Rev.*, **96**, 669-700

Gray, W. M., 1998: The formation of tropical cyclones, *Meteor. Atmos. Phys.*, **67**, 37-69

Hendricks, E. A., M. T. Montgomery, and C. A. Davis, 2004: The role of "vortical" hot towers in the formation of Tropical Cyclone Diana (1984), *J. Atmos. Sci.*, **61**, 1209-1232.

Holton, J. R.: 2004, *An tntroduction to dynamic meteorology*, Fourth Ed., Elsevier Academic Press, 535 pp.

Hoskins, B. J., M. E. McIntyre, and A. W. Robertson, 1985: On the use and

significance of isentropic potential vorticity maps, *Q. J. R. Meteor. Soc.*, **111**, 877-946

Houze, R. A. Jr., 1989: Observed structure of mesoscale convective systems and implications for large-scale heating, *Q. J. R. Metorol. Soc.*, **115**, 425-461

Johnson, D. E., W.-K. Tao, J. Simpson, and C.-H. Sui, 2002: A study of the response of deep tropical clouds to large-scale thermodynamic forcing. part I: modeling strategies and Simulations of TOGA COARE convective system, *J. Atmos. Sci.*, **59**, 3492-3518

Jones, S. C., 1995: The evolution of vortices in vertical shear. I: initially barotropic vortices, *Q. J. R. Metorol. Soc.*, **121**, 821-851

Jones, S. C., 2000a: The evolution of vortices in vertical shear. II: large-scale asymmetries, *Q. J. R. Metorol. Soc.*, **126**, 3137-3159

Jones, S. C., 2000b: The evolution of vortices in vertical shear. III: baroclinic vortices, *Q. J. R. Metorol. Soc.*, **126**, 3161-3185

Jordan, C. L.. 1958: Mean soundings for the West Indies area, *J. Meteor.*, **15**, 91-97

Kessler, E., 1969: On the Distribution and Continuity of water substance in atmospheric circulation, *Meteor Monogr.*, No. 32, Amer Meteor. Soc., 84 pp.

Klemp, J. B., and R. B. Wilhelmson, 1978: The simulation of three-dimensional convective storm dynamics, *J. Atmos. Sci*, **35**, 1070-1096

Lafore, J. P., J. Stein, N. Asencio, P. Bougeault, V. Ducrocq, J. Duron, C. Fischer, P. Héreil, P. Mascart, V. Masson, J. P. Pinty, J. L. Redelsperger, E. Richard, and J. Vilá-Guerau de Arellano, 1998: The meso-NH atmosperic simulation system. part I: adiabatic formulation and control simulations, *Ann. Geophysicae*, **16**, 90-109

Latif, M., N. Keenlyside, and J. Bader, 2007: Tropical sea surface temperature, vertical wind shear, and hurricane development, *Geophys. Res. Lett.*, **34**, L01710, doi:10.1029/2006GL027969

Leary, C. A., and R. A. Houze, Jr, 1979: Melting and evaporation of hydrometeors in precipitation from the anvil clouds of deep tropical convection, *J. Atmos. Sci.*, **36**, 669-679

McBride, J. k., and R. Zehr, 1981: Observational analysis of tropical cyclone formation. part II: comparison of Non-developing versus Developing systems, *J. Atmos. Sci.*, **38**, 1132-1151

Molinari, J., D. Vollaro, and K. L. Corbosiero, 2004: Tropical cyclone formation in a sheared environment: a case study, *J. Atmos. Sci.*, **61**, 2493-2509

Möller, J. D., and M. T. Montgomery, 2000: Tropical cyclone evolution via potential vorticity anomalies in a three-dimensional balanced model, *J. Atmos. Sci.*, **57**, 3366-3387

Montgomery, M. T., and B. F. Farrell, 1993: Tropical Cyclone formation, *J. Atmos. Sci.*, **50**, 285-310

Montgomery, M. T., and J. Enagonio, 1998: Tropical cyclogenesis via convectively fored vortex Rossby waves in a three-dimensional quasigeostrophic model, *J. Atmos. Sci.*, **55**, 3176-3207

Montgomery, M. T., M. E. Nicholis, T. A. Cram, and A. B. Saunders, 2006: A vortical hot tower route to tropical cyclogenesis, *J. Atmos. Sci.*, **63**, 355-386

Ogura, Y., T. Takahashi, 1971: Numerical simulation of the life cycle of a thunderstorm cell, *Mon. Wea. Rev.*, **99**, 895-911

Ooyama, K., 1964: A dynamical model for the study of tropical cyclone development., *Geofys. Int.*, **4**, 187-198

Ooyama, K., 1969: Numerical simulation of the life cycle of tropical cyclones, J. Atmos. Sci., **26**, 3-40

Raymond, D. J., and H. Jiang, 1990: A theory for long-lived mesoscale convective systems, *J. Atmos. Sci.*, **47**, 3067-3077

Raymond, D. J., C. López-arrillo, and L. L. Cavazos, 1998: Case studies of developing East Pacific easterly waves, *Quart. J. Roy. Meteor. Soc.*, **124**, 2005-2034

Reasor, P. D., M. T. Montgomery, and L. D. Grasso, 2004: A new look at the

problem of tropical cyclones in vertical shear flow: Vortex resiliency, *J. Atmos. Sci.*, **61**, 3-22

Riehl, H., 1954: *Tropical Meteorology*, McGraw-Hill, 392 pp.

Ritchie, E. A., and G. J. Holland, 1997: Scale interactions during the formation of Typhoon Irving, *Mon. Wea. Rev.*, **125**, 1377-1396

Rotunno, R., and K. Emanuel, 1987: An air-sea interaction theory for tropical cyclones. part II: evolutionary study using a nonhydrostatic axisymmetric numerical model, *J. Atmos. Sci.*, **44**, 542-561

Simpson, J., J. B. Halverson, B. S. Ferrier, W. A. Petersen, R. H. Simpson, R. Blakeslee, and S. L. Durden, 1998: On the role of "Hot Towers" in tropical cyclone formation, *Meteor. Atmos. Phys.*, **67**, 15-35

Skamarock, W. C., and J. B. Klemp, 1992: The stability of time-split numerical methods for the hydrostatic and the nonhydrostatic elastic equations, *Mon. Wea. Rev.*, **120**, 2109-2127

Smagorinsky, J., 1963: General circulation experiments with the primitive equations: 1. The basic experiment. *Mon. Wea. Rev.*, **91**, 99-164

Soong, S-T, and Y. Ogura, 1973: A comparison between axi-symmetric and slab-symmetric cumulus cloud models, *J. Atmos. Sci.*, **30**, 879-893

Webster, P. J., and R. Lukas, 1992: TOGA COARE: The Coupled Ocean-Atmosphere Response Experiment, *Bull. Amer Meteor. Soc.*, **73**, 1377-

1416

WMO, 2006: Workshop topic reports sixth WMO international workshop on tropical cyclones (IWTC-VI), World Meteorological Organization, WMO/TD, No. 1353. 596 pp.

Zehr, R., 1992: Tropical cyclogenesis in the western North Pacific, NOAA Tech. Rep. NESDIS 61, 181 pp.

Tables

$U_{7.5}$	C_0	50km	100km	200km
0 m s^{-1}	5 K day^{-1}	3.5	3.4	2.0
	10 K day^{-1}	7.9	9.8	8.8
	20 K day^{-1}	15.5	14.2	13.5
1 m s^{-1}	5 K day^{-1}	3.2	3.5	2.4
	10 K day^{-1}	6.6	9.7	8.2
	20 K day^{-1}	15.5	15.9	14.7
3 m s^{-1}	5 K day^{-1}	1.7	3.3	2.4
	10 K day^{-1}	6.3	7.1	8.8
	20 K day^{-1}	10.4	15.6	13.2
6 m s^{-1}	5 K day^{-1}	0.7	1.8	2.1
	10 K day^{-1}	3.1	6.1	12.3
	20 K day^{-1}	8.9	14.3	11.3
9 m s^{-1}	5 K day^{-1}	0.4	0.5	1.6
	10 K day^{-1}	1.3	4.3	6.2
	20 K day^{-1}	5.6	12.6	20.2

Table 1: Maximum values of vorticity at z=750 m ($\times 10^{-4}$ s^{-1}) for all the dry experiments.

$U_{7.5}$	C_0	50km	100km	200km
0 m s^{-1}	5 K day^{-1}	◯	◯	◯
	10 K day^{-1}	◯	◯	◯
	20 K day^{-1}	◯	◯	◯
1 m s^{-1}	5 K day^{-1}	◯	◯	◯
	10 K day^{-1}	◯	◯	◯
	20 K day^{-1}	◯	◯	◯
3 m s^{-1}	5 K day^{-1}	◯	◯	◯
	10 K day^{-1}	◯	◯	◯
	20 K day^{-1}	◯	◯	◯
6 m s^{-1}	5 K day^{-1}	×	◯	◯
	10 K day^{-1}	×	◯	◯
	20 K day^{-1}	◯	◯	◯
9 m s^{-1}	5 K day^{-1}	×	×	◯
	10 K day^{-1}	×	×	◯
	20 K day^{-1}	×	◯	◯

Table 2: The judgement for vortex touchdown based on the ratio of deformation to vorticity at z=750 m for the dry experiments.

$U_{7.5}$	C_0	50km	100km	200km
1 m s^{-1}	5 K day^{-1}	◯	◯	◯
	10 K day^{-1}	◯	◯	◯
	20 K day^{-1}	◯	◯	◯
3 m s^{-1}	5 K day^{-1}	×	◯	◯
	10 K day^{-1}	◯	◯	◯
	20 K day^{-1}	◯	◯	◯
6 m s^{-1}	5 K day^{-1}	×	×	◯
	10 K day^{-1}	×	◯	◯
	20 K day^{-1}	◯	◯	◯
9 m s^{-1}	5 K day^{-1}	×	×	×
	10 K day^{-1}	×	◯	◯
	20 K day^{-1}	×	×	◯

Table 3: The final judgement of vortex touch down for the dry experiments.

$U_{7.5}$	C_0	50km	100km	200km
1 m s^{-1}	5 K day^{-1}	2	1	0.5
	10 K day^{-1}	1	0.5	0.25
	20 K day^{-1}	0.5	0.25	0.125
3 m s^{-1}	5 K day^{-1}	6	3	1.5
	10 K day^{-1}	3	1.5	0.75
	20 K day^{-1}	1.5	0.75	0.375
6 m s^{-1}	5 K day^{-1}	12	6	3
	10 K day^{-1}	6	3	1.5
	20 K day^{-1}	3	1.5	0.75
9 m s^{-1}	5 K day^{-1}	18	9	4.5
	10 K day^{-1}	9	4.5	2.25
	20 K day^{-1}	4.5	2.25	1.125

Table 4: The values of SI for the dry experiments.

$U_{7.5}$	C_0	50km	100km	200km
1 m s^{-1}	5 K day^{-1}	0.8	0.7	0.35
	10 K day^{-1}	0.4	0.2-0.35	0.175
	20 K day^{-1}	0.2	0.1	0.05-0.0875
3 m s^{-1}	5 K day^{-1}	2.4-3.6	1.8	0.9-1.2
	10 K day^{-1}	1.8	0.6-0.9	0.3-0.6
	20 K day^{-1}	0.6	0.15-0.45	0.075-0.225
6 m s^{-1}	5 K day^{-1}	7.2	3.6-4.2	1.8-2.1
	10 K day^{-1}	3-3.6	1.5	0.75-0.9
	20 K day^{-1}	1.2-1.5	0.6-0.75	0.225-0.375
9 m s^{-1}	5 K day^{-1}	14.4	6-6.6	3-3.3
	10 K day^{-1}	4.2-6	2.4-3	1.05-1.25
	20 K day^{-1}	1.5-2.1	0.75-1.05	0.375-0.525

Table 5: The values of SI' for the dry experiments.

shear	shower intensity	HR	CR	DR
0 m s^{-1}	HI	1.2	0.9	1.1
	CI	2.3	24.0	24.5
	DI	7.6	4.2	54.1
20 m s^{-1}	HI	0.2	1.1	5.1
	CI	1.8	3.4	2.2
	DI	4.4	38.8	38.2
40 m s^{-1}	HI	0.1	0.9	5.3
	CI	3.0	4.6	9.3
	DI	3.6	10.6	28.5

Table 6: The values of maximum vorticity ($\times 10^{-4}$ s^{-1}) on $z = 250$ m surface at $t = 36$ hours for the moist experiments. The values $< 2.0 \times 10^{-4}$ s^{-1} are shaded.

shear	shower intensity	HR	CR	DR
0 m s^{-1}	HI	◯	◯	◯
	CI	◯	◯	◯
	DI	◯	◯	◯
20 m s^{-1}	HI	×	×	×
	CI	×	◯	◯
	DI	◯	◯	◯
40 m s^{-1}	HI	×	×	×
	CI	×	×	×
	DI	×	◯	◯

Table 7: The judgement of vortex touchdown based on the connection of vorticity maxima for the moist experiments.

shear	shower intensity	HR	CR	DR
0 m s^{-1}	HI	◯	◯	◯
	CI	◯	◯	◯
	DI	◯	◯	◯
20 m s^{-1}	HI	×	×	×
	CI	×	◯	◯
	DI	◯	◯	◯
40 m s^{-1}	HI	×	◯	×
	CI	×	×	×
	DI	◯	◯	◯

Table 8: The judgement of vortex touchdown based on the ratio of deformation to vorticity at $z = 250$ m for the moist experiments.

shear	shower intensity	HR	CR	DR
0 m s^{-1}	HI	×	×	×
	CI	◯	◯	◯
	DI	◯	◯	◯
20 m s^{-1}	HI	×	×	×
	CI	×	◯	◯
	DI	◯	◯	◯
40 m s^{-1}	HI	×	×	×
	CI	×	×	×
	DI	×	◯	◯

Table 9: The final judgement of vortex touchdown based on logical multiplication of above three results for the moist experiments.

shear	shower intensity	HR	CR	DR
0 m s^{-1}	HI	3.4	11.3	14.9
	CI	8.3	24.0	27.4
	DI	17.0	50.1	33.3
20 m s^{-1}	HI	3.3	11.0	15.0
	CI	8.2	24.6	27.6
	DI	17.4	50.1	32.8
40 m s^{-1}	HI	3.3	11.0	15.1
	CI	8.0	25.0	27.8
	DI	17.5	50.2	35.4

Table 10: The values of cooling rate (K day^{-1}) averaged spatially (z = 250-3750 m below the rain shower) and temporally (0-36 hours) in the moist experiments.

shear	shower intensity	HR	CR	DR
20 m s^{-1}	HI	14.7	2.2	0.8
	CI	5.9	1.0	0.4
	DI	2.8	0.5	0.4
40 m s^{-1}	HI	29.5	4.4	1.6
	CI	12.2	1.9	0.9
	DI	5.6	1.0	0.7

Table 11: The values of SI for all the moist experiments with shear.

Figures

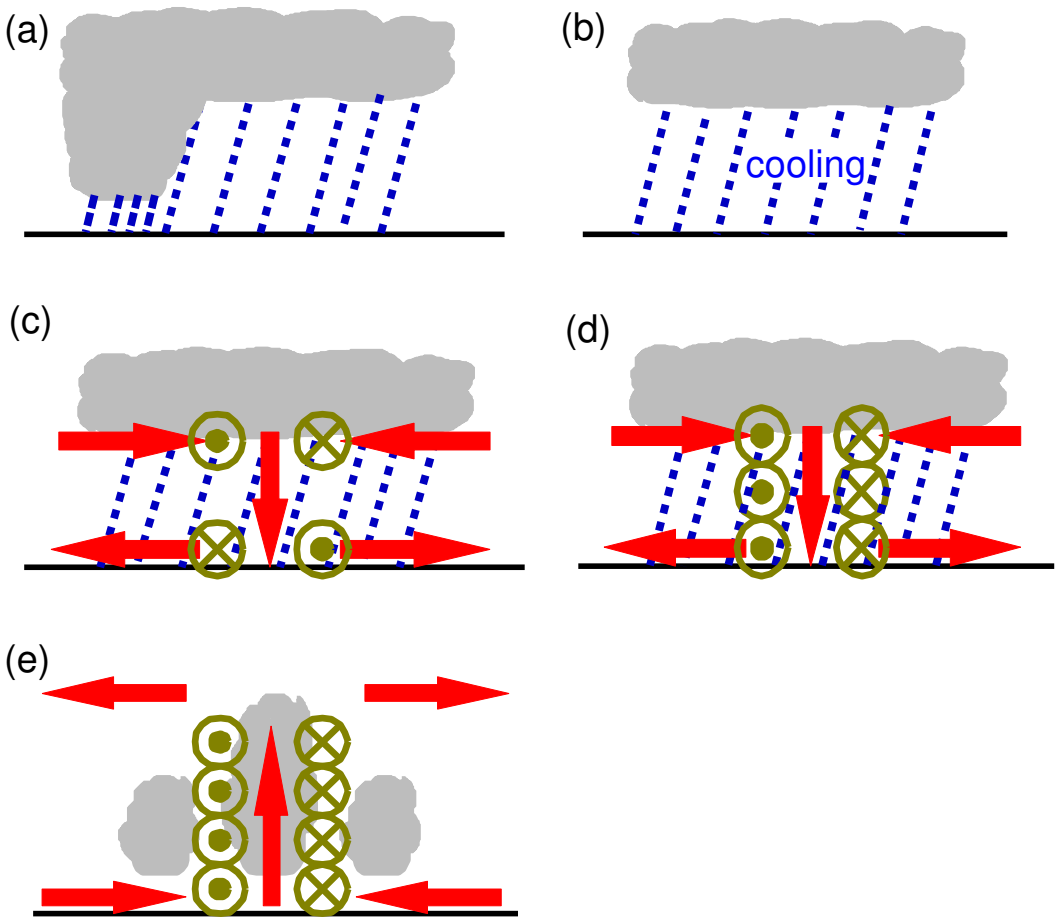

Figure 1: Schematic view of TC genesis reported by BE. (a) Stratiform region develops in later stage of life cycle of tropical cloud cluster. (b) Cooling driven by evaporation of raindrops occurs below stratiform cloud. (c) The cooling drives in-down-out circulation. The convergence (divergence) of planetary vorticity makes cyclonic (anticyclonic) vortex just beneath the cloud (on the ground surface). (d) The anticyclonic vortex on the ground is dissipated and the cyclonic vortex is extended to the ground surface by downward advection. (d) After death of stratiform precipitation, vortex can intensify to TC.

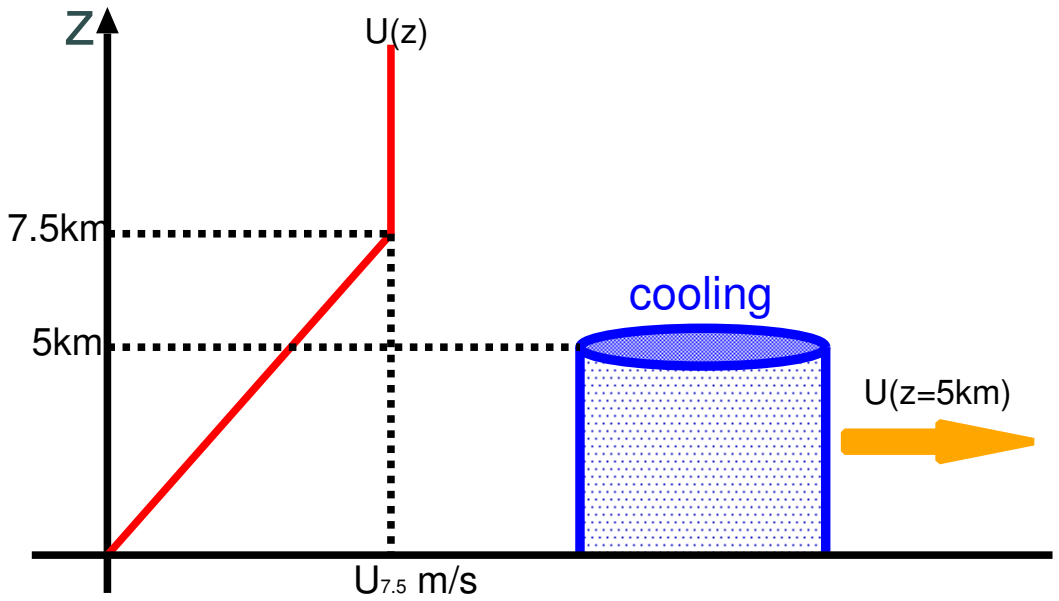

Figure 2: Schematic view of the configuration of the cooling and the initial wind in the dry experiments

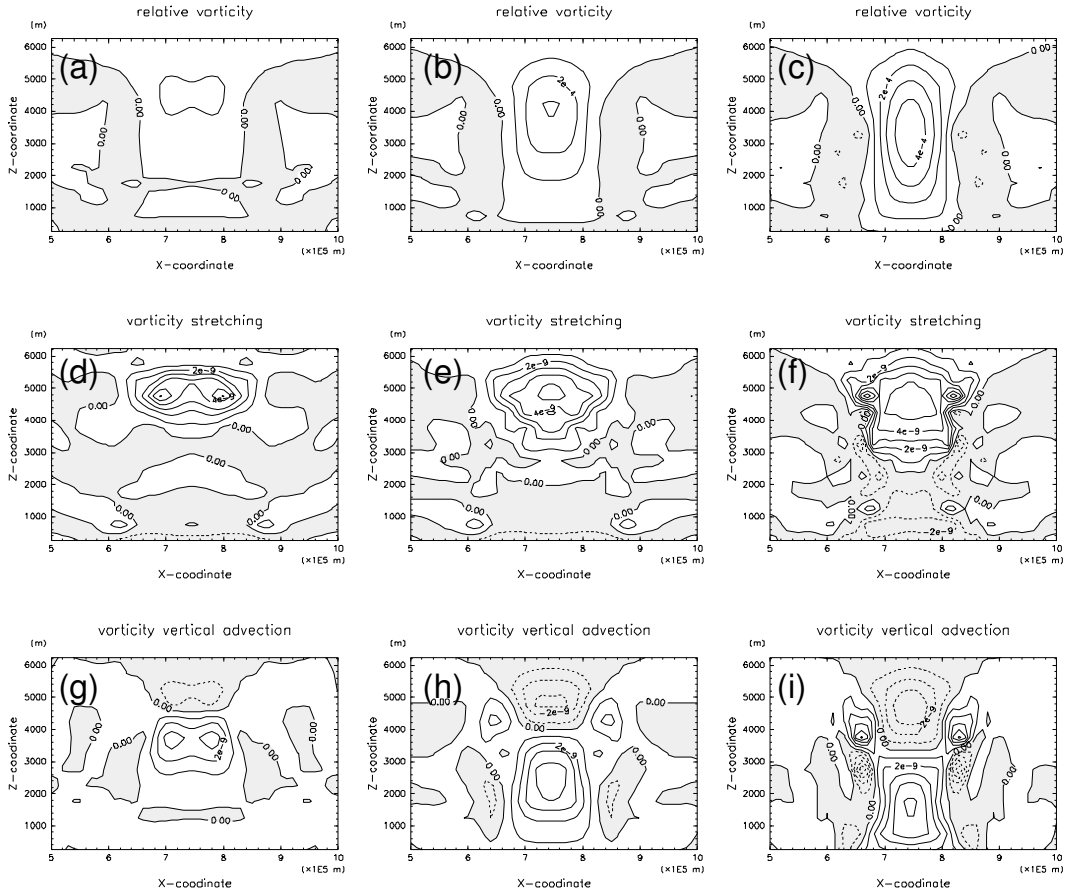

Figure 3: (Upper panels) The vorticity at $y = 750$ km for the experiment C10R100S0 at (a) 15 h, (b) 30 h, and (c) 45 h. The contour interval is 1×10^{-4} s^{-1}. (Mid-panels) The vorticity production by stretching at (d) 15 h, (e) 30 h, and (f) 45 h. The contour interval is 1×10^{-9} s^{-2}. (bottom-panels) The vertical advection at (g) 15 h, (h) 30 h, and (i) 45 h. The contour interval is 1×10^{-9} s^{-2}.

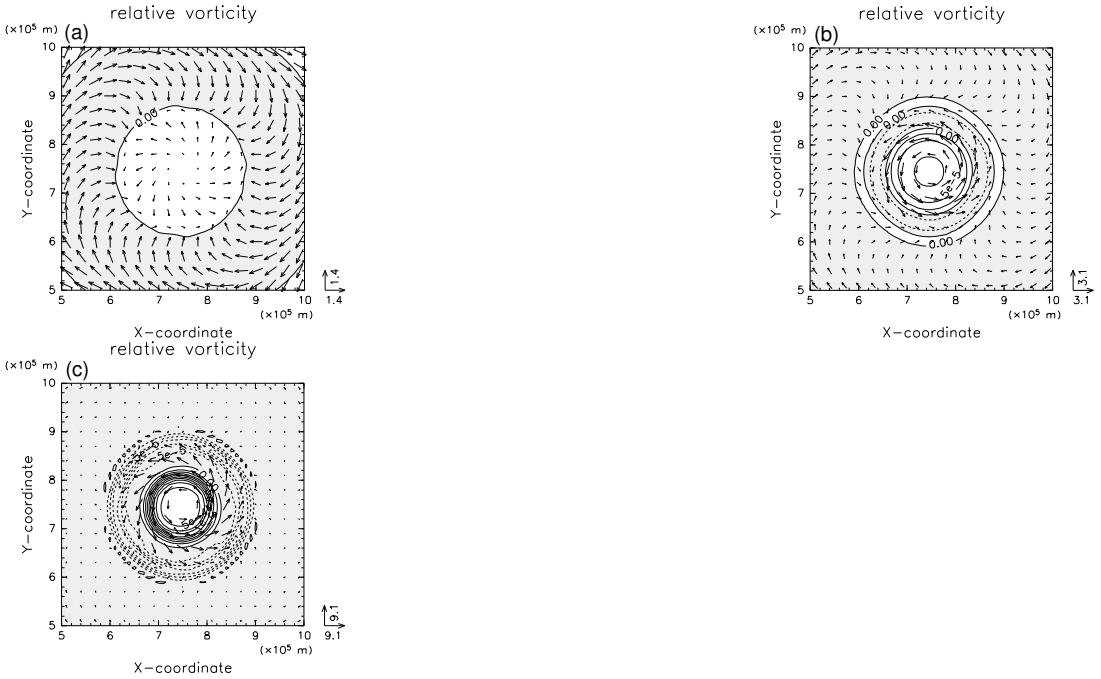

Figure 4: The vorticity and wind vector relative to translate velocity of cooling on $z = 750$m surface. (a) 20h, (b) 40h and (c) 60h. Contour interval is 2.5×10^{-5} s^{-1}.

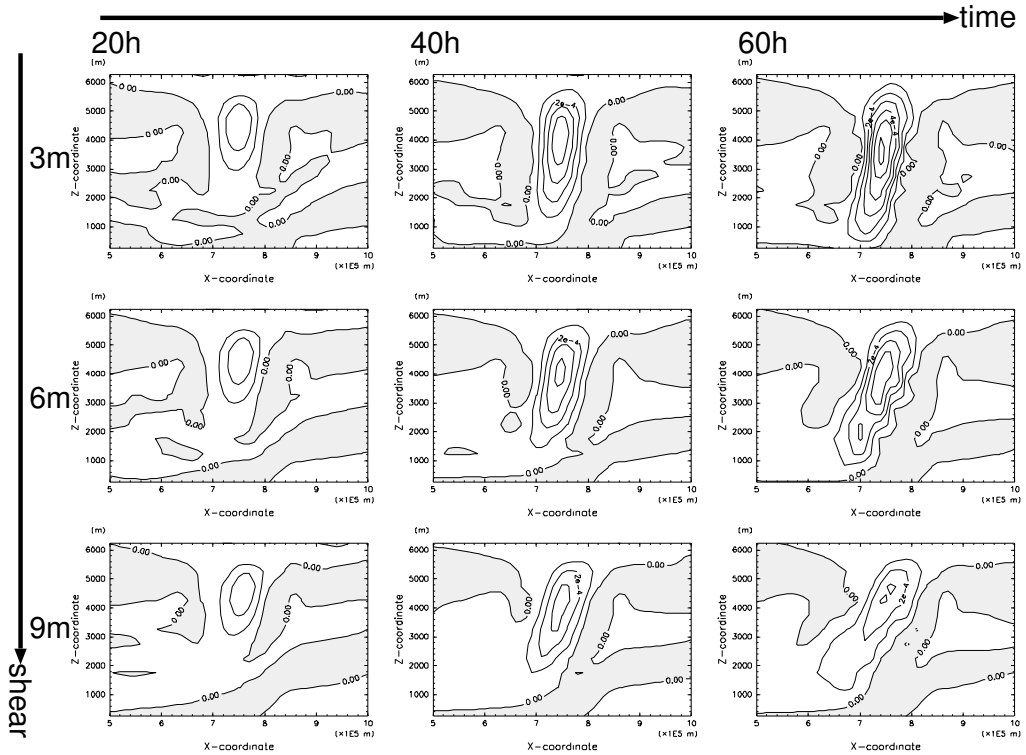

Figure 5: Time series of the vorticity at $y = 750$ km for the experiments C10R100S3, C10R100S6 and C10R100S9.

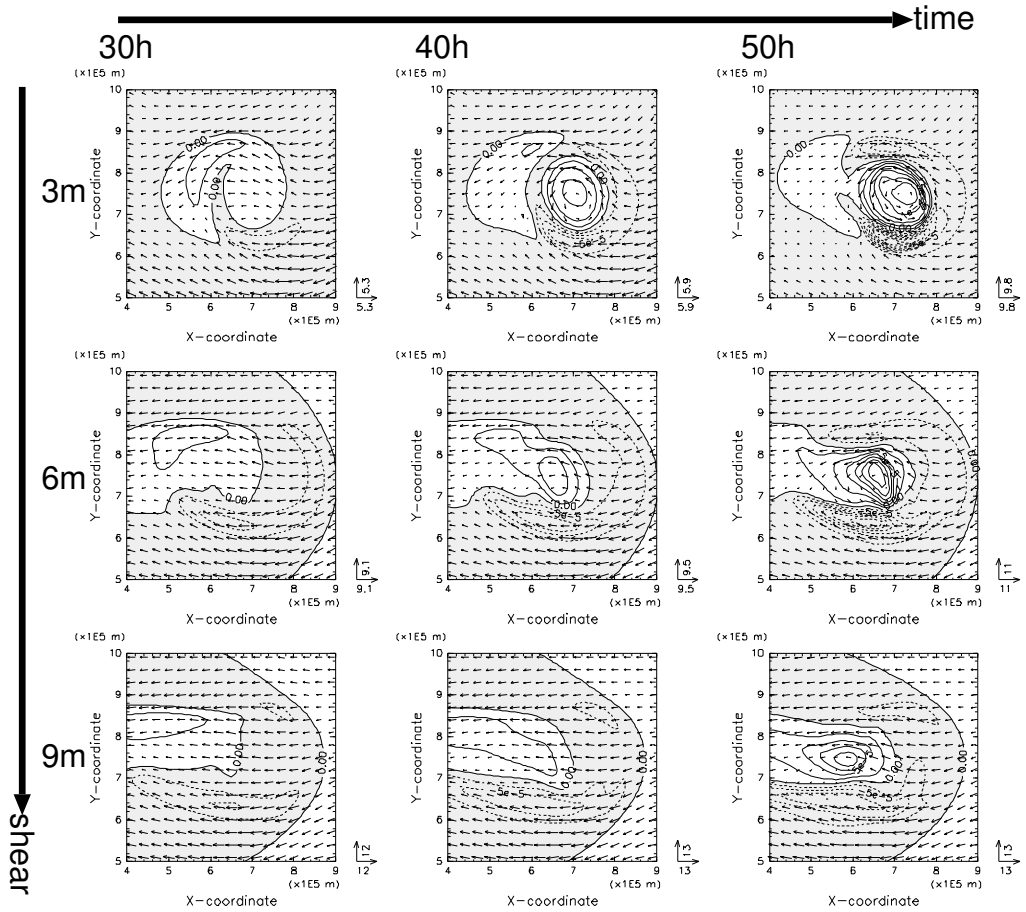

Figure 6: Time series of the vorticity and wind vector relative to the translation velocity of cooling on $z = 750$ m surface for the experiments C10R100S3, C10R100S6 and C10R100S9. Contour interval is 2.5×10^{-5} s^{-1}.

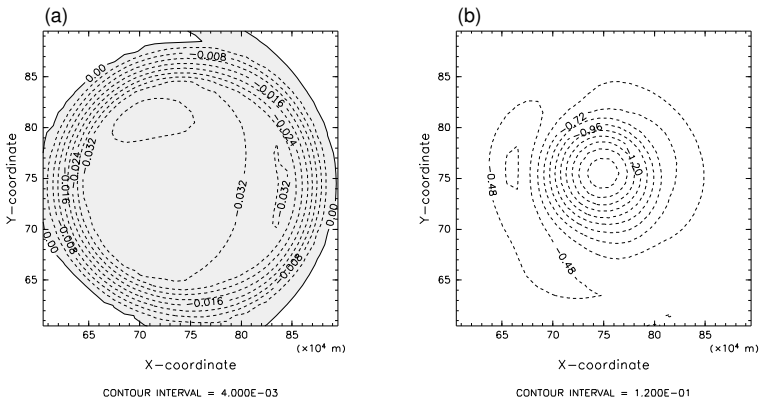

Figure 7: (a) time mean (0-40 hours) vertical velocity, (b) potential temperature anomaly at $t = 40$ hours on $z = 2250$ m surface for the experiment C10R100S3.

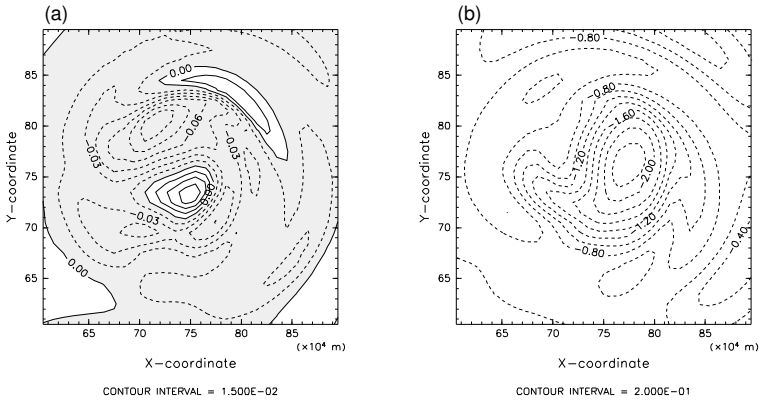

Figure 8: (a) vertical velocity and (b) potential temperature on $z = 2250$ m surface at 60 hours for the experiment C10R100S3.

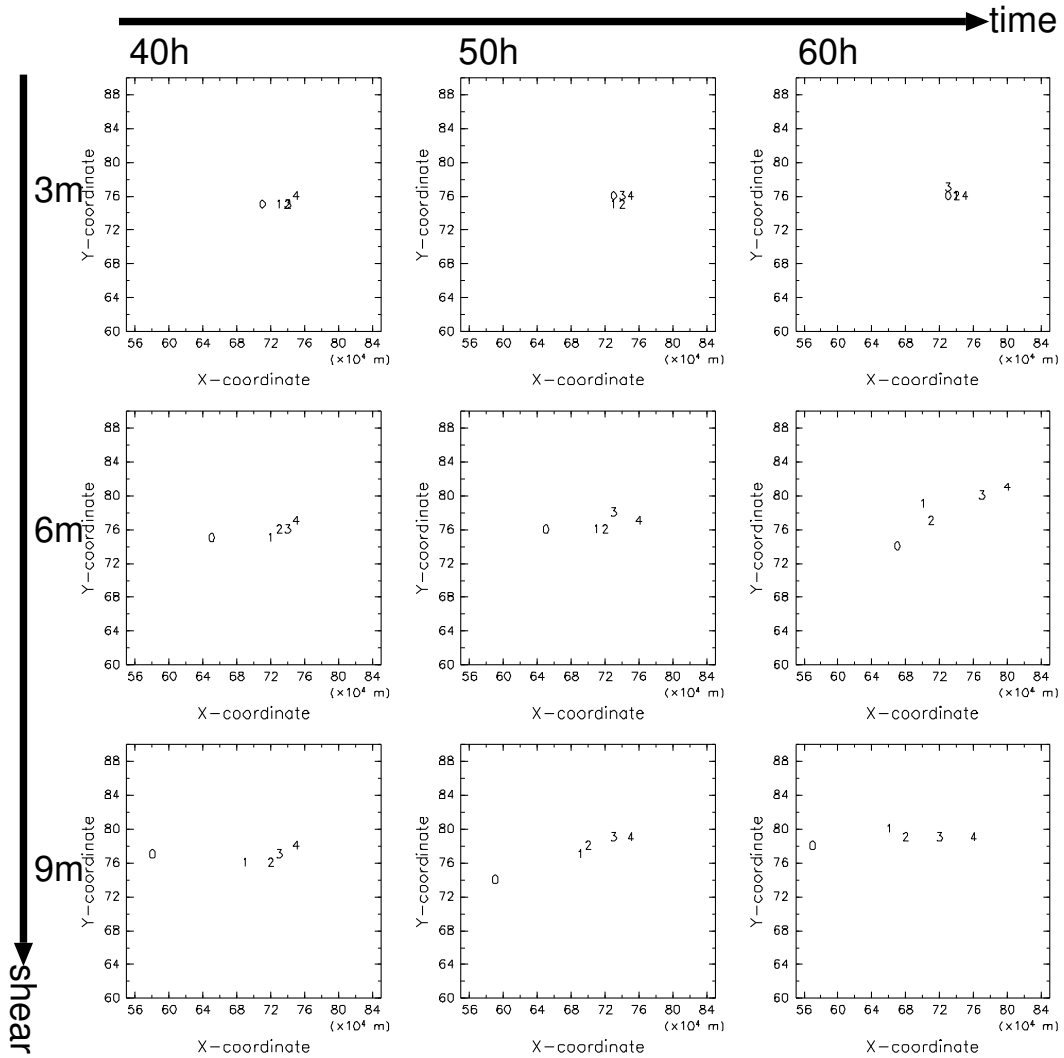

Figure 9: Time series of the positions of vorticity maxima for the experiments C10R100S3, C10R100S6 and C10R100S9. Each symbol 0: z =750 m, 1: z =1750 m, 2: z =2750 m, 3: z =3750 m, 4: z =4750 m represents vorticity maximum on each level respectively.

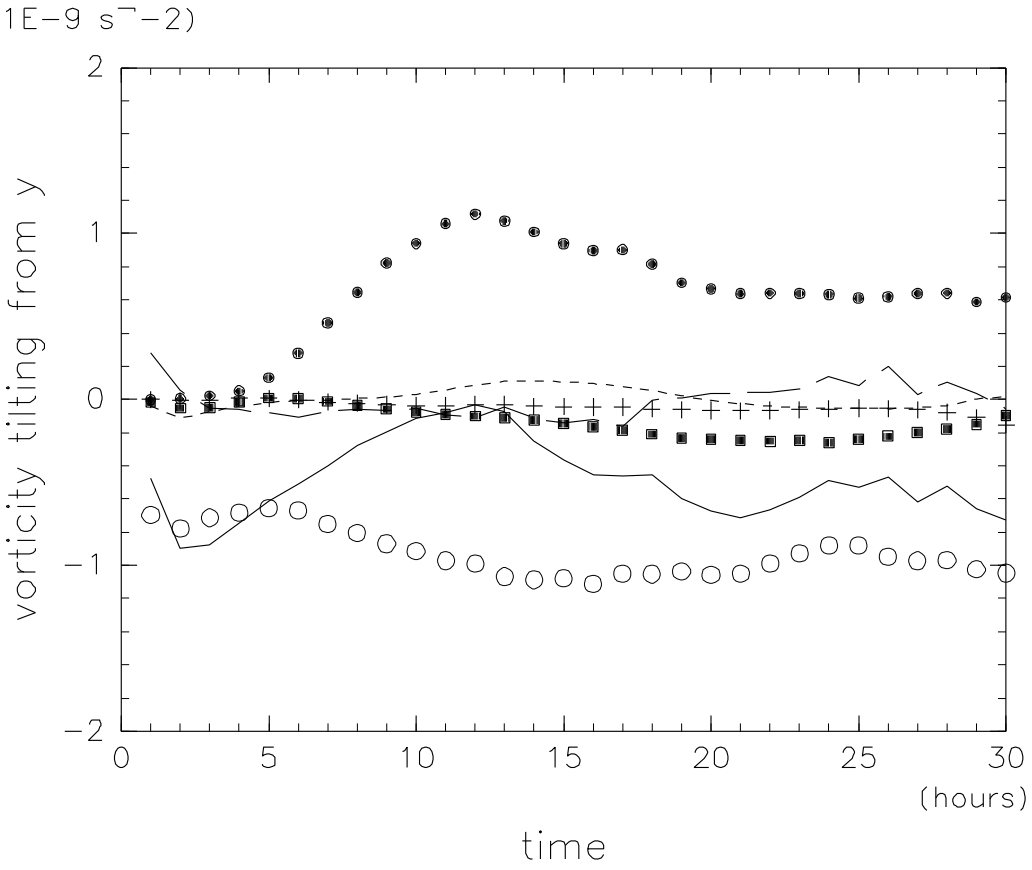

Figure 10: Time evolution of all terms of vorticity equation for the experiment C10R100S3 on $z = 1250$ m at the southern edge of the cooling ($y = 620$ km) 0-30 hours. solid line: total tendency, ○: tilting of y-component of vorticity, ■: tiltitng of x-component of vorticity, ●: horizontal advection, +: vertical advection, dotted line: stretching and broken line: residual.

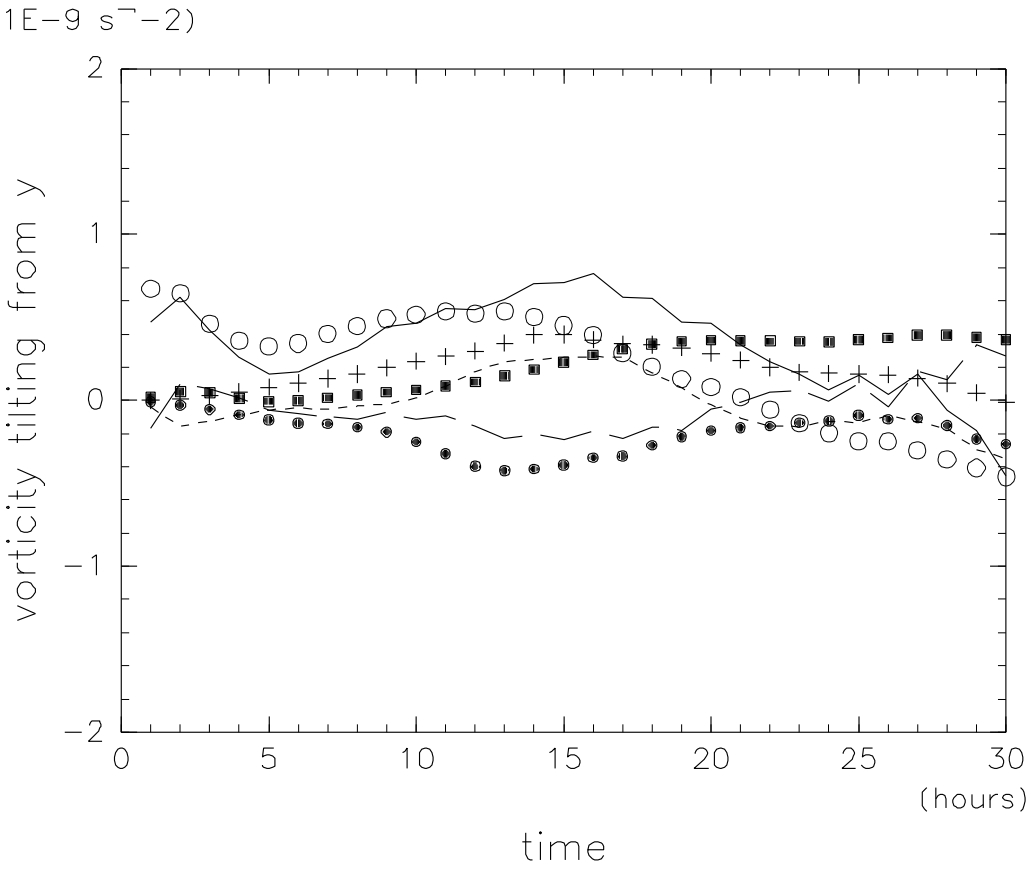

Figure 11: Same as Fig. 10. But at the northern edge of the cooling ($y = 870$ km).

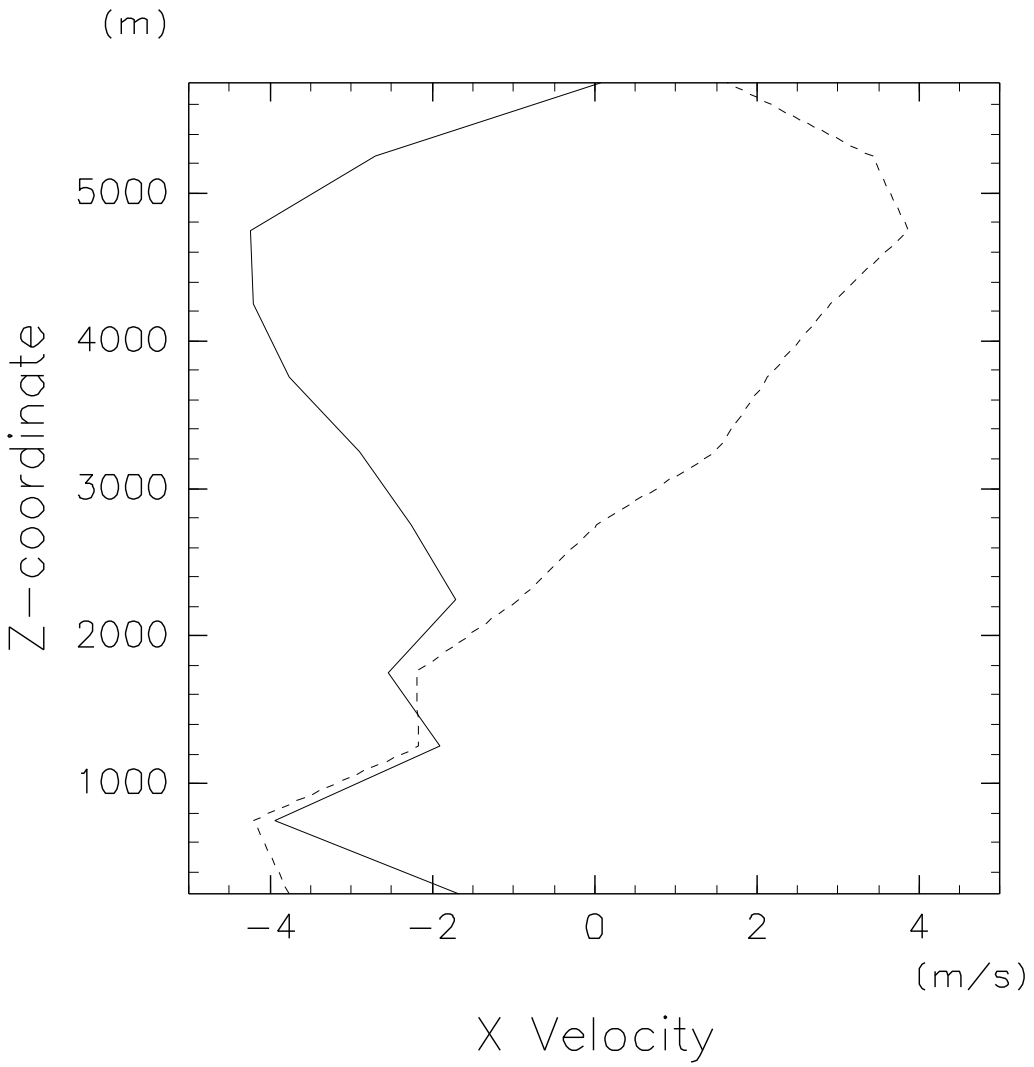

Figure 12: Vertical profile of the westerly wind for experiment C10R100S6 at the northern edge (solid line; $y = 850$ km) and southern edge (broken line; $y = 650$ km) of the cooling at $t = 20$ hours.

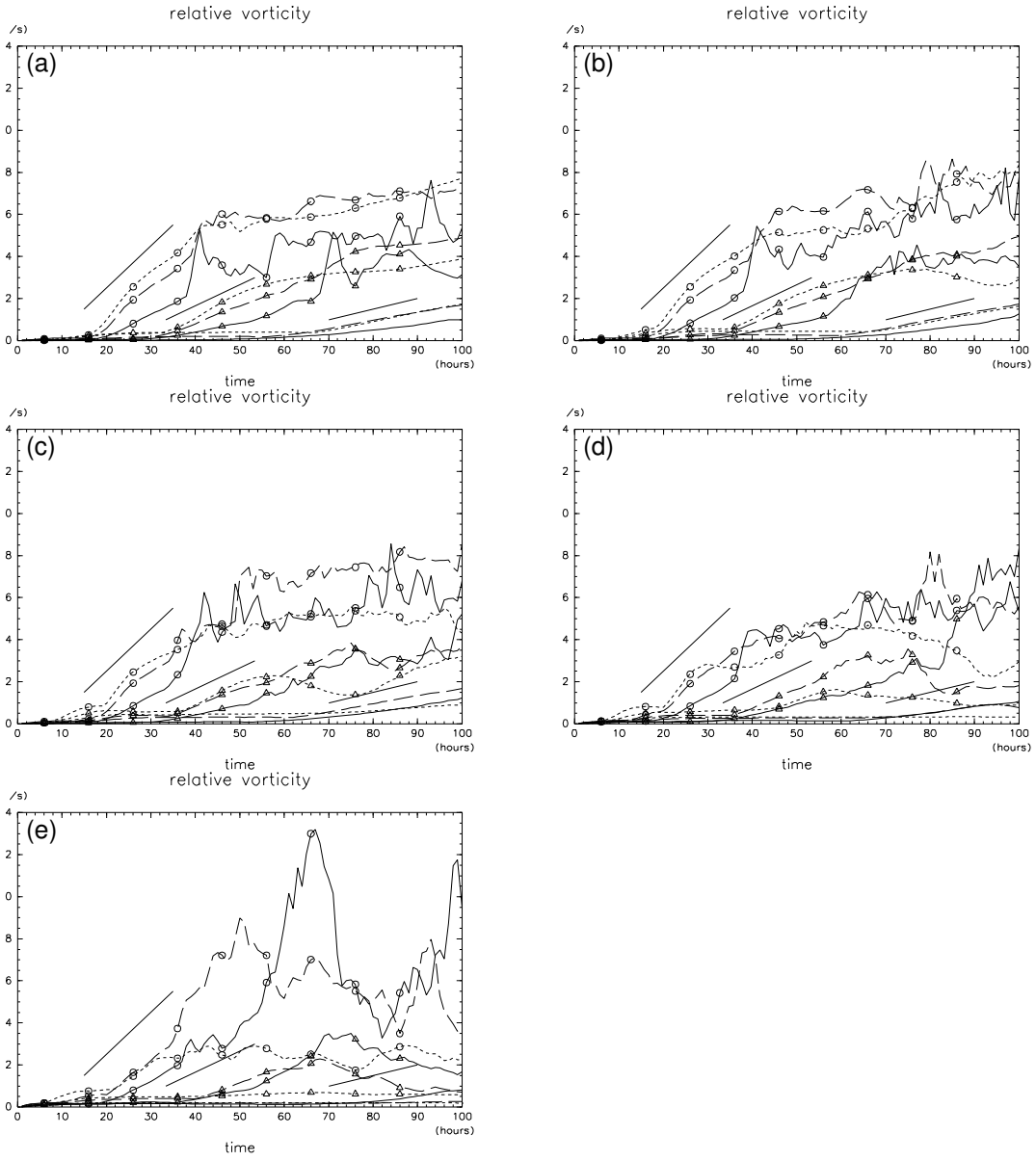

Figure 13: Time evolution of maximum value of vorticity (s^{-1}) at z =750 m for (a) $U_{7.5}$=0 m s^{-1}, (b) $U_{7.5}$=1 m s^{-1}, (c) $U_{7.5}$=3 m s^{-1}, (d) $U_{7.5}$=6 m s^{-1} and (e)$U_{7.5}$=9 m s^{-1}. Symbols denote magnitude of C_0; ○: 20 K day^{-1}, △: 10 K day^{-1}, none: 5 K day^{-1}. Line types denote radius of cooling; solid: 200 km, broken: 100 km, dotted: 50 km. Three solid line segments in each panel denote slope of 4×10^{-4}, 2×10^{-4} and 1×10^{-4} (/72000 s^{-2}), respectively for reference.

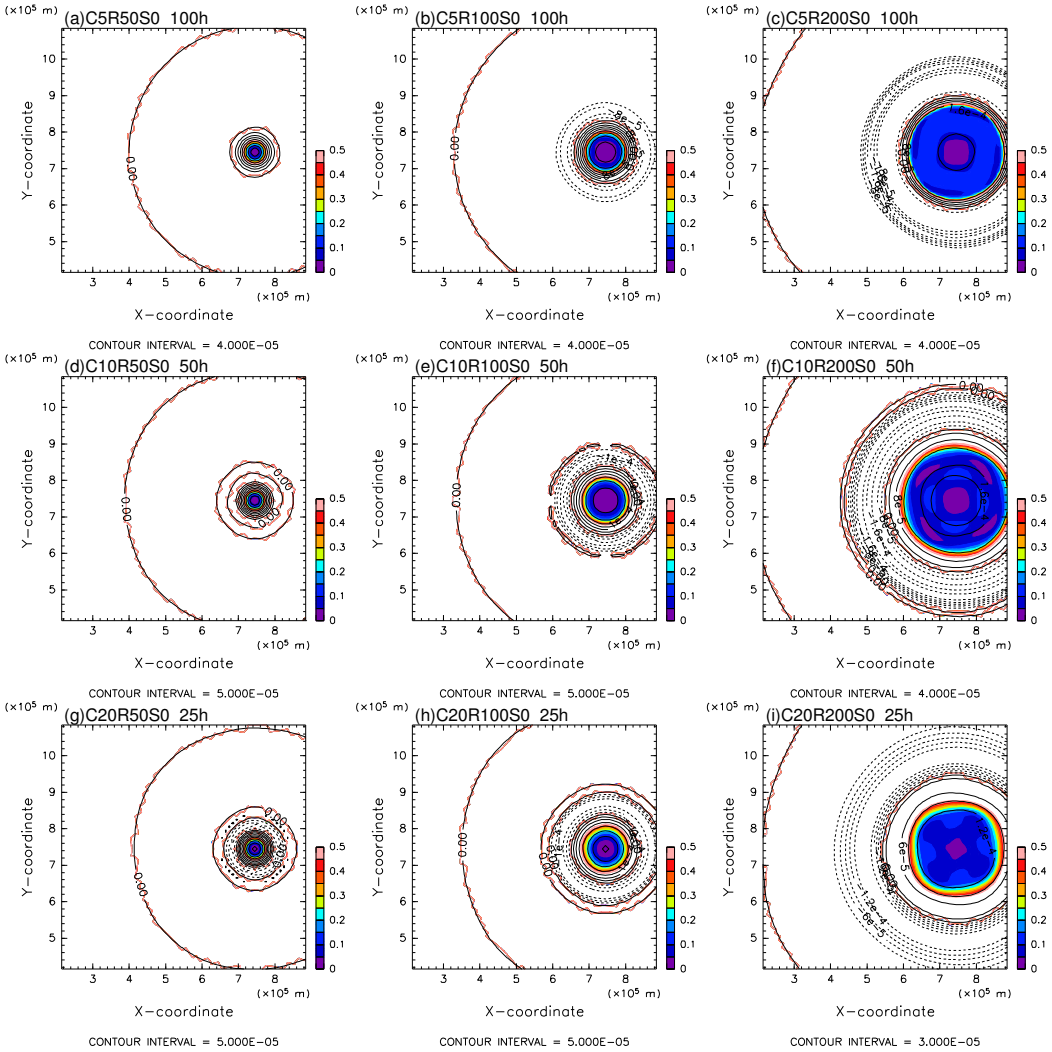

Figure 14: The vorticity (contour, s^{-1}) and ratio of deformation to the vorticity (colored < 0.5) for the dry experiments with $U_{7.5}$ of 0 m s^{-1}.

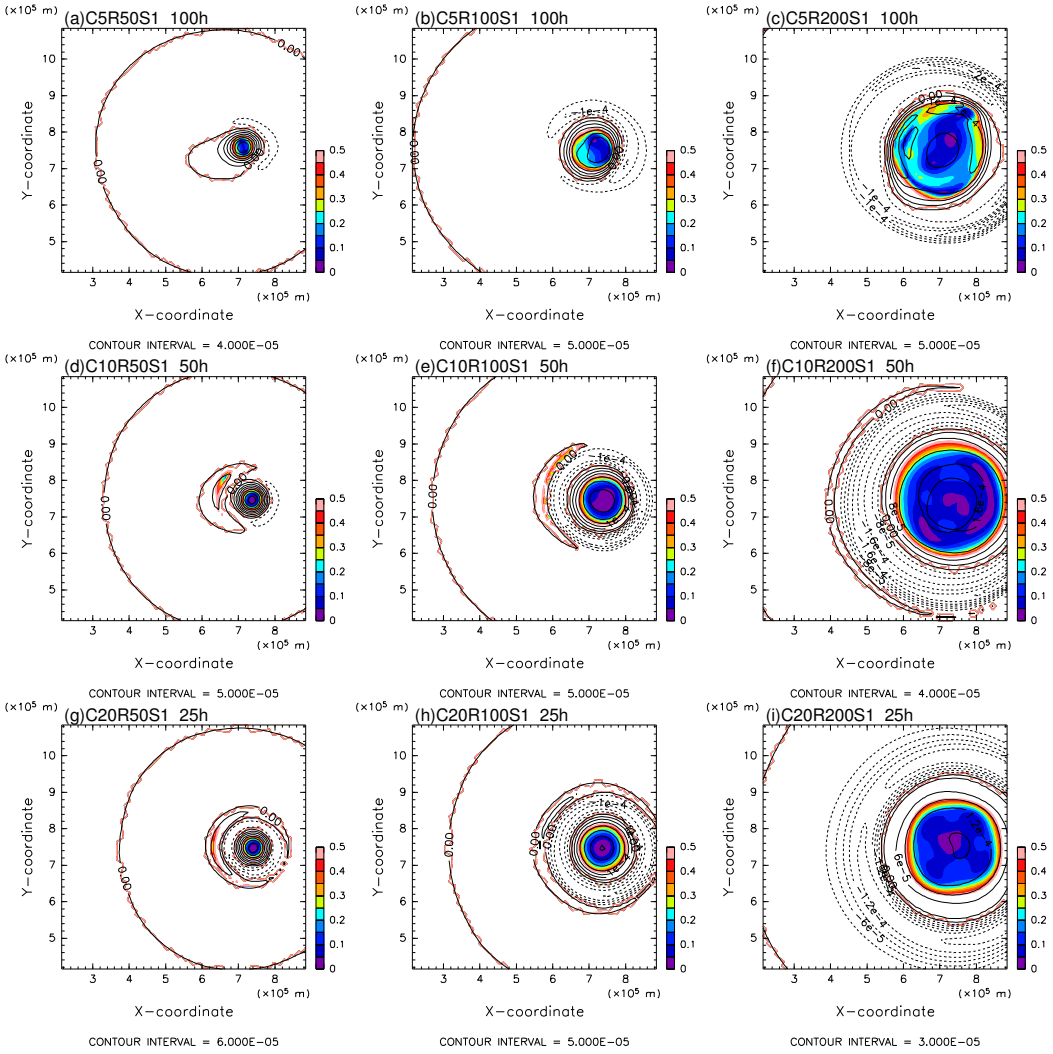

Figure 15: The vorticity (contour, s^{-1}) and ratio of deformation to the vorticity (colored < 0.5) for the dry experiments with $U_{7.5}$ of 1 m s^{-1}.

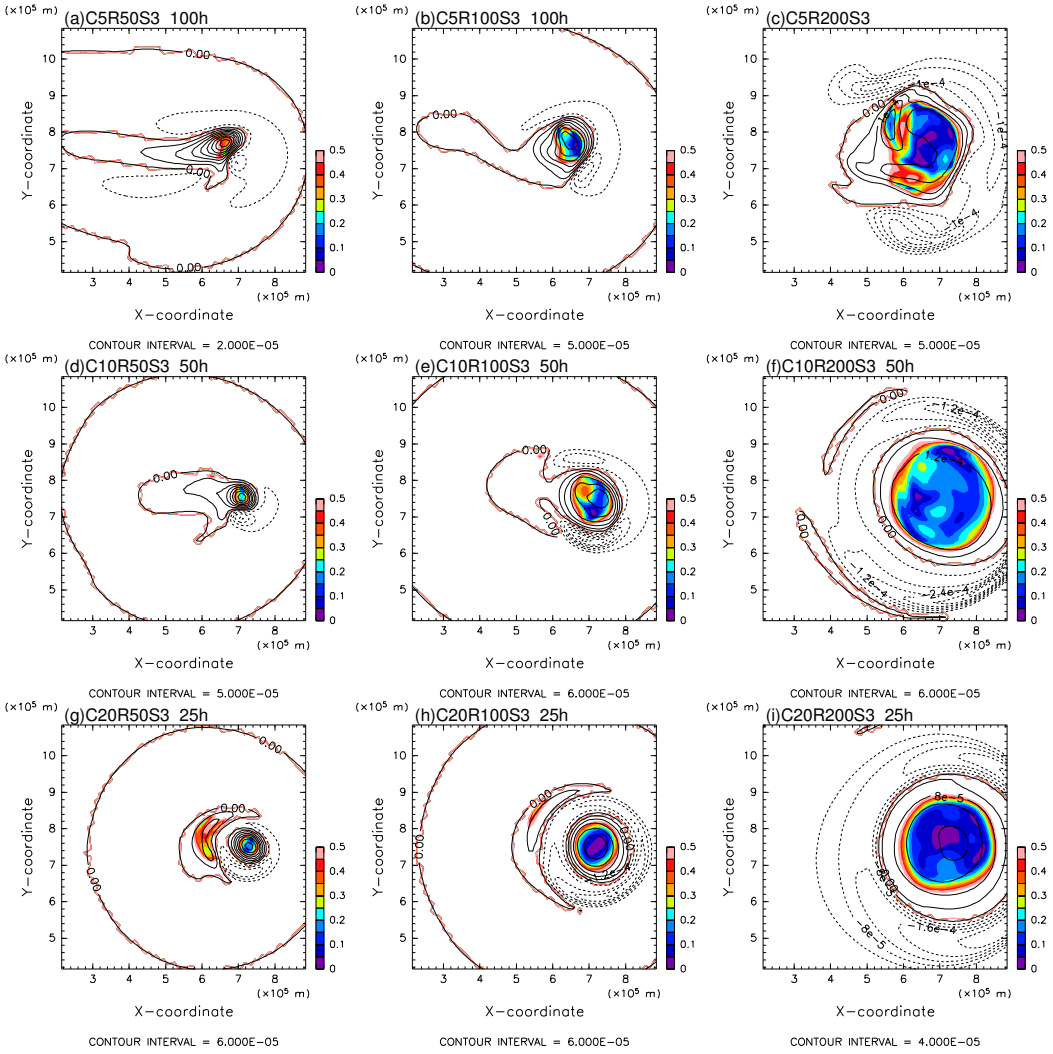

Figure 16: The vorticity (contour, s^{-1}) and ratio of deformation to the vorticity (colored < 0.5) for the dry experiments with $U_{7.5}$ of 3 m s^{-1}.

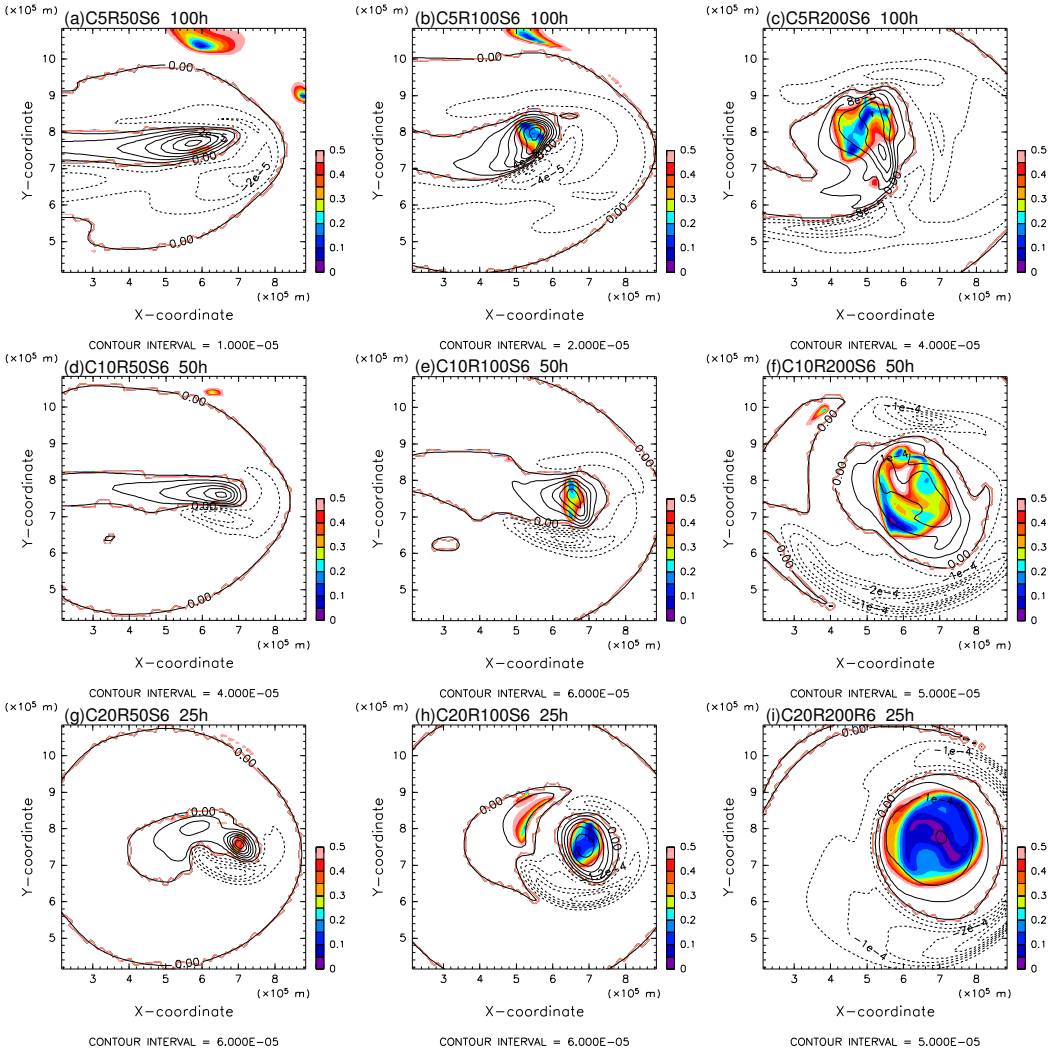

Figure 17: The vorticity (contour, s^{-1}) and ratio of deformation to the vorticity (colored < 0.5) for the dry experiments with $U_{7.5}$ of 6 m s^{-1}.

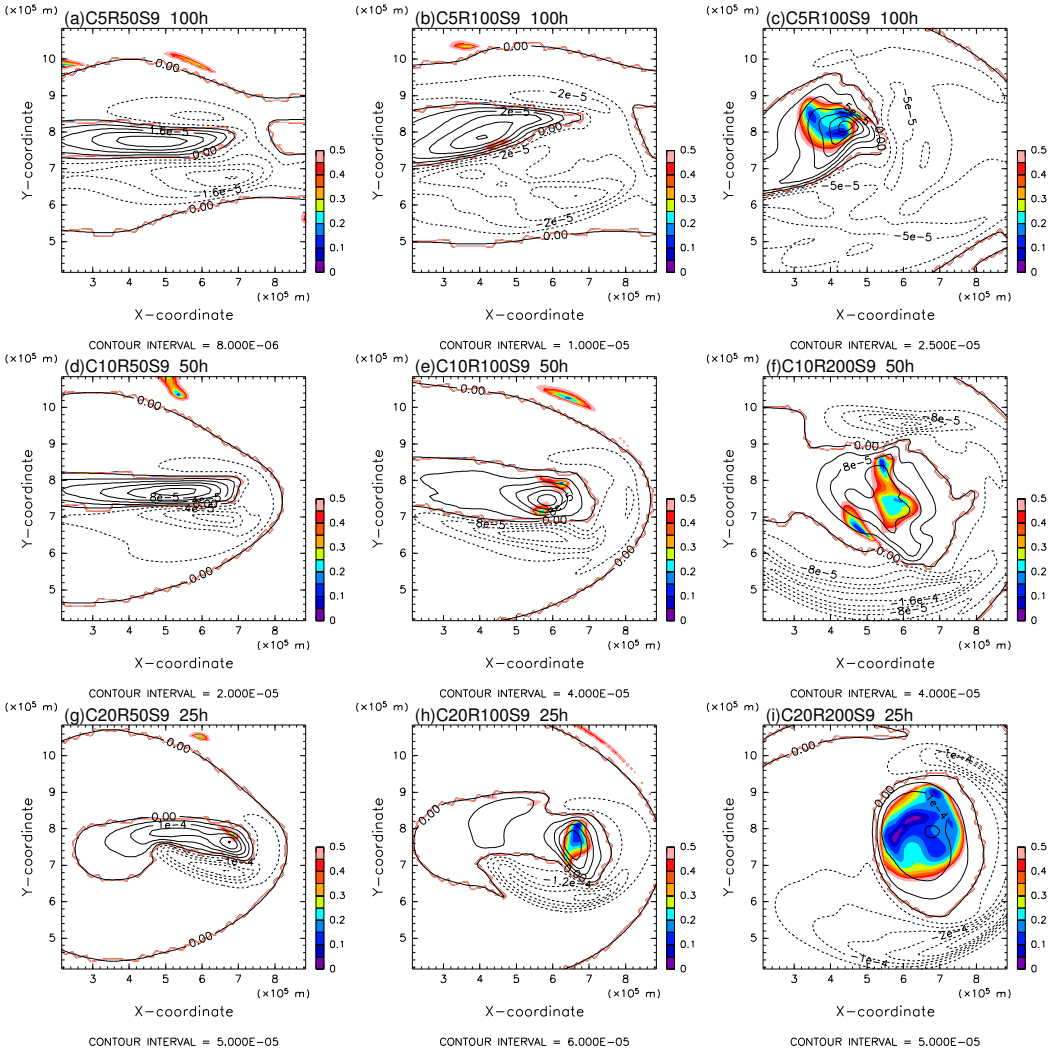

Figure 18: The vorticity (contour, s^{-1}) and ratio of deformation to the vorticity (colored < 0.5) for the dry experiments with $U_{7.5}$ of 9 m s^{-1}.

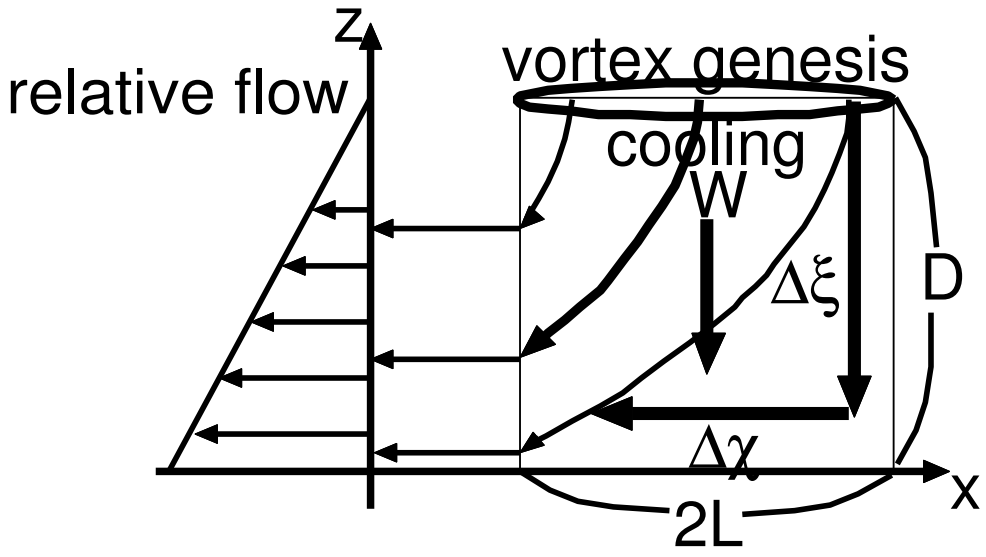

Figure 19: Schematic diagram of trajectory of parcels which start from the top of the cooling for very large vertical shear. Therefore parcels cannot reach the ground.

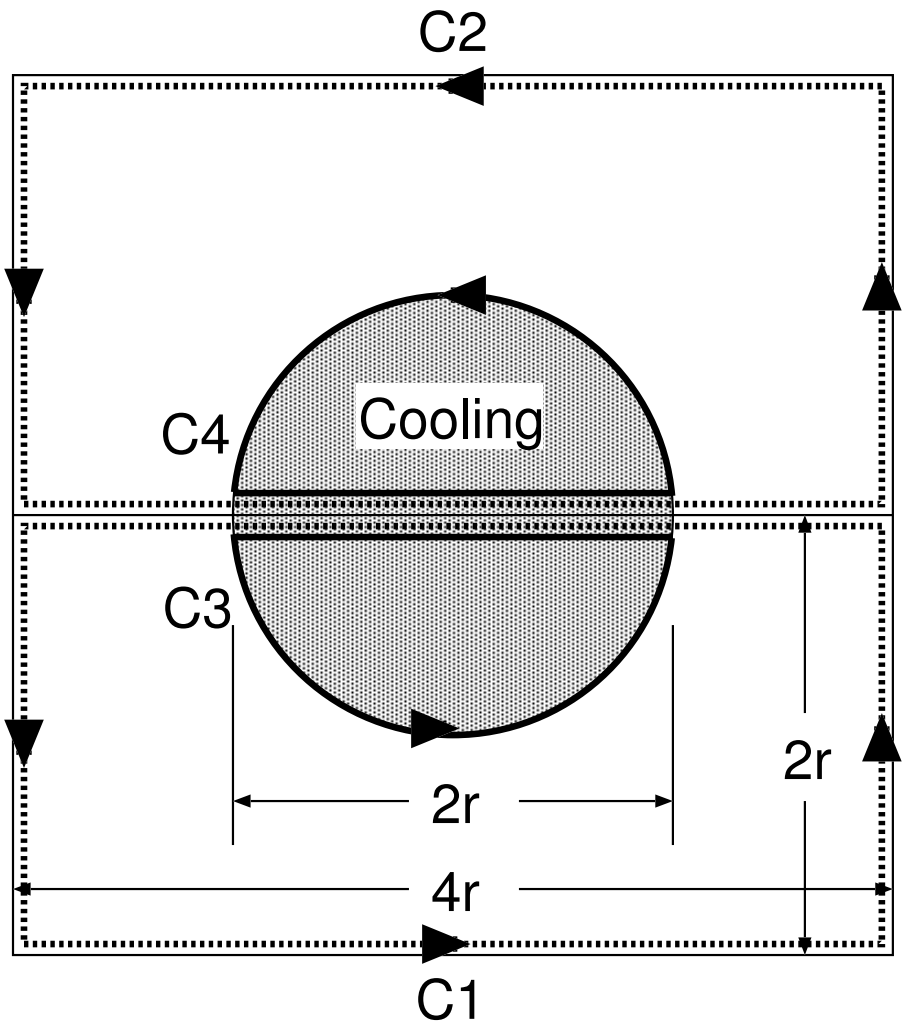

Figure 20: Schematic diagram for calculating circulation.

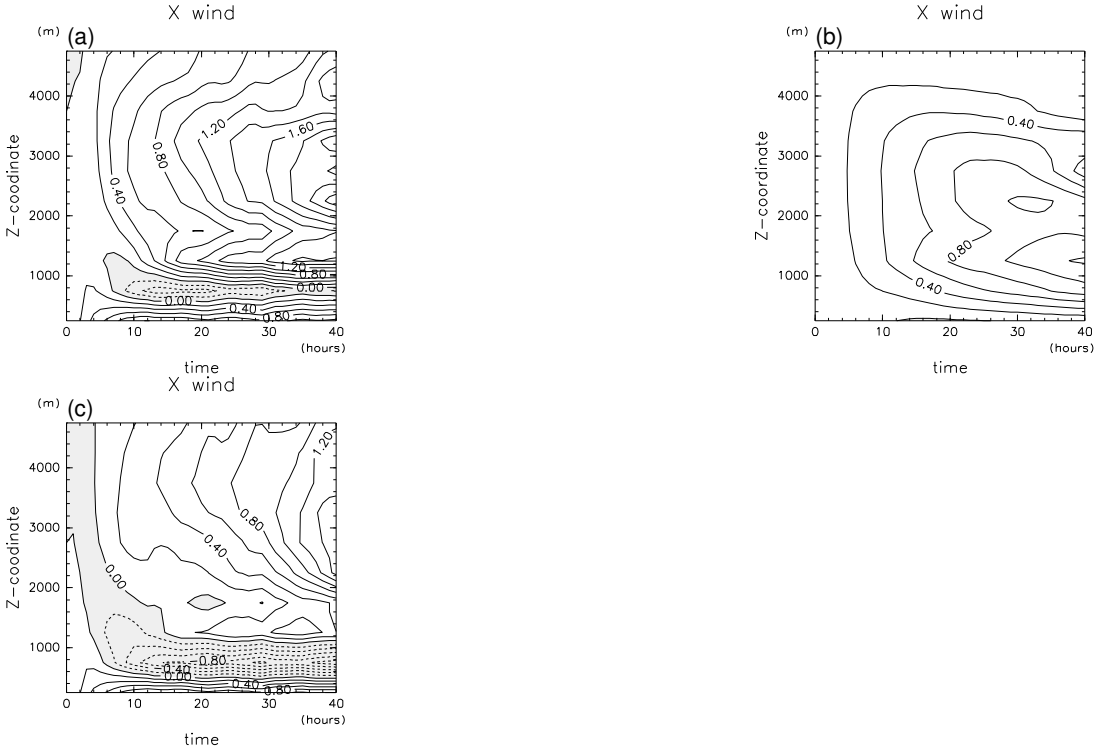

Figure 21: (a) Averaged value of zonal wind u minus $\overline{u}$ (m s^{-1}), (b) $u_{C1} + u_{C2}$ (m s^{-1}) calculated from circulation, (c) difference value of (a) from (b) (m s^{-1}) for the experiment C10R100S6.

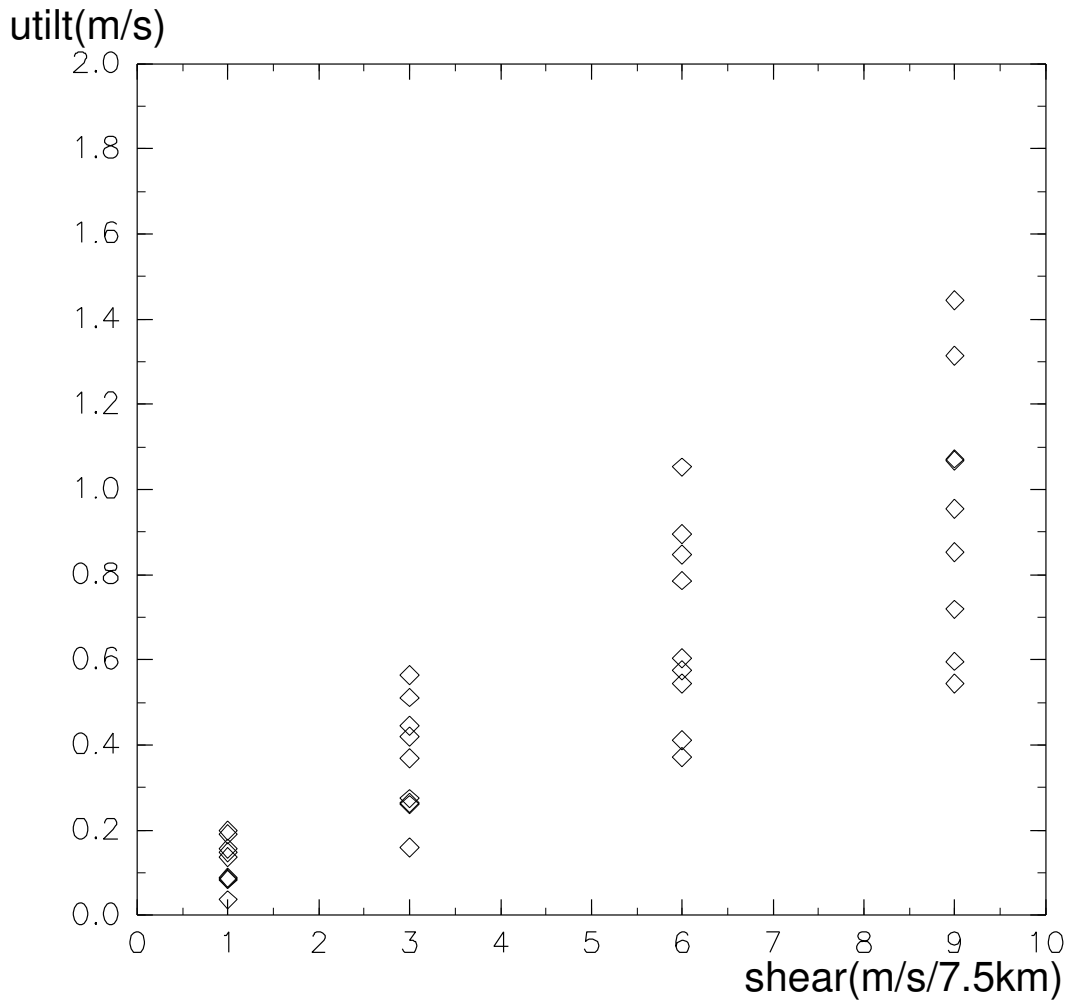

Figure 22: Distribution of u_{tilt} for all the dry experiments with shear.

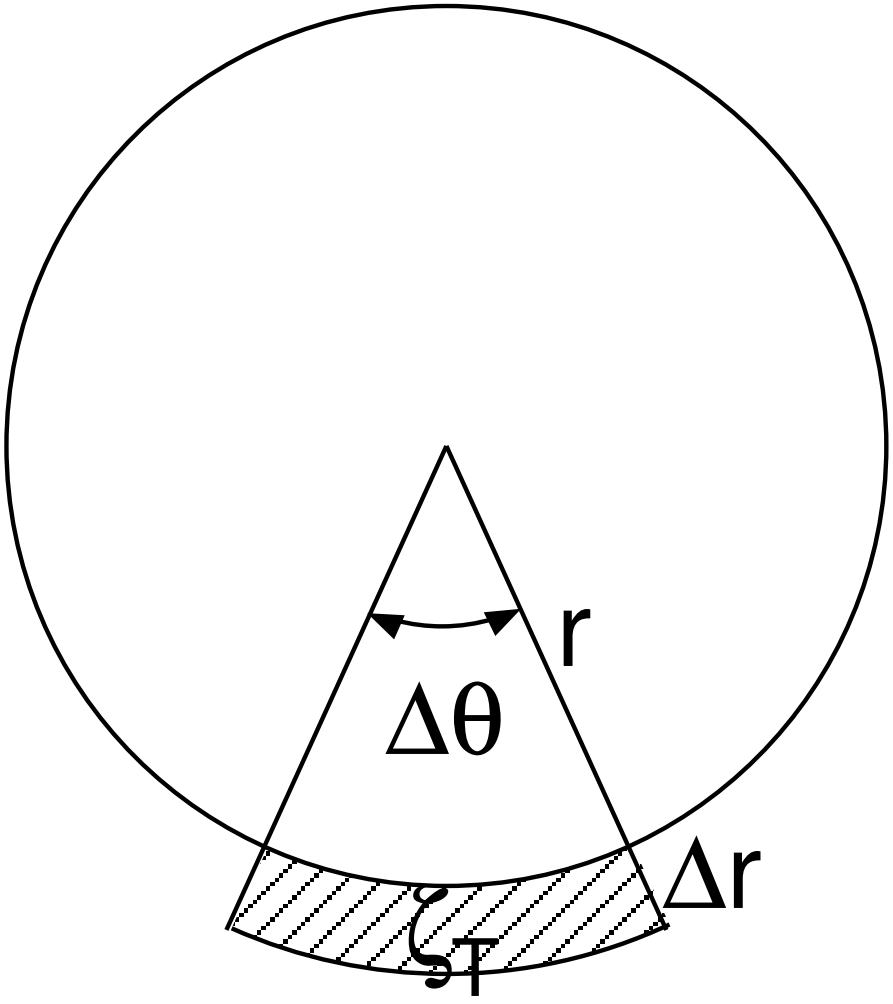

Figure 23: Schematic diagram of concentrated negative vorticity at the southern edge of cooling.

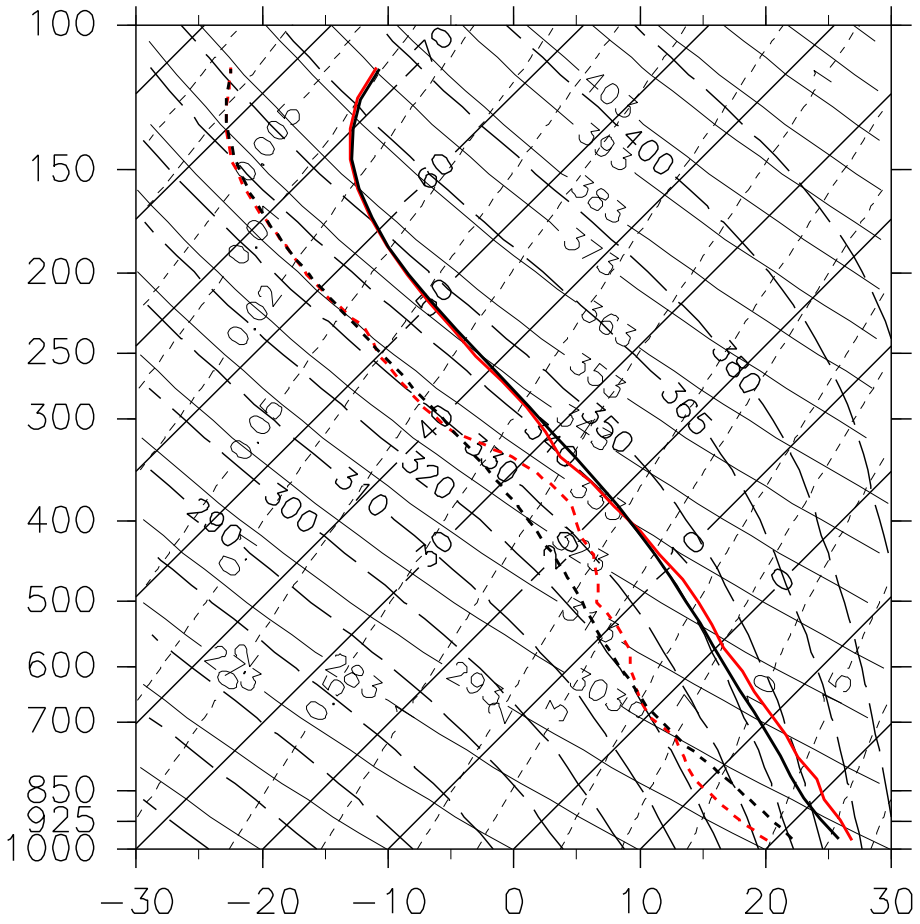

Figure 24: Skew T diagram depicting initial temperature and moisture profiles. Black lines show Jordan's (1958) profiles and red lines show the profiles used in the moist experiments.

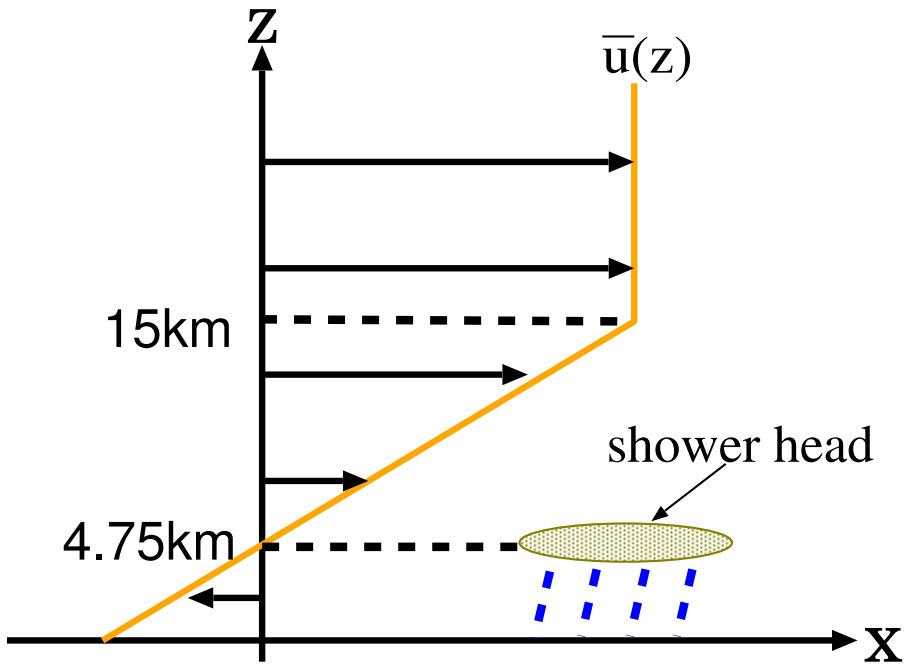

Figure 25: Schematic view of the configuration of $\overline{u}$, "shower head" and initial wind.

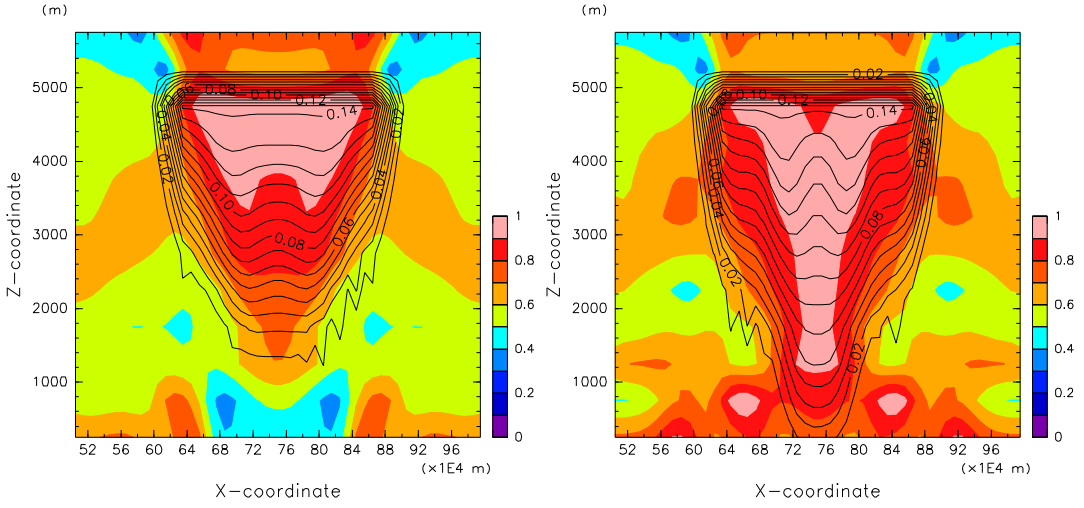

Figure 26: Mixing ratio of rain water (contour; g kg^{-1}) and relative humidity (shade; $\times 100\%$) for the experiment 0mCICR at $t = 10$ hours (left) and $t = 20$ hours (right). The contour interval is 0.02 g kg^{-1}.

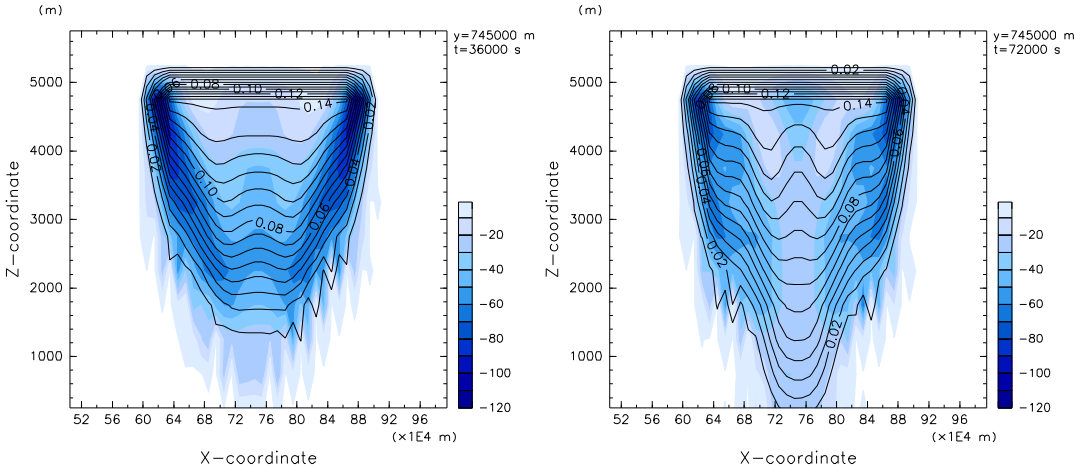

Figure 27: Mixing ratio of rain water (contour; g kg^{-1}) and cooling rate (shade; K day^{-1}) for the experiment 0mCICR at $t = 10$ hours (left) and $t = 20$ hours (right). The contour interval is 0.02 g kg^{-1}.

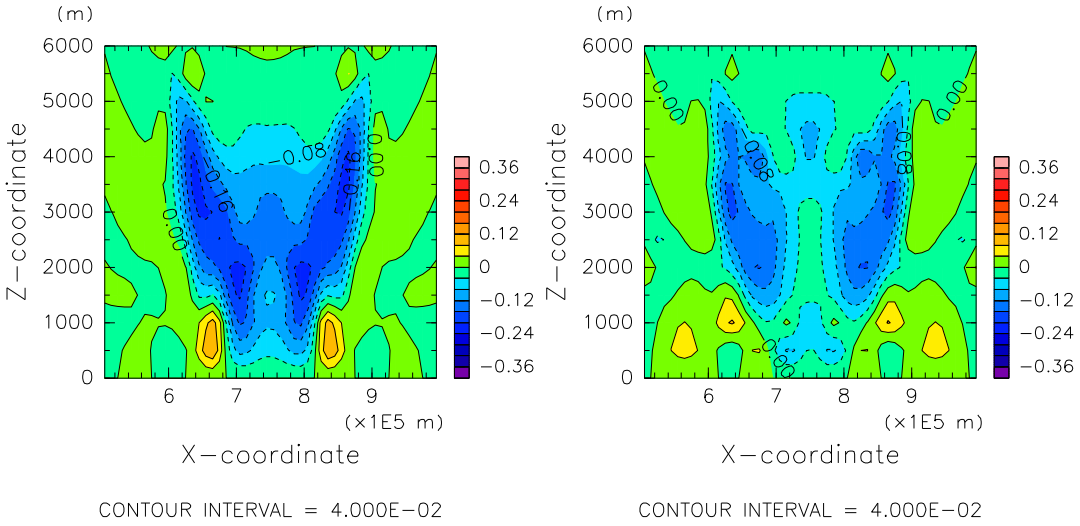

Figure 28: Vertical velocity for the experiment 0mCICR at $t = 10$ hours (left) and $t = 20$ hours (right). The contour interval is 0.04 m s^{-1}.

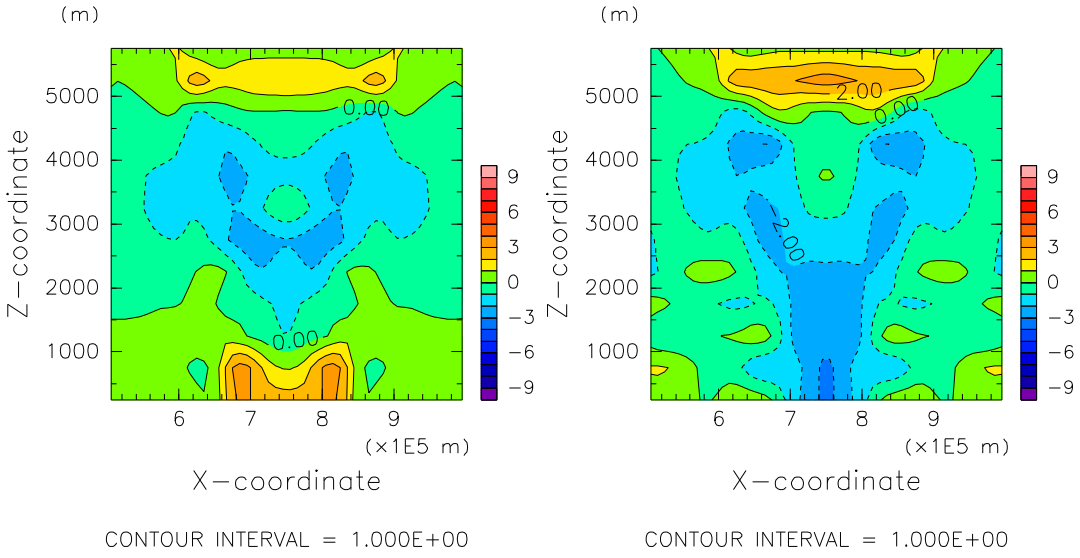

Figure 29: Potential temperature deviation for the experiment 0mCICR at $t = 10$ hours (left) and $t = 20$ hours (right). The contour interval is 1 K.

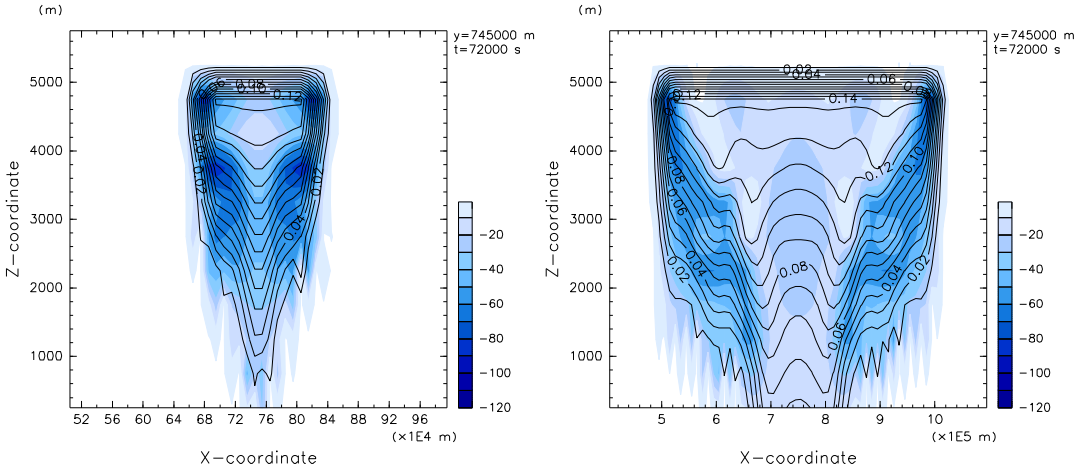

Figure 30: Mixing ratio of rainwater (contour; g kg^{-1}) and cooling rate (shade; K day^{-1}) at 20 hours for the experiments 0mCIHR and 0mCIDR. The contour interval is 0.01 g kg^{-1}.

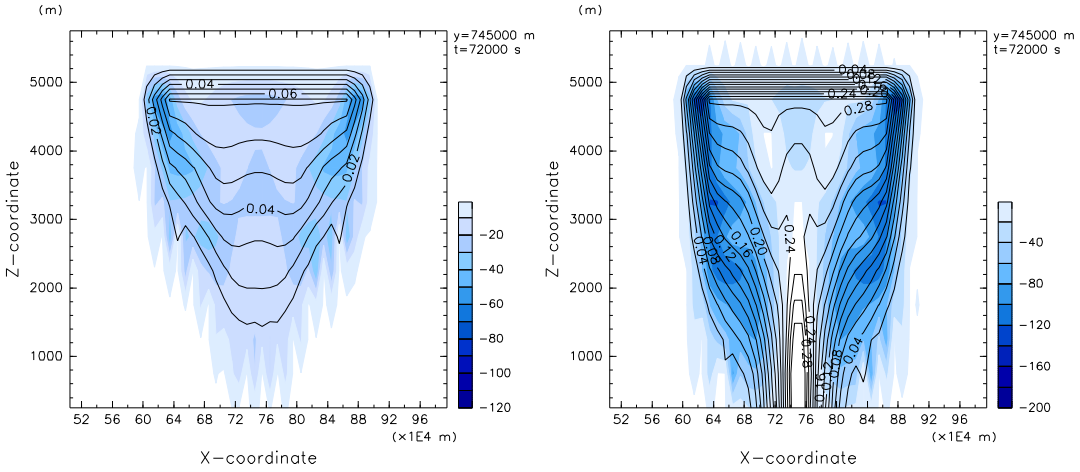

Figure 31: Mixing ratio of rainwater (contour; g kg^{-1}) and cooling rate (shade; K day^{-1}) at 20 hours for experiments 0mHICR (left) and 0mDICR (right). The contour intervals are 0.01 g kg^{-1} (left) and 0.02 g kg^{-1} (right).

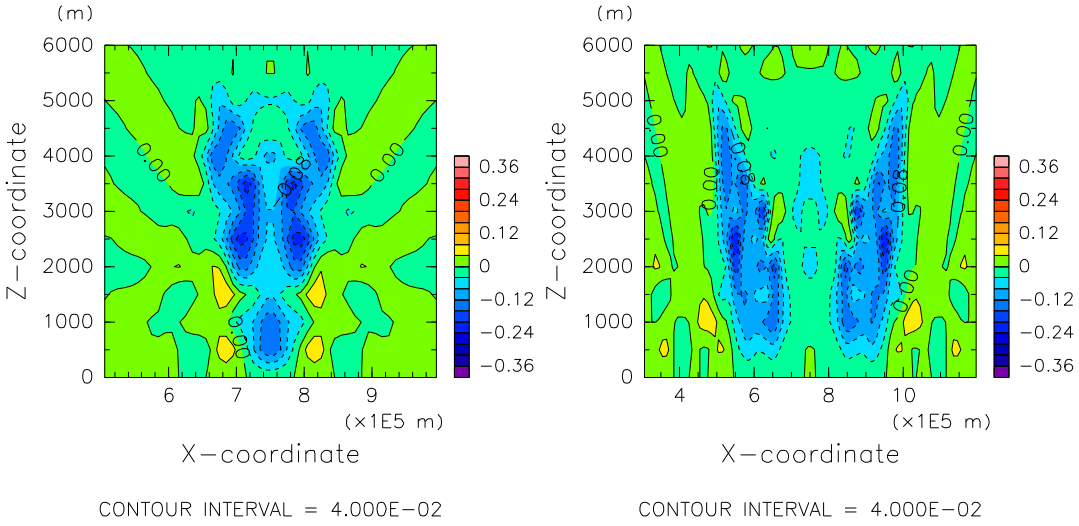

Figure 32: Vertical velocity at $t = 20$ hours for the experiments 0mCIHR (left) and 0mCIDR (right). The contour interval is 0.04 m s^{-1}.

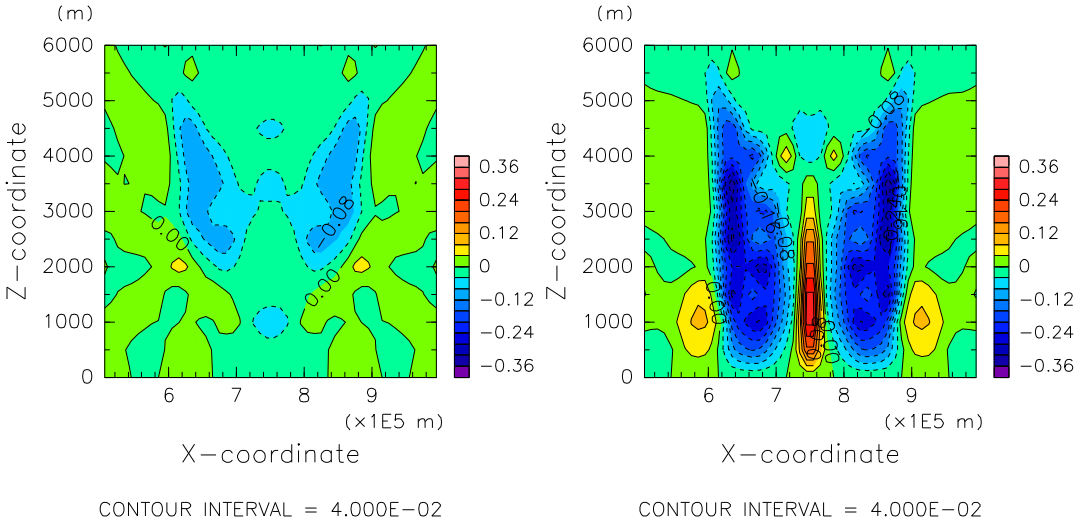

Figure 33: Vertical velocity at $t = 20$ hours for the experiments 0mHICR (left) and 0mDICR (right). The contour interval is 0.04 m s^{-1}.

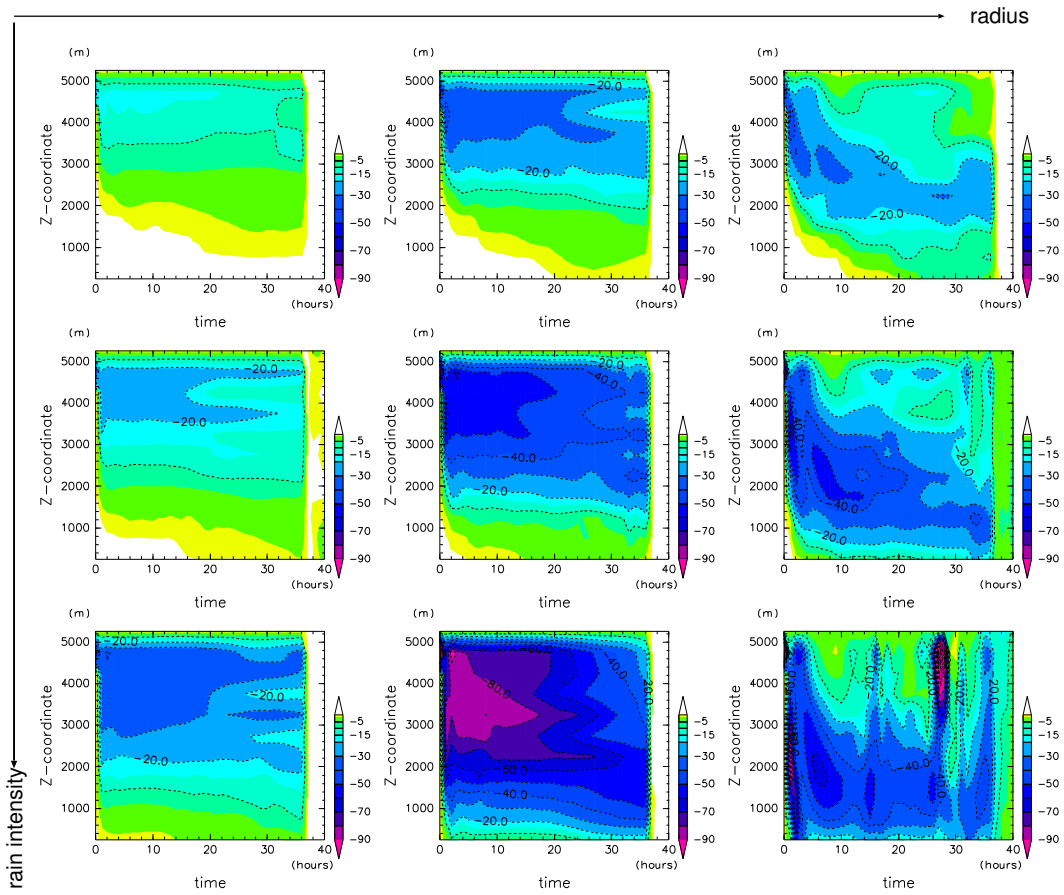

Figure 34: Time evolution of cooling rate profiles (K day^{-1}) averaged in the shower region for the no shear experiments. rows: rain intensity, (1st raw) intensity halved, (2st raw) standard intensity, (last raw) intensity doubled. column: radius of shower, (1st colomn) radius halved, (2nd column) standard radius, (last column) radius doubled.

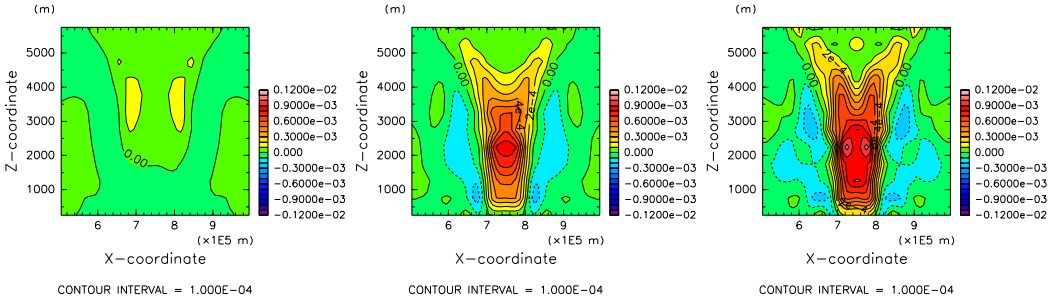

Figure 35: Time evolution of the vorticity at y=750 km at t=4 hours (left), 8 hours (middle), and 12 hours (right) for the experiments 0mCICR.

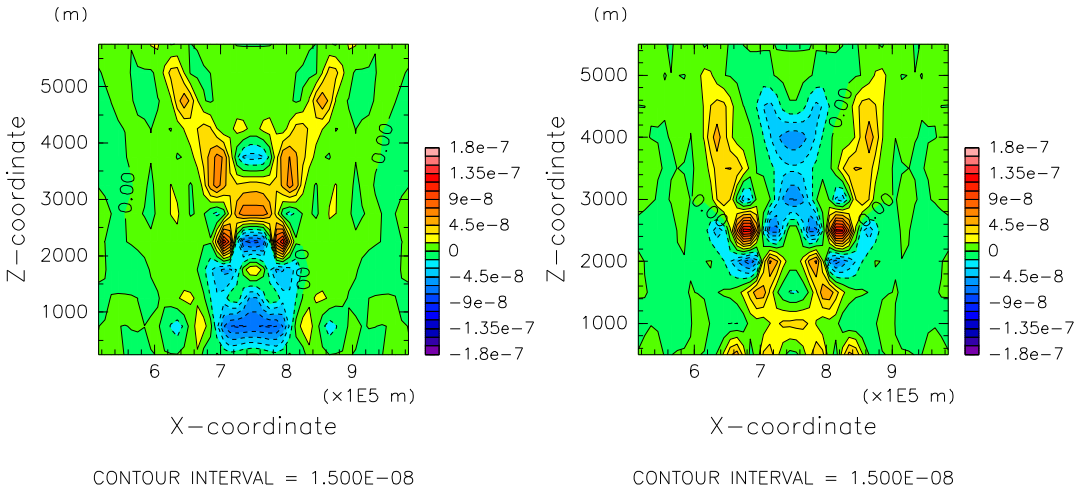

Figure 36: The vertical section of the vorticity production by stretching (left, s^{-2}) and by vertical advection at $t = 12$ hours for the experiments 0mCICR. The contour interval is 1.5×10^{-8} s^{-2}.

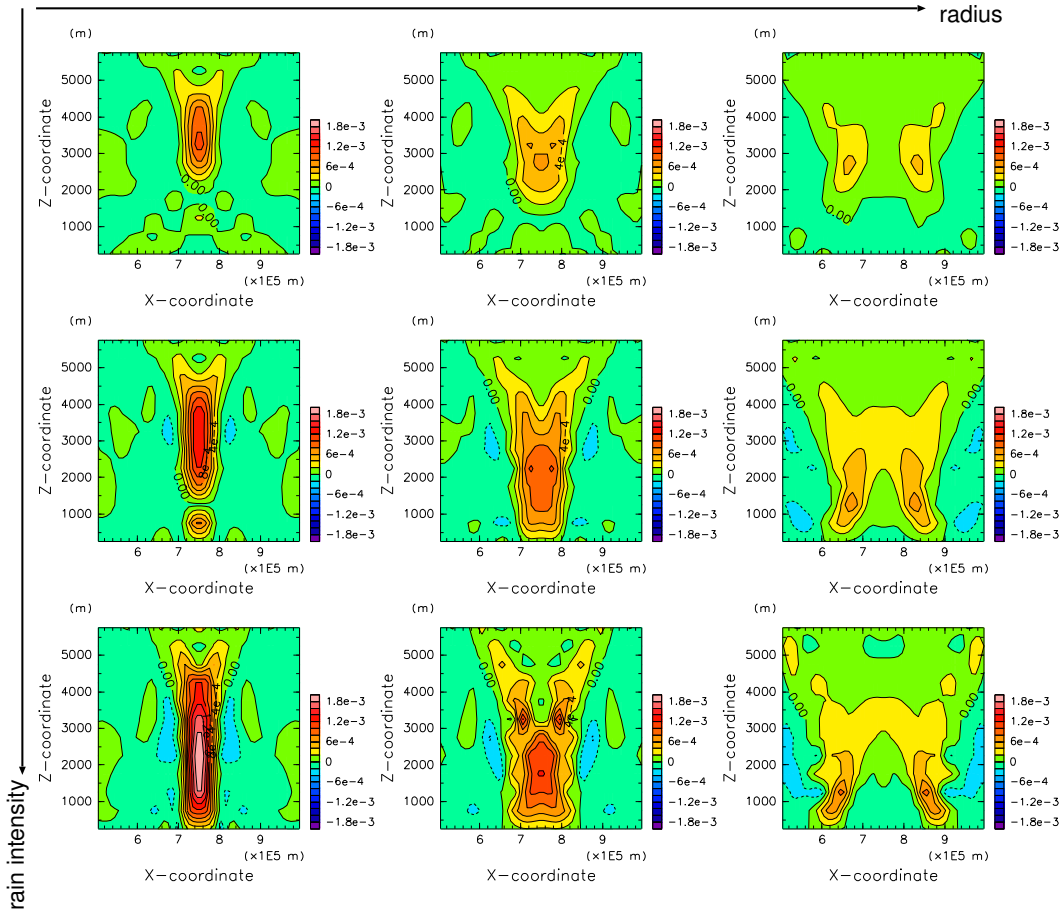

Figure 37: The vertical section of the vorticity at $t = 12$ hours for the no shear experiments. rows: rain intensity, (1st raw) intensity halved, (2st raw) standard intensity, (last raw) intensity doubled. column: radius of shower, (1st colomn) radius halved, (2nd column) standard radius, (last column) radius doubled. The contour interval is 2.0×10^{-4} s^{-1}.

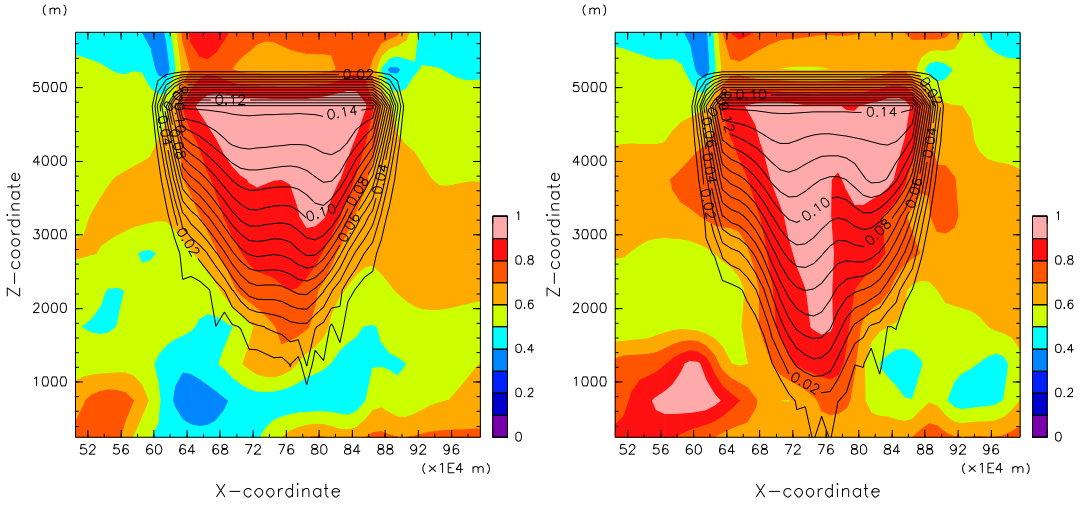

Figure 38: Mixing ratio of rainwater (contour; g kg^{-1}) and relative humidity (shade; $\times 100\%$) for the experiment 20mCICR at $t = 10$ hours (left) and $t = 20$ hours (right). The contour interval is 0.01 g kg^{-1}.

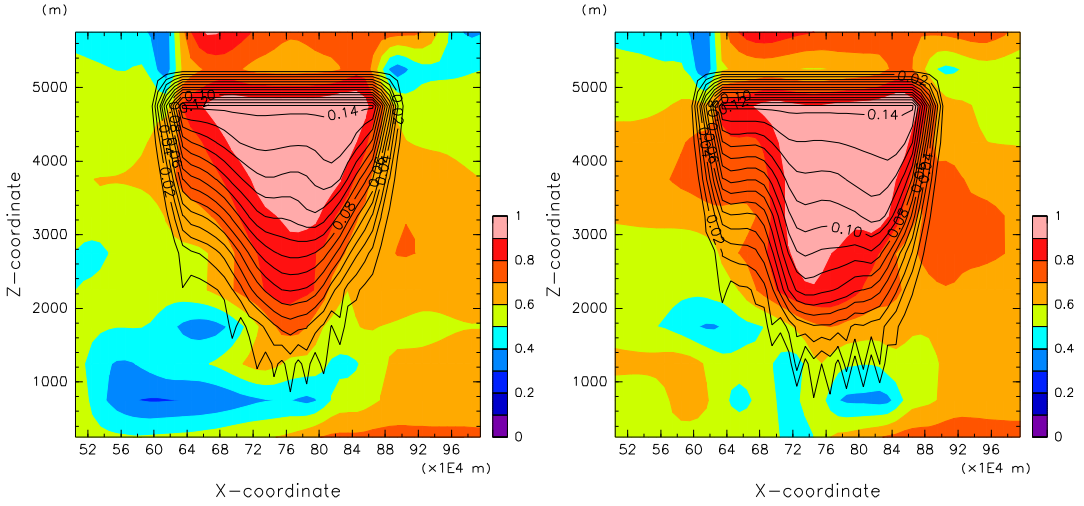

Figure 39: Mixing ratio of rainwater (contour; g kg^{-1}) and relative humidity (shade; $\times 100\%$) for the experiment 40mCICR at $t = 10$ hours (left) and $t = 20$ hours (right). The contour interval is 0.01 g kg^{-1}.

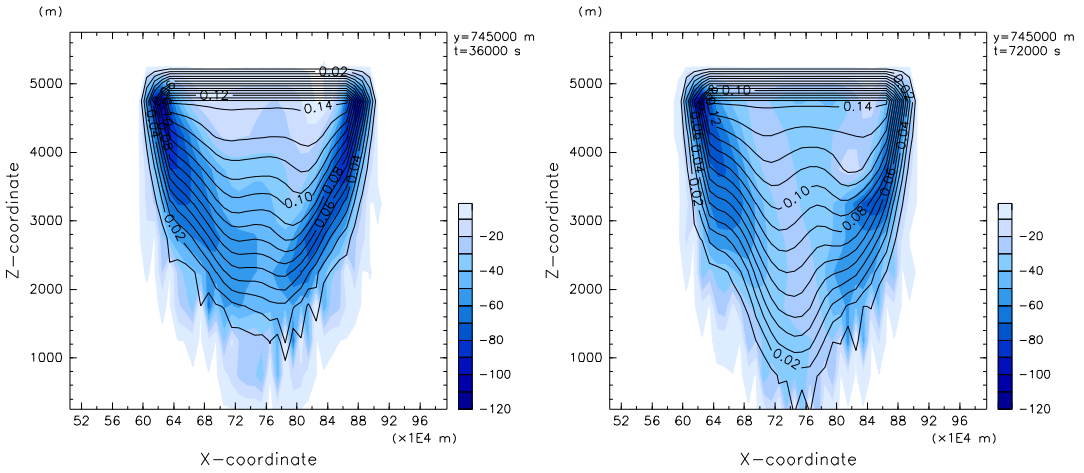

Figure 40: Mixing ratio of rainwater (contour; g kg^{-1}) and cooling rate (shade; K day^{-1}) for the experiment 20mCICR at $t = 10$ hours (left) and $t = 20$ hours (right). The contour interval is 0.01 g kg^{-1}.

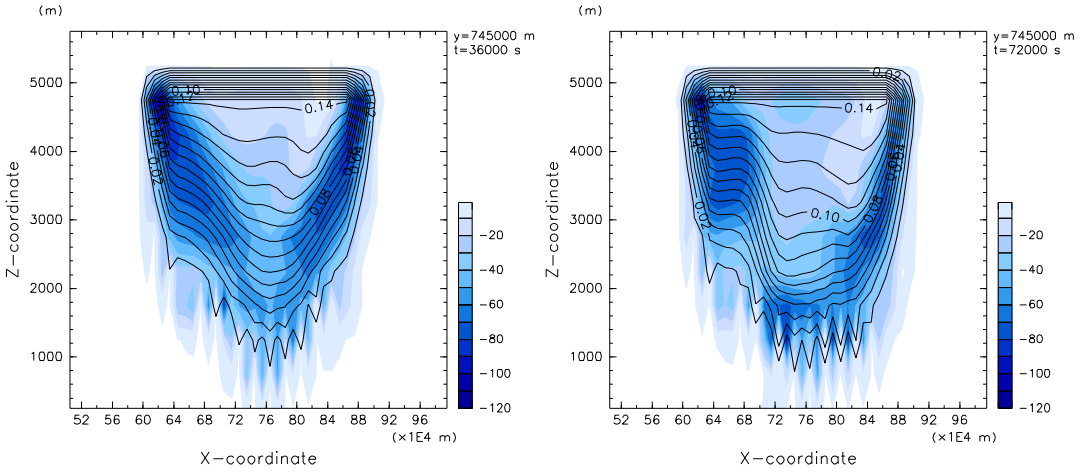

Figure 41: Mixing ratio of rainwater (contour; g kg^{-1}) and cooling rate (shade; K day^{-1}) for the experiment 40mCICR at $t = 10$ hours (left) and $t = 20$ hours (right). The contour interval is 0.01 g kg^{-1}.

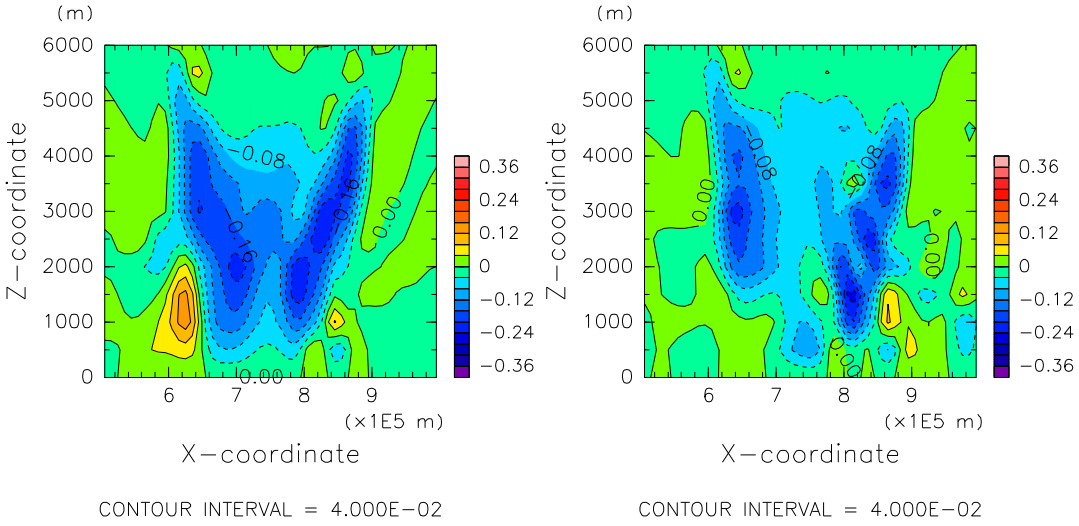

Figure 42: The vertical velocity for the experiment 20mCICR at $t = 10$ hours (left) and $t = 20$ hours (right). The contour interval is 0.04 m s^{-1}.

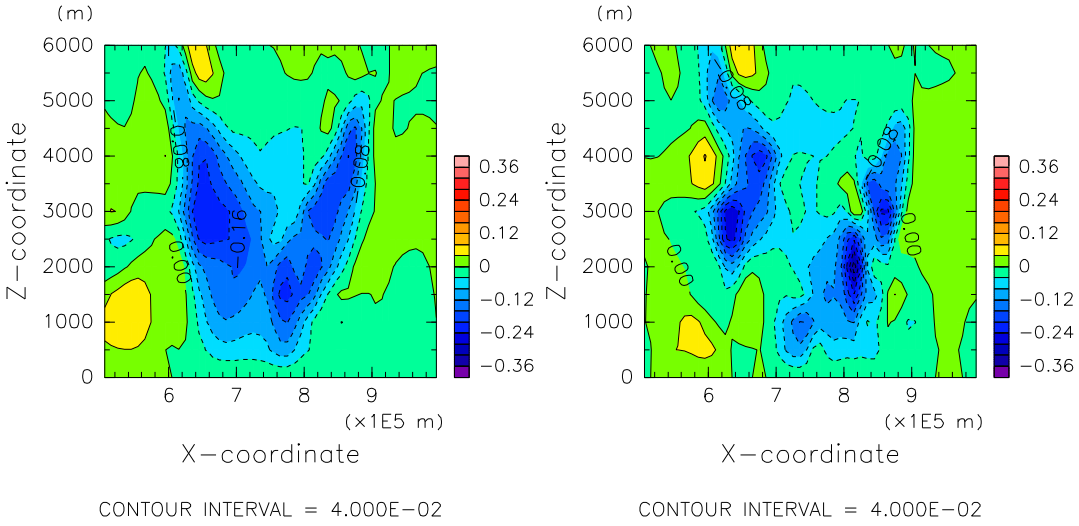

Figure 43: The vertical velocity for the experiment 40mCICR at $t = 10$ hours (left) and $t = 20$ hours (right). The contour interval is 0.04 m s^{-1}.

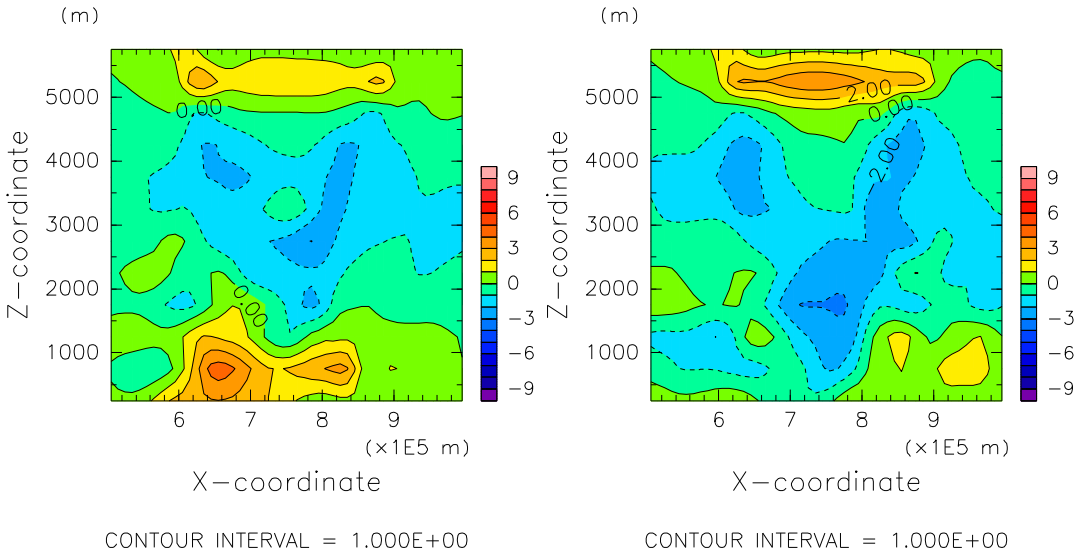

Figure 44: Potential temperature deviation for the experiment 20mCICR at $t =$ 10 hours (left) and $t = 20$ hours (right). The contour interval is 1 K.

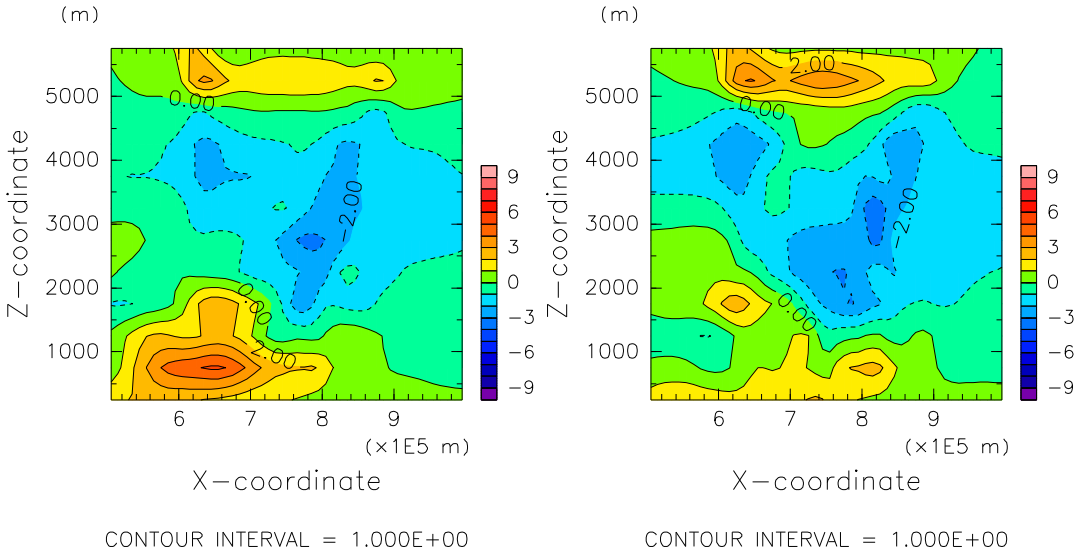

Figure 45: Potential temperature deviation for the experiment 40mCICR at $t =$ 10 hours (left) and $t = 20$ hours (right). The contour interval is 1 K.

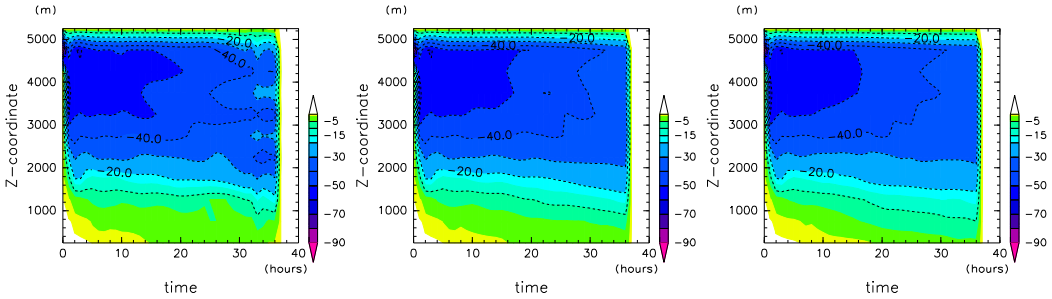

Figure 46: Time evolution of cooling rate profiles (K day^{-1}) averaged in the shower region for the experiments 0mCICR (left), 20mCICR (middle), and 40mCICR (right).

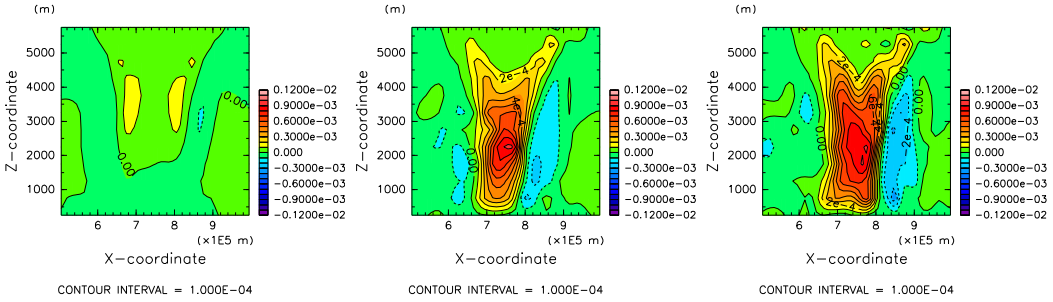

Figure 47: Time evolution of the vorticity at y= 750 km at t= 4 hours (left), 8 hours (middle), and 12 hours (right) for the experiments 20mCICR.

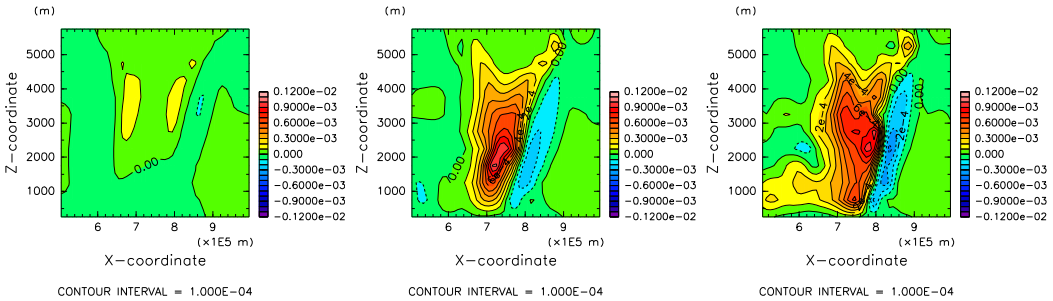

Figure 48: Time evolution of the vorticity at y= 750 km at t= 4 hours (left), 8 hours (middle), and 12 hours (right) for the experiments 40mCICR.

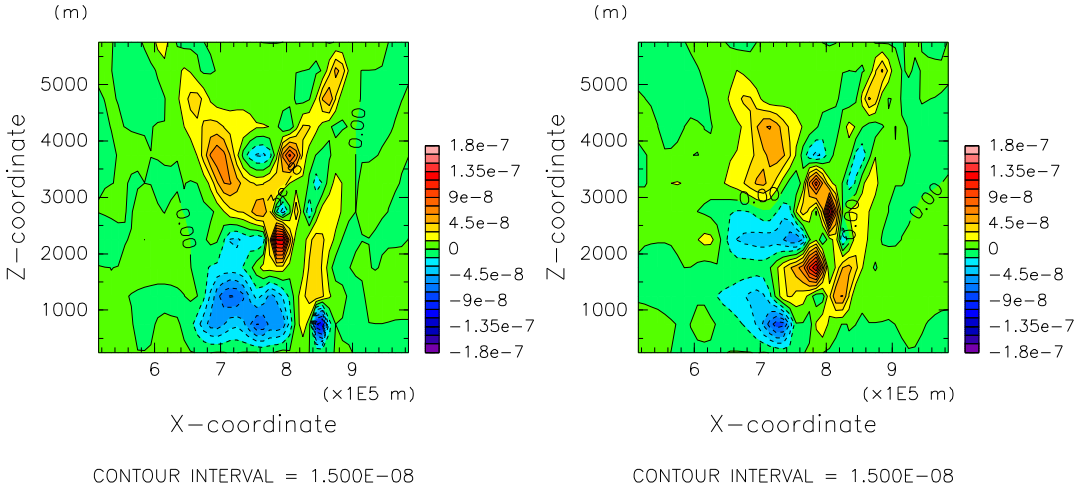

Figure 49: The vertical section of the vorticity production by stretching at $t =$ 12 hours for experiments 20mCICR (left), and 40mCICR (right). The contour interval is 1.5×10^{-8} s^{-2}.

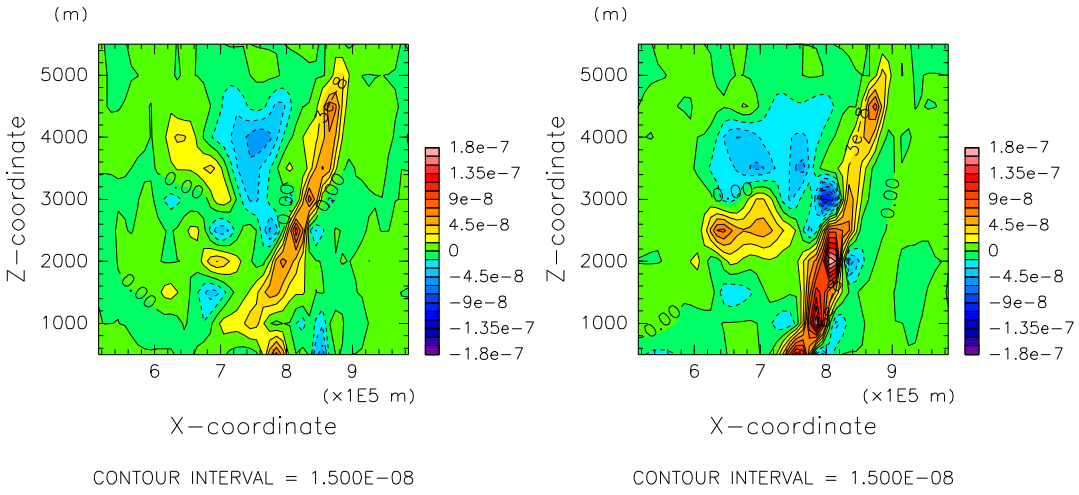

Figure 50: The vertical section of the vorticity production by vertical advection at $t = 12$ hours for the experiments 20mCICR (left) and 40mCICR (right). The contour interval is 1.5×10^{-8} s^{-2}.

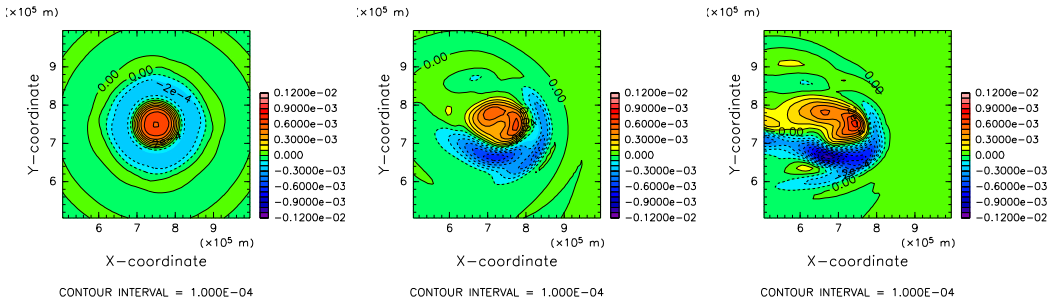

Figure 51: The vertical section of the vorticity at $t = 12$ hours for the experiments 0mCICR (light), 20mCICR (middle), and 40mCICR (right). The contour interval is 1.0×10^{-4} s^{-1}.

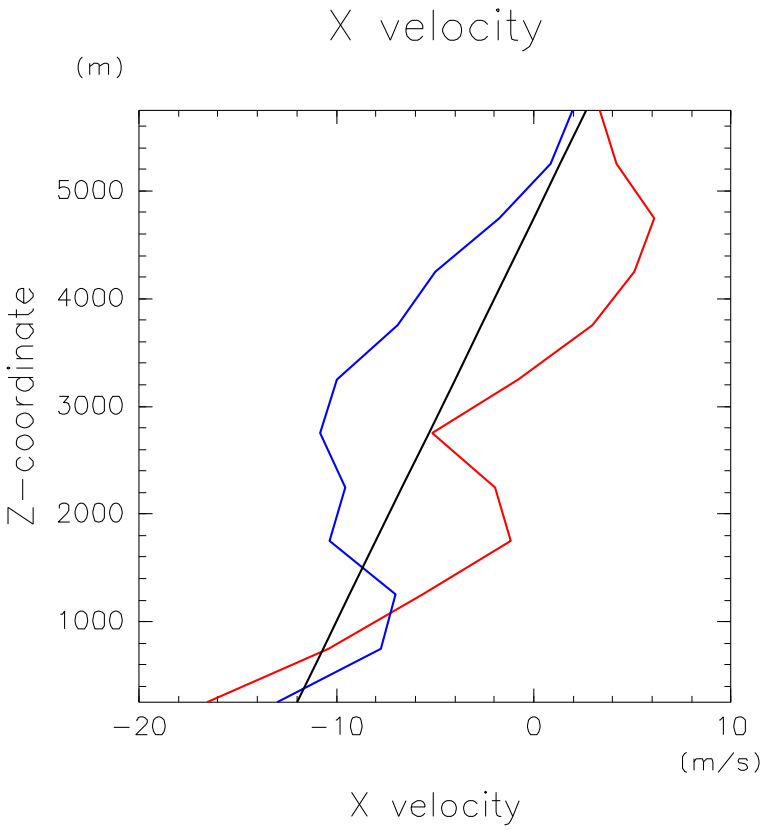

Figure 52: Vertical profiles of the westerly wind for the experiment 40mCICR at the northern edge (x=750 km and y=850 km; blue) and sourthern edge (x=750 km and y=650 km; red) of the shower region at t= 10 hours. The black line shows the initial shear.

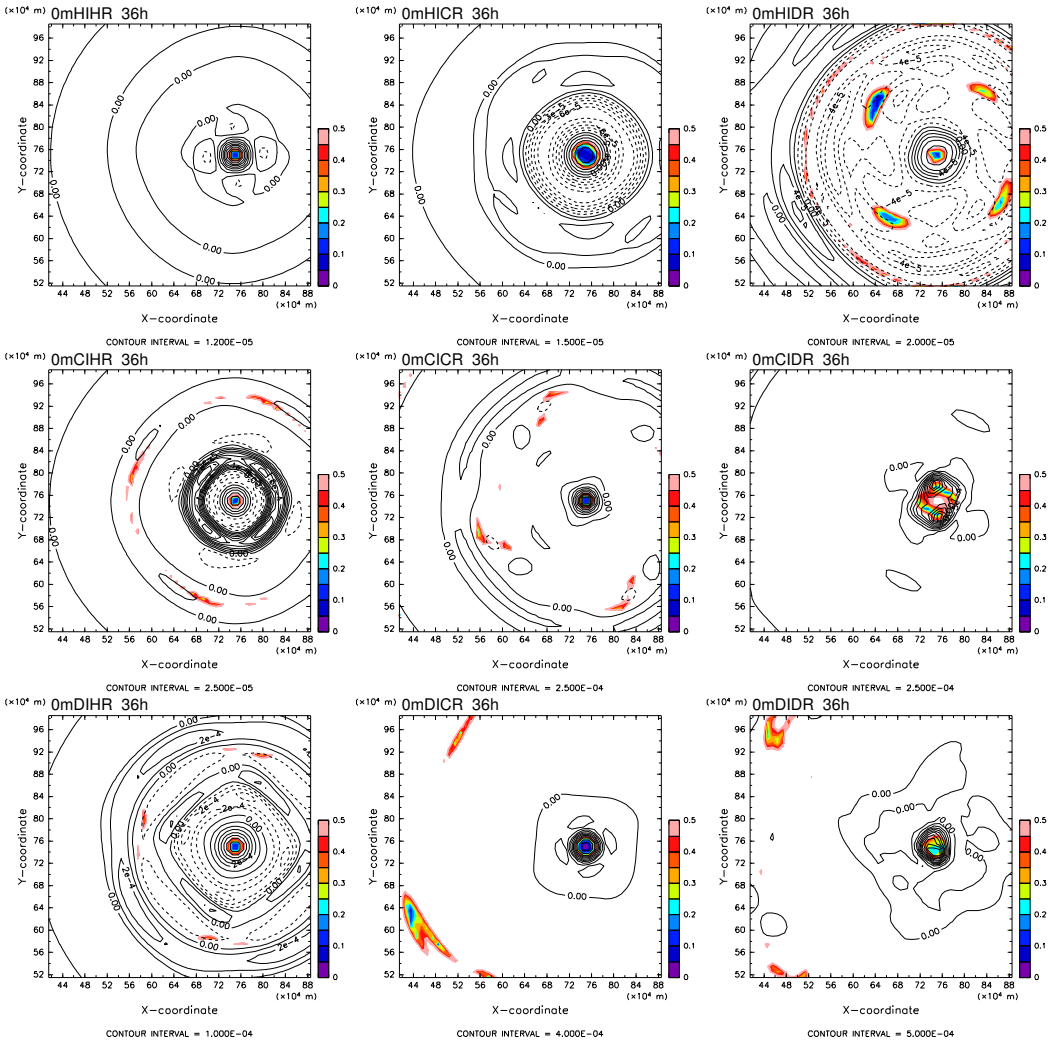

Figure 53: The vorticity (contour, s^{-1}) and ratio of deformation to vorticity (colored < 0.5) for the experiments with no shear.

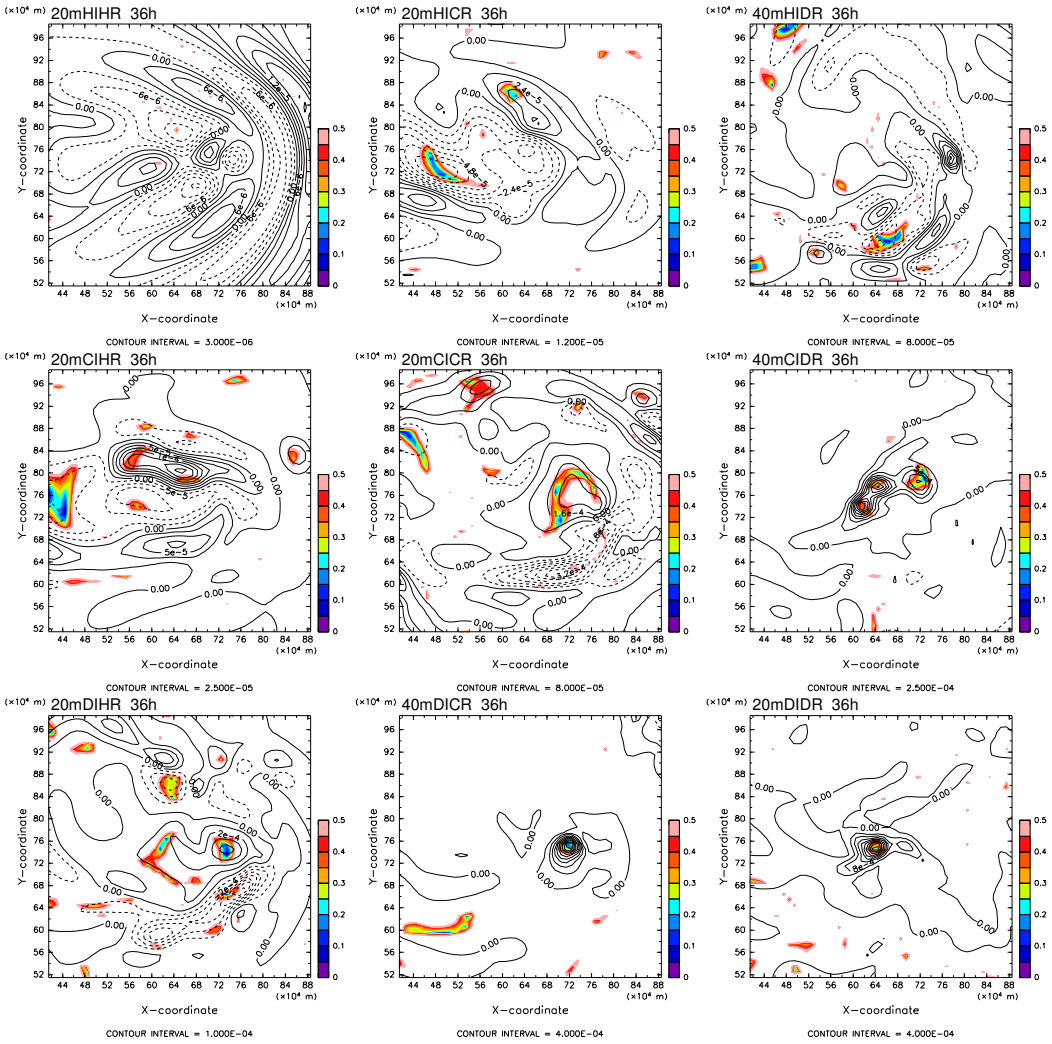

Figure 54: The vorticity (contour, s^{-1}) and ratio of deformation to vorticity (colored < 0.5) for the experiments with shear of 20 m s^{-1}.

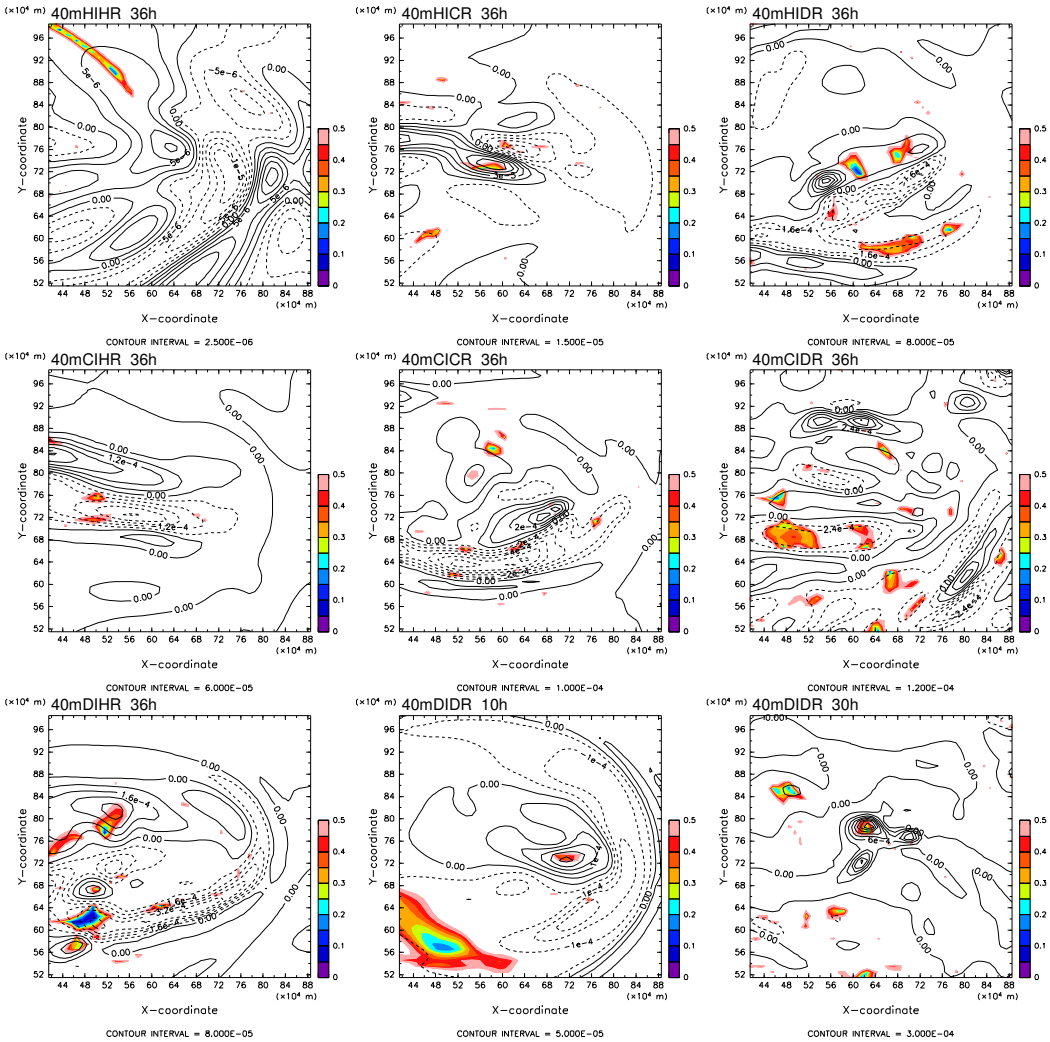

Figure 55: The vorticity (contour, s^{-1}) and ratio of deformation to vorticity (colored < 0.5) for the experiments with shear of 40 m s^{-1}.